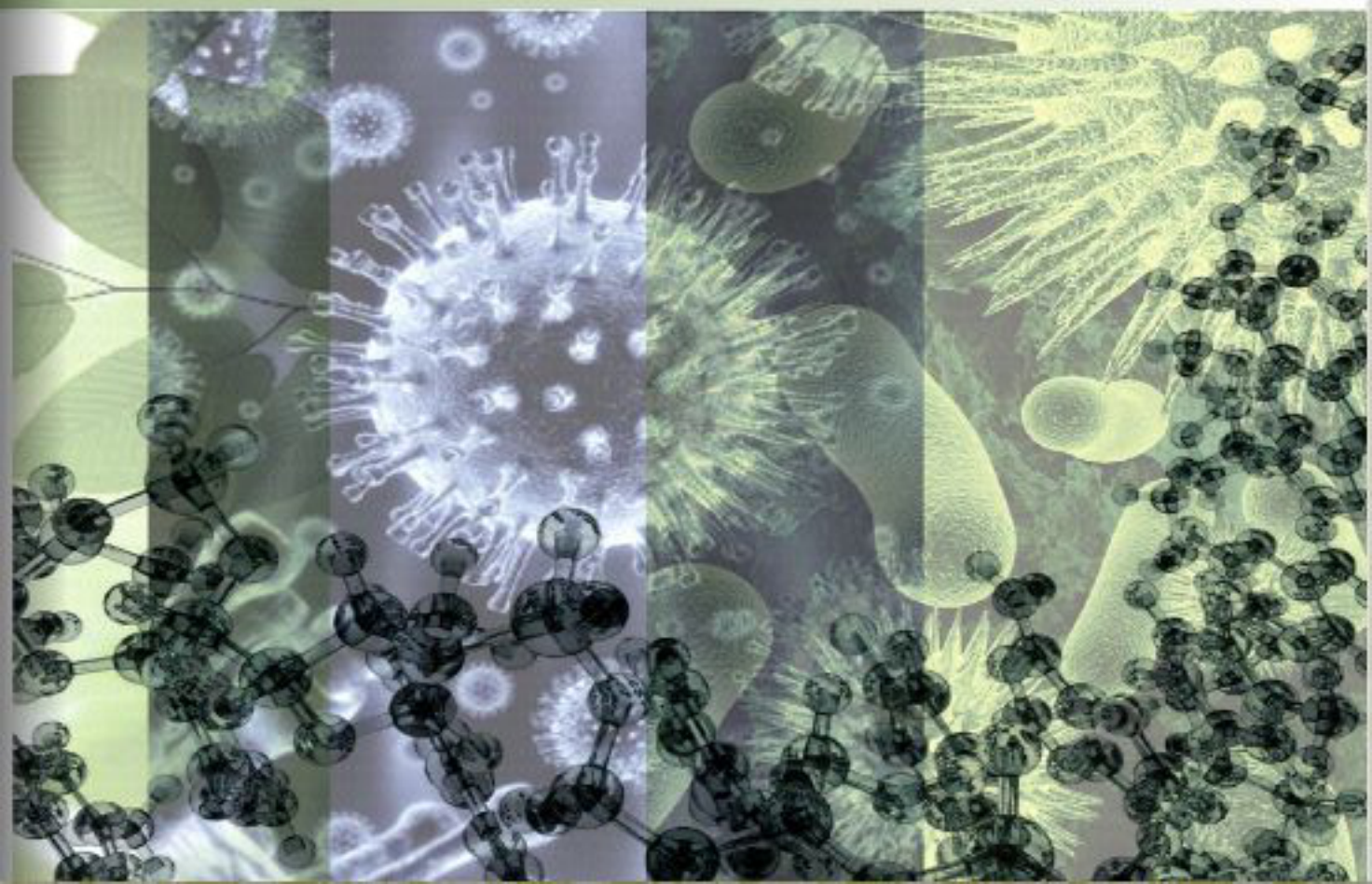


RECENT ADVANCES IN PHARMACEUTICAL SCIENCES

VOL. VIII

Editors

Diego Muñoz-Torrero, Yolanda Cajal and Joan Maria Llobet





Research Signpost
Trivandrum
Kerala, India

Recent Advances in Pharmaceutical Sciences VIII, 2018: 1-18 ISBN: 978-81-308-0579-5
Editors: Diego Muñoz-Torrero, Yolanda Cajal and Joan Maria Llobet

1. Magnetic nanoparticles: From diagnosis to therapy

M. Antònia Busquets and Joan Estelrich

*Department of Pharmacy, Pharmaceutical Technology and Physical Chemistry
Institute of Nanoscience and Nanotechnology, IN2UB
Faculty of Pharmacy and Food Sciences, University of Barcelona
Avda Joan XXIII, 27-31, 08028 Barcelona*

Abstract. Magnetic nanoparticles have proven to be promising theranostic agents, namely tools for therapy and diagnosis. Among them, superparamagnetic iron oxide nanoparticles (SPIONs) highlight for their biocompatibility and reduced toxicity. Here, we describe the synthesis and characterization of SPIONs by co-precipitation of ferric and ferrous salts under mild conditions. These particles were able to accumulate in inflamed areas fact that was increased upon the application of an external magnetic field. Resonance magnetic imaging studies have shown their suitability as negative contrast agents for diagnosis. In addition, hybrid nanoparticles were obtained by incorporating the above described SPIONs into liposomes or nanoemulsions. The findings have confirmed the high potential of these systems for biomedical applications.

Introduction

The impact of nanotechnology is strongly associated to the development of nanomaterials and nanoparticles (NPs) [1,2]. In particular, magnetic nanoparticles (MNs) present a number of advantages if compared to other

Correspondence/Reprint request: Dr. M. Antònia Busquets, Department of Pharmacy, Pharmaceutical Technology and Physical Chemistry, Faculty of Pharmacy and Food Sciences, University of Barcelona, Avda Joan XXIII, 27-31, 08028 Barcelona. E-mail: mabusquetsvinas@ub.edu

nanosystems. Their magnetic properties can be exploited for the targeting of drugs and as contrast agents. The duality that involves both therapy and diagnosis, all in one, or theranostic effect [3] has gained interest in the biomedical field, becoming an encouraging approach towards a personalized medicine. For that purpose, the design of nanosystems often requires the combination of one or several modifications of traditional NPs. It usually involves changes in their surface or their incorporation into other NPs conferring in this way also versatile, multifunctional, biocompatible and biodegradable properties [4,5].

There is a great variety of materials that show magnetism in some extent depending on their atomic structure and temperature. The compounds with stable magnetic properties are classified into two main groups: ferromagnets, with permanent magnetism, and paramagnets, with magnetism that appears upon the application of an external magnetic field [6]. On the other hand, the size is a decisive aspect concerning to the functionality of the MNs. A ferromagnet of macroscopic size contains numerous regions called magnetic domains in the demagnetized state. Within each domain all the atomic moments (represented as arrows in Fig 1) are aligned in one of the directions leading to spontaneous magnetization.

The direction of the magnetization, however, varies from domain to domain so as to minimize the magnetostatic energy. On a purely statistical basis, all available easy directions will be used equally in the material. Hence the particle as a whole will only show a net magnetization when submitted to an applied field [7]. A ferromagnet below a certain critical diameter (D_{CR}) shows a single domain. Further reduction in size results in a superparamagnetic (D_{SPM}) behavior meaning that magnetic properties are only present upon the application of an external magnetic field.

Among the several types of MNs, up to now, iron oxide nanoparticles (IONs) have proven to be the most promising MNs for theranostic applications mainly for their high imaging sensitivity, therapeutic efficacy, inherent biocompatibility and low cost [8]. This group comprises different chemical combinations of iron such as ferrites with a general formula MFe_2O_4 ($M = Co, Ni, Zn, Mn$), magnetite (Fe_3O_4), maghemite ($\gamma-Fe_2O_3$) or the non-stoichiometric mixture of the last two, with diameters comprised between 1 and 100 nm. This array of sizes supposes an additional advantage in the design of IONs with different magnetic behavior and consequently for a variety of applications. Therefore, below a certain diameter, D_{SPM} , they are superparamagnetic being magnetized only in presence of a magnetic field. Superparamagnetic IONs (SPIONs) can be directed by an external magnet

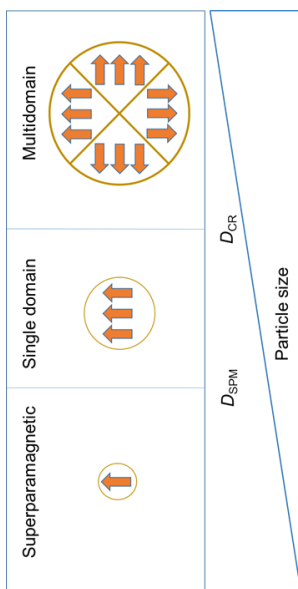
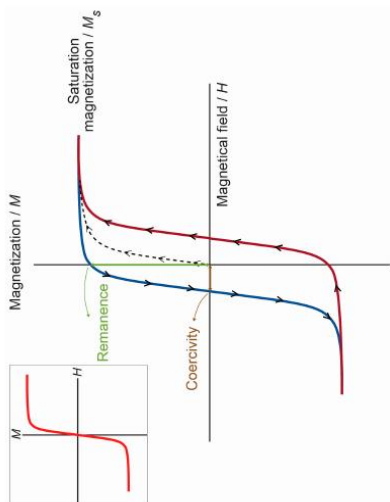


Figure 1. Left) Magnetic regimes of ferromagnetic materials classified according to their size. Right) Changes of magnetization (M) for a ferromagnetic material depending on the application of an external magnetic field (H). The arrows on the cycle indicate the direction in the increase or decrease of the field amplitude. The inset shows the behavior of a superparamagnetic material submitted to the same external magnetic field [6].

towards a given target zone (Figure 2). Then, the application of a magnetic field moves the SPIONs toward the magnet and concentrates near its location. SPIONs revert to a non-magnetic state upon removal of the external magnet [9].

The application of a high-frequency alternating magnetic field can selectively heat SPIONs resulting in a hyperthermia effect that can be exploited for drug targeting. Therefore, their responsiveness to a magnetic field makes these particles suitable stimuli-sensitive systems as they can change their physical properties in response to an external stimulus and, in case of carrying drugs, these can be selectively delivered to the target site, minimizing any side effects [10].

The magnetic properties SPIONs make them suitable candidates for molecular imaging (MI), a diagnostic approach that combines molecular biology and in vivo imaging performed in real time with the possibility of sequential and longitudinal monitoring. MI has the advantage over other diagnostic tools that allows high soft tissue contrast, spatial resolution and penetration depth for what it is considered one of the most powerful noninvasive imaging techniques in diagnostic [11,12,13]. In particular, SPIONs have shown interesting results as negative contrast agents in magnetic

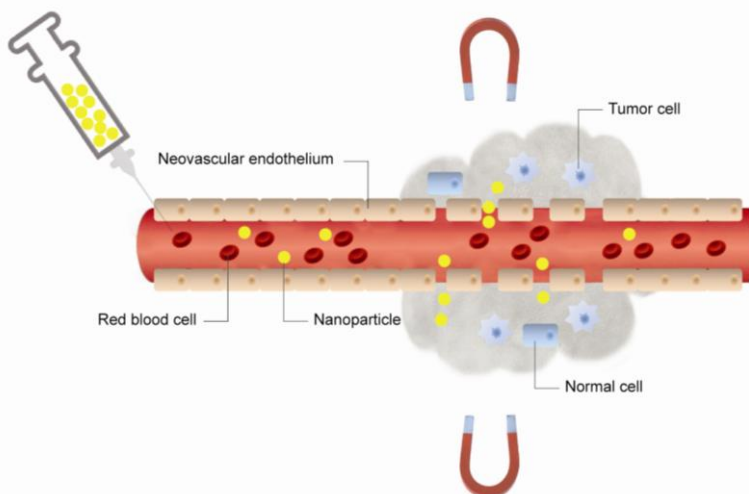


Figure 2. Procedure for magnetically-guided drug targeting of nanoparticles. The enhanced permeability and retention effect facilitates the extravasation of the nanoparticles from the pores in leaky tumor blood vessel walls [6].

resonance imaging (MRI) [14,15]. SPIONs improved the contrast-to-noise ratio in MRI by shortening the spin-spin T_2 relaxation times of the water protons within the tissues or regions of interest, enhancing in this way the image contrast.

The versatility and functionality of SPIONs can be enhanced by modifications of their surface consisting mainly on coating the surface with ligands or by their inclusion into other nanoparticles giving hybrid nanosystems such as liposomes or nanoemulsions [16,17]. The combination of liposomes and SPIONs results in multifunctional magnetoliposomes (MLs) or *all in one* system that can also incorporate a variety of molecules. The first reference on MLs is found in a 1989 publication by Kiwada [18]. These MLs had a size in the micrometer range, far too big for biological applications. From then, several procedures have been described resulting in nanometer-sized MLs [19,20]. Figure 3 shows a prototype of multifunctional or hybrid liposome (large unilamellar liposome, LUV), composed of phospholipids, with theranostic properties. Thus, encapsulated SPIONs in the inner core or embedded into the lipid bilayer provide a tool for magnetic targeting; the presence of a peptide such as the cyclic arginine-aspartic acid-glutamine motif, allows

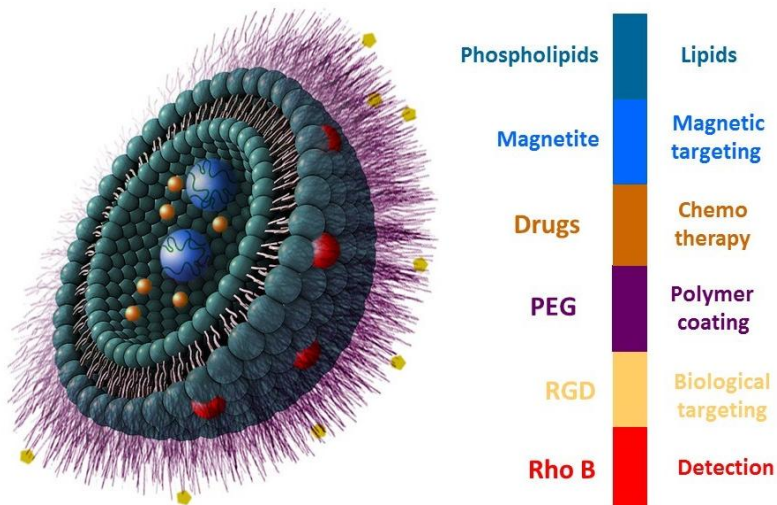


Figure 3. Prototype of a multifunctional large unilamellar magnetoliposome with the associated properties provided by each component. PEG: Polyethylene glycol; RGD: Arginine (R)-Glycine (G)-Aspartic acid (D); Rho-B: Lissamine Rhodamine B

for biological targeting; drugs located depending on their hydrophilic or hydrophobic character as SPIONs in the aqueous compartment or among the lipid acyl-chains, respectively, make the systems appropriate for chemotherapy. On another hand, the presence of polymers (e.g. polyethylene glycol, PEG) on the outer leaflet of the vesicles, protect them from the opsonization and rapid uptake from the bloodstream once administered. Finally, fluorescent probes can be incorporated to the lipid bilayer for detection purposes.

Similarly, the incorporation of SPIONs into oil-in-water nanoemulsions results in magnetic nanoemulsions (MNEs). MNEs can include the same components as mentioned for liposomes and are particularly interesting as drug delivery systems of hydrophobic drugs. Both, MNEs and MLs are biodegradable and show low toxicity [22].

1. Synthesis and characterization of iron oxide nanoparticles

SPIONs were synthesized according to the method described by Berger et al. [22]. Briefly, a mixture of $\text{Fe}(\text{OH})_2$ and $\text{Fe}(\text{OH})_3$ was obtained after the stoichiometric reaction of Fe^{2+} and Fe^{3+} in presence of strong alkali and under vigorous stirring. Subsequent fast aging of those hydroxides generates magnetite. The overall reaction is:



In order to provide colloidal stability to the particles and prevent their aggregation, they are usually coated with other nanoscale materials, resulting in the so named ferrofluids. Hydrophilic polymers such as dextran and its

Table 1. Physicochemical parameters of ALG or CHI coated NPs.

Coating	Size ¹ / nm	PDI ²	Magnetization/ emu g ⁻¹	ζ potential/ mV
ALG	50 ± 5	0.15± 0.02	56.8±0.2	-34±1
CHI	100 ± 7	0.18± 0.01	59.3±1.0	25±1

¹Hydrodynamic diameter measured by dynamic light scattering

²Polydispersity index. Its value varies from 0 for a monodisperse sample to 1 for a polydisperse population.

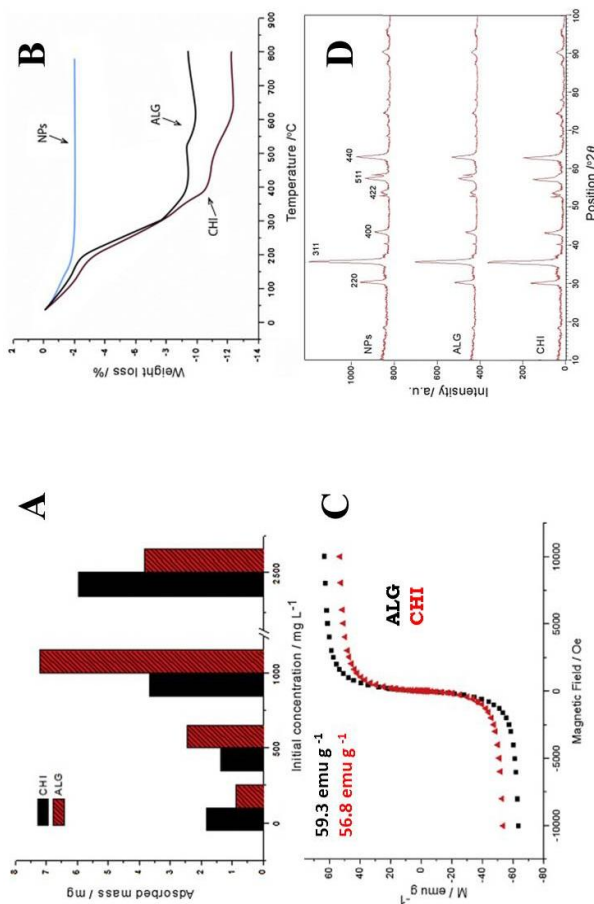


Figure 4. Physicochemical characteristics of SPIONs coated with CHI or ALG. A) Mass of polymer adsorbed at 300 K depending on the initial amount of polymer; B) thermogravimetric analysis of the coated (CHI, ALG) and uncoated NPs; C) magnetic behavior and, D) XRD patterns [23].

derivatives, polyethylene glycol (PEG), chitosan (CHI) and alginate (ALG) are among the most used for the stabilization of naked magnetic nanoparticles [23]. We have studied the influence of the initial amount of CHI, ALG and PEG of different molecular weights in the stabilization of the magnetite. The optimal concentration of polymer needed for coating the NPs was calculated through adsorption isotherms and the amount coated was measured by thermogravimetry.

The ferrofluids were also characterized by measuring their size and size distribution by dynamic light scattering (DLS) and charge (ζ potential) with a Zetasizer Nano ZS90 (Malvern Instruments, UK). High-resolution TEM (HR-TEM, 2010F Jeol Microscope, Japan) indicated that the particle diameter was around 11 nm, value that was confirmed by X ray diffraction (XRD). Some of the above results are illustrated in Table 1 and Figure 4.

The magnetic properties of the ferrofluids under the influence of a magnetic field were measured with a superconducting quantum interference device (SQUID) magnetometer (Quantum design MPMS XL, San Diego, California, USA) at room temperature. All samples showed superparamagnetism without magnetic hysteresis at room temperature.

2. Synthesis and characterization of hybrid nanoparticles

2.1. Magnetoliposomes

A lipid or lipid mixture of interest in chloroform/methanol (2:1, v/v) was introduced into a round bottom flask and the organic solvent was evaporated in a rotavapor under reduced pressure until the formation of a thin film. The dried mixture was then hydrated with an aqueous suspension of hydrophilic magnetic particles. In the case of hydrophobic SPIONs and hydrophobic drugs as indomethacin, they were added to the organic mixture and proceed as mentioned before. Up to now, the samples consist on a heterogeneous population of MLs. In order to obtain homogeneous samples, MLs were sonicated in an ultrasonic processor (Hielscher, Teltow, Germany) or submitted to extrusion cycles through a 200 nm polycarbonate filters (Extrude device, Avestin, Ottawa, Canada). Ligand-targeted MLs with the arginine-glycine-aspartic acid motif (RGD) were also designed to study their ability to interact with cancer cells [24]. MLs were characterized as mentioned for SPIONs and additionally, the amount of lipid, encapsulated drug and SPIONs were measured as described in [9]. The average size of MLs was around 200 nm with low polydispersity (< 0.2).

2.2. Magnetic nanoemulsions

The advantage of MNEs over MLs is their higher loading capacity of hydrophobic materials. Oil in water MNEs were prepared by mixing olive oil, cholesterol (CHOL) and the phospholipids 1,2-distearoyl-*sn*-glycero-3-phosphoethanolamine (DSPE-PEG) and 1,2-distearoyl-*sn*-glycero-3-phosphocholine (DSPC) dissolved in organic solvent. Hydrophobic SPIONs and indomethacin were also added to the organic phase. Then, the organic solvent was removed by rotary evaporation at 35 °C and the dried mixture was hydrated with water or buffered saline solution. The resulting crude emulsion was homogenized by spontaneous emulsification (low energy) or ultrasonication with an UP200 St ultrasonic processor (Hielscher, Teltow, Germany) (high energy) (Figure 5) [26,27]. NEs were characterized as described for MLs.

For internalization studies in cells, MLs and MNEs were labeled with the fluorescent probe 1,2-dimyristoyl-*sn*-glycero-3-phosphoethanolamine-N-(lissamine rhodamine B sulfonyl) (ammonium salt) (Rho-PE). In both hybrid nanosystems, SPIONs kept their original superparamagnetic properties.

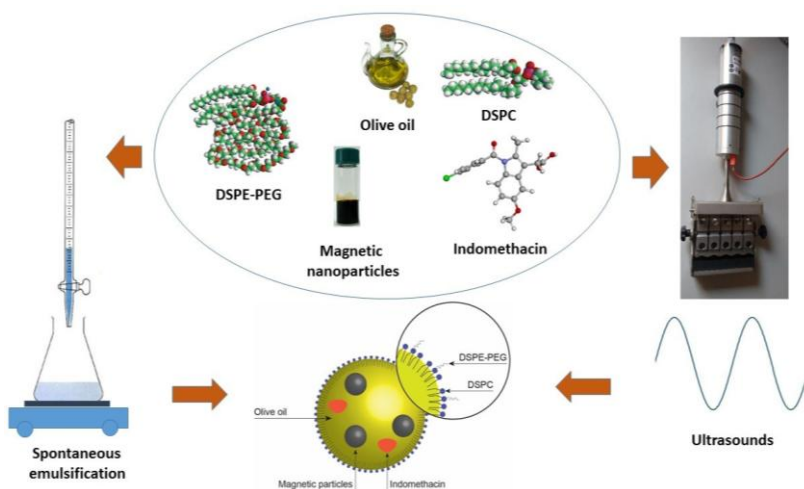


Figure 5. Schematic representation of the magnetic NEs loading indomethacin and SPIONs obtained by high energy method (ultrasounds) or low energy method (spontaneous emulsification). On top components of the NEs [27].

3. Magnetoliposomes accumulate in inflamed sites

The ability of MLs to reach inflamed areas was studied in a first assay by administering intravenously bare MLs to mice, namely MLs containing only phospholipids with encapsulated SPIONs [25]. Previously, sterile air pouches were produced by injecting air subcutaneously into the back of the mice. Then, animals were divided in four groups. In two of them, acute inflammation was induced by injecting 1.2 % carrageenan (phologen) to the pouch (inflammation groups). The injection in the other two groups (control groups) consisted on sterile saline. MLs were then injected i.v. to one of the two inflammation (I + MLs), and control groups (C + MLs). Mice were sacrificed 20 min after the injection.

The iron content in exudates (pouch), plasma and organs was analyzed by inductively coupled plasma atomic emission spectroscopy (ICP-AES, Perkin Elmer Optima 3200RL, Massachusetts, USA). Iron levels were higher in animals with inflammation than in control animals. After the administration of MLs to the control group, iron content increased similarly to the measured for animals with inflammation and MLs. There was no change in the concentration of iron in the liver after i.v. administration, whereas there was an increase in the spleen compared to the control group (Figure 6).

Iron biodistribution indicated that MLs accumulated mainly in the inflammation zone without the need of an external magnet to potentiate the migration of MLs to the target site. A possible explanation to this fact is the enhanced permeability and retention effect as a consequence of the leaky vasculature of the tumor or in inflamed areas that allows the intratumoral accumulation of particles smaller than 200 nm [28].

In a later study [9], a similar experiment was performed in which an external magnetic field induced a selective biodistribution of bare MLs to the inflamed area (Figure 7).

By this magnetically guided drug targeting approach, MLs accumulated at the site of inflammation (exudates) and simultaneously were removed from the blood. In addition, their content decreased in the liver and spleen. The increase in iron levels in exudates depended on the time of exposure of the external magnetic field (Table 2).

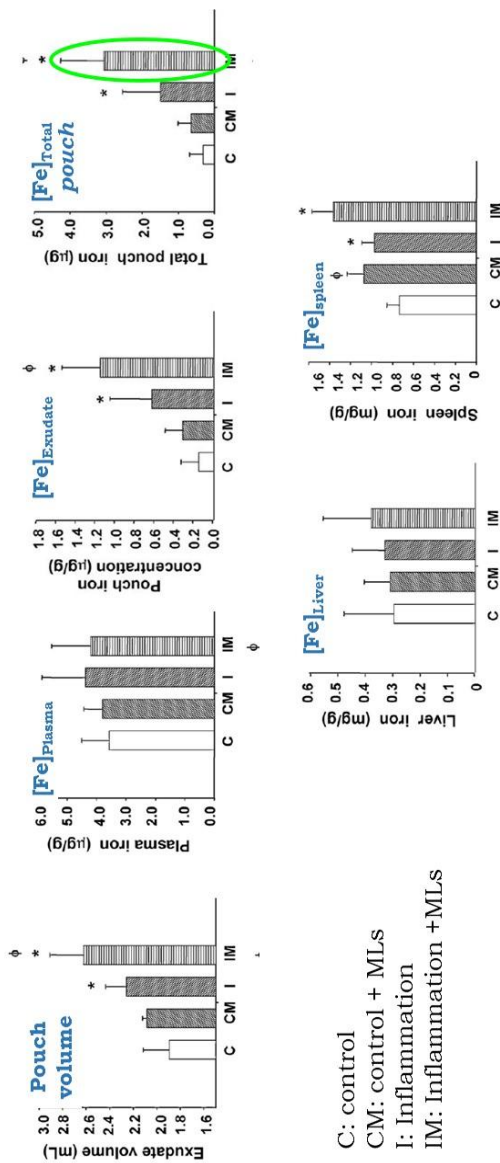


Figure 6. Pouch volume and iron concentration in plasma, pouch, liver and spleen 20 min after sterile saline (control and inflammation groups) or MLs (control and inflammation groups) i.v. injection. In these experiments inorganic iron can not be distinguished from endogenous iron. Total iron content in the pouch for the group IM (green circle) was significantly higher than in the other groups confirming the accumulation of SPIONs [25].

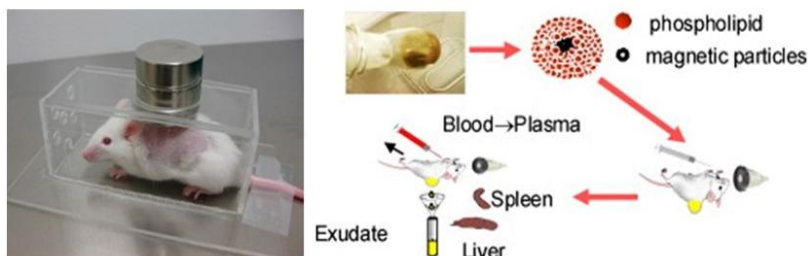


Figure 7. Experimental device to measure the effect of an external magnetic field on the biodistribution of MLs (left) after i.v. injection into mice (right). An inflammatory focus was introduced on their backs. Two $\text{Nd}_2\text{Fe}_{12}\text{B}$ disk magnets (25 x 10 mm, of 600 mT per side) were placed over the hole in the Plexiglas cages [9].

Table 2. Iron concentration ($\mu\text{g} \cdot \text{g}^{-1}$) in exudates, plasma, liver and spleen.

Groups	Exudates	Plasma	Liver	Spleen
C	0.04 ± 0.04	4.04 ± 1.02	621 ± 310	665 ± 180
I	0.26 ± 0.13	4.01 ± 1.27	712 ± 224	836 ± 278
IN	0.33 ± 0.11	4.12 ± 1.07	873 ± 99	$1,446 \pm 390$
INM	0.56 ± 0.12	2.89 ± 0.42	674 ± 64	$1,264 \pm 35$

C: control, mice with back air pouch receiving sterile saline; I: inflammation control group, animals with carrageenan-induced inflammation in the air pouch receiving saline; IN: as I but receiving MLs i.v.; and INM as IN but under the effect of a magnet located just above the inflammatory pouch for 20 min (Figure 7) [9].

TEM micrograph of the exudates showed the presence of intact MLs 20 min after the injection. This is a consequence of the size of the SPIONs (~ 12 nm) that is too large to passively cross the phospholipid bilayer. Iron release is only possible after the action of opsonins and cells of the mononuclear phagocyte system or other destabilizing agents.

4. Ligand-targeted Magnetoliposomes

It is described that nanoparticles can be directed to a target site by functionalization of the external core. Insertion of peptides is one of the most

successful strategies [29]. For instance, the cyclic RGD peptide, bounded to the outer leaflet of the liposomal bilayer through a lipid-PEG-maleimido group, can bind vascular endothelial cells at inflammation sites [30]. Dubey et al. [31] indicated that cyclic RGD peptide anchored sterically stabilized liposomes bearing 5-FU were significantly more active against primary tumor and metastasis than the non-targeted sterically stabilized liposomes and free drug. Therefore cyclic RGD peptide anchored sterically stabilized liposomes hold potential of targeted cancer chemotherapeutics. Based on this premise, we designed an experiment aimed to study the targeting of RGD-MLs to integrin $\alpha_v\beta_3$ expressed in many cancer cells as the HeLa cellular line. Bare MLs and PEG-sterically stabilized MLs were used as control (Figure 8).

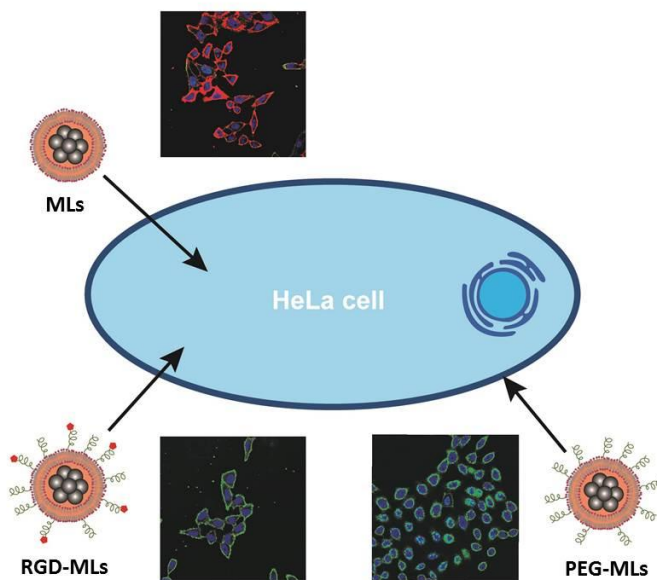


Figure 8. Magnetoliposomes, MLs, composed of phosphatidylcholine (PC)/cholesterol (CHOL) (8:2 mol/mol) synthesized for internalization studies in HeLa and 3T3 cells. PEG-MLs: pegilated MLs (long circulating) and RGD-MLs: functionalized MLs (biological targeting). The images correspond to confocal observations (Leika TCS-SP2, Heidelberg, Germany) after the incubation of MLs with HeLa cells for 4 h. MLs were labeled with rhodamine-PE (red), the nucleus with membrane-permeable dye Hoeschst 33342 (blue) and the cell membrane with cell membrane-impermeable Alexa Fluor 488-conjugated wheat germ agglutinin (green).

Previously to the cellular internalization studies, the cytotoxicity of naked SPIONs and MLs was analyzed in Hela and 3T3 (control) cellular lines by two typical assays, MTT that measures the metabolic activity in the mitochondria of viable cells and NR that gives information about the membrane integrity. MLs were viable at the concentrations studied [24].

Unexpectedly, confocal microscopy and flow cytometry showed that bare MLs were internalized in higher extent than the MLs displaying the targeting moiety [24]. Apparently, cellular uptake of ligand-targeted MLs was inhibited by the PEG chains of the surface. To overcome this drawback, MLs surface should display PEG chains of different length, short to prevent the adsorption of proteins on the surface of the proteins and a long chain to favor the interaction with the cellular receptor.

5. Magnetoliposomes as contrast agents for Magnetic Resonance Imaging

Agar phantoms with MLs or SPIONs were prepared to avoid particle aggregation during the application of the magnetic field. Then MRI measurements were performed on a 7.0 T BioSpec 70/30 horizontal animal scanner (Bruker BioSpin, Ettlingen, Germany). T_1 (positive contrast) and T_2 (negative contrast) relaxometry maps as well as the relaxation rates r_1 ($1/T_1$) and r_2 ($1/T_2$) were obtained as described in [14]. The relaxivity for a MRI contrast agent calculated from equation 1 is described as the increase of the relaxation rate of the water (solvent) induced by 1 mmol.L⁻¹ of the active ion.

$$r_{i,obs} = \left[\frac{1}{T_{i,obs}} - \frac{1}{T_{i,water}} \right] / C_{CA} \quad \text{Equation 1}$$

where i refers to 1 (r_1) or 2 (r_2), and C_{CA} , to the iron concentration of the contrast agent (SPIONs).

Table 3 shows the relaxivity values for the SPIONs alone and incorporated into liposomes of different composition. r_1 is poorly sensitive to SPIONs at 7 T due to the reduced susceptibility to dipolar contributions at high field, in addition to the presence of bulky surface groups hindering the surface accessibility of water to the magnetic cores. Contrarily, r_2 values are bigger because transversal relaxivities are highly sensitive to the presence of substances around the magnetic core.

Table 3. r_1 , r_2 and r_2/r_1 ratio of magnetic hydrophobic (O) and hydrophilic (H) nanoparticles alone or encapsulated in liposomes of different lipid composition.

MLs	$r_1/\text{mM}^{-1} \text{ s}^{-1}$	$r_2/\text{mM}^{-1} \text{ s}^{-1}$	r_2/r_1
O	0.96	74.5	78
H	0.80	50.7	63
O-DMPC	0.90	340	378
H-DMPC	9.10	1282	140
O-DMPC-CHOL	0.80	230	288
O-DMPC-PS	0.80	798	1000
O-DOPC	0.90	630	700
H-DOPC	3.40	678	199
O-DOPC-PS	0.90	995	1000

DMPC: 1,2-dimyristoyl-*sn*-glycero-3-phosphocholine; DOPC: 1,2-dioleoyl-*sn*-glycero-3-phosphocholine; CHOL: cholesterol; PS: phosphatidylserine.

MLs composed of saturated (DMPC) or unsaturated phospholipids (DOPC), with or without CHOL or PS (negatively charged phospholipid) showed higher transverse reaction rates r_2 compared to the values obtained for SPIONs alone as a consequence of the reduction of the diffusion coefficient of water near the nanoparticles. The coating of SPIONs with lipid bilayers provided a longer interaction between the water protons and the magnetic field at the surface of the magnetic core than in absence of coating.

6. Magnetic nanoemulsions are suitable vehicles for hydrophobic drugs

NEs were chosen for their high payload, fact that favors the loading of large amounts of drugs. Therefore, multifunctional MNEs were prepared encapsulating indomethacin and SPIONs. Cytotoxicity studies were performed as described for MLs in HeLa and 3T3 cellular lines. Then, the anti-inflammatory

activity of indomethacin loaded into MNEs, compared to the effect of free drug, was studied in a carrageenan-induced paw edema in rat model [26]. The height of the paw edema was measured at different times. Therefore, the study was performed with three groups of animals: A) carrageenan; B) carrageenan and indomethacin and, C) carrageenan and MNEs loaded with indomethacin. The peak of the edema was observed at 4 h for group A), and 6 h for the remaining two. The analysis of the area below the curve (Figure 9), with the Turkey-Kramer statistical test, indicated the lack of differences between groups A and B or B and C, while significant differences ($p < 0.05$) were noticed between groups A and C.

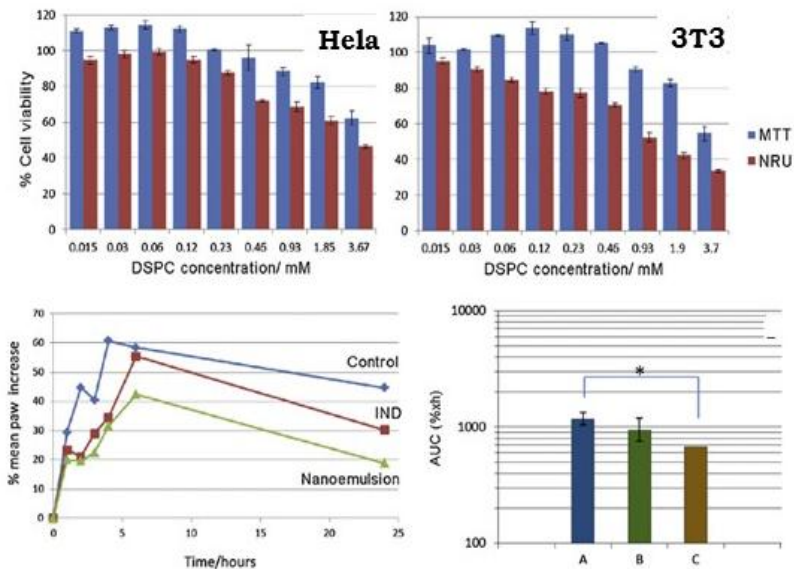


Figure 9. Top: viability of HeLa and 3T3 cells after the incubation with magnetic-NEs for 24 h. Bottom left: changes in paw edema induced by carrageenan in rats at different times, after administration of saline (control), free indomethacin (IND) (2mg kg^{-1}) or indomethacin loaded MNEs (Nanoemulsion). Bottom right: area under the curve of the paw increase obtained from the data of the previous figure [26].

Ulcers in the stomachs were observed only in the group that was administered with free drug, thus confirming protective role of the NEs in reducing the drug side effects.

7. Conclusion

Stable aqueous suspensions of superparamagnetic iron oxide nanoparticles stabilized with polyethylene glycol, chitosan or alginate (ferrofluids) were successfully prepared by a co-precipitation method under mild conditions. Their incorporation into liposomes gave also stable systems that showed ability to accumulate in inflamed areas, fact that increased upon the application of an external magnetic field. Magnetoliposomes presented enhanced negative transversal relaxivity (r_2) compared to SPIONs, fact that indicates their suitability as negative contrast agents for magnetic resonance imaging. On another hand, magnetic nanoemulsions showed to be good vehicles for indomethacin with reduced side effects in comparison with the administration of the free drug. In summary, MLs and MNEs are good candidates as nanosystems for magnetic resonance imaging, for delivering hydrophobic drugs and can behave as stimuli-responsive drug delivery systems.

Acknowledgements

The authors are grateful to Dr. M. Carmen Morán for the cellular studies and to Dr. Elvira Escribano and Dr. Josep Queralt for the *in vivo* experiments.

References

1. Attama, A. A.; Charles, L. 2014, Handbook of Functional Nanomaterials. Edited by Aliofkhaezrai, M., 2, 1-41.
2. Sapsford, K. E., Algar, W. R., Berti, L., Gemmill, K. B., Casey, B. J., Oh, E., Stewart, M. H.; Medintz, I. L. 2013, *Chem. Rev.*, 113, 1904.
3. Warner, S. 2004 *Scientist*, 18, 38
4. Hassanzadeh, P., Atyabi, F., Dinarvand, R., 2018, *J. Controlled Release*, 270, 260.
5. Bhise, K., Sau, S., Alsaab, H., Kashaw, S. K., Tekade, R. K., Iyer, A. K., 2017, *Ther. Deliv.*, 8, 1003.
6. Estelrich, J., Escribano, E., Queralt, J., Busquets, M. A. 2015, *Int. J.Mol. Sci.*, 16, 8070.
7. Subhankar B., Kleemann, W. 2008, *J. Phys. D: Appl. Phys.*, 42, 013001
8. Busquets, M. A., Espargaró, A., Sabaté, R. Estelrich, J. 2015, *Nanomaterials*, 5, 2231.
9. García-Jimeno, S., Escribano, E., Queralt, J., Estelrich, J. 2012, *Nanoscale Res. Lett.*, 7, 452
10. Kalber, T.L., Ordidge, K.L., Southern, P., Loebinger, M. R., Kyrtatos, P.G., Pankhurst, Q.A., Lythgoe, M.F., Janes, S.M., 2016, *Int J Nanomedicine*, 11: 1973.
11. Atukorale, P. U., Covarrubias, G., Bauer, L., Karathanasis, E. 2017, *Adv. Drug Deliv. Rev.*, 113, 141.

12. James, M. L., Gambhir, S.S., 2012, *Physiol. Rev.*, 92, 897.
13. Huang, Y., He, S., Cao, W., Cai, K., Liang, X. J. 2012, *Nanoscale*, 4, 6135.
14. Martínez-González, R., Busquets, M.A., Estelrich, J. 2016, *Int. J. Mol. Sci.*, 17, 1209.
15. Laurent, S., Vander, E. L., Muller, R. N. 2013 Edited by Merbach, Andre; Helm, Lothar; Toth, Eva, *Chemistry of Contrast Agents in Medical Magnetic Resonance Imaging (2nd Edition)* 427-447.
16. Prasad, A. I., Parchur, A. K., Juluri, R. R., Jadhav, N., Pandey, B. N., Ningthoujam, R. S., Vatsa, R. K. 2013 *Dalton Trans.* 42, 4885.
17. Kirui, D. K., Khalidov, I., Wang, Y., Batt, C. A. 2013 *Nanomedicine* 9, 702.
18. Kiwada, H., Sato, J., Yamada, S., Kato, Y. 1986, *Chem. Pharm. Bull.*, 34, 4253
19. De Cuyper, M., Noppe, W. 1996 *J. Colloid Interf. Sci.*, 182, 478
20. Sabate, R., Barnadas-Rodriguez, R., Callejas-Fernandez, J., Hidalgo-Alvarez, R. Estelrich, J. 2008, *Int. J. Pharm.*, 347, 156
21. Lahiri, B. B., Ranoo, S., Zaibudeen, A. W., Philip, J. 2017, *J. Magnetism Magnetic Mat.* 441, 310.
22. Berger, P., Adelman, N. B., Beckman, K. J., Campbell, D. J., Ellis, A. B., Lisensky, G.C. 1999, *J. Chem. Ed.*, 76, 943.
23. Castelló, J., Gallardo, M., Busquets, M. A., Estelrich, J. 2015, *Colloids Surf., A: Physicochem. Eng. Aspects* 468, 151.
24. Estelrich, J., Busquets, M.A., Morán, M.C. 2017, *ACS Omega* 2, 6544.
25. García-Jimeno, S., Escribano, E., Queralt, J., Estelrich, J. 2011, *Int. J. Pharm.* 405, 181.
26. Kwasigroch, B., Escribano, E., Morán, M.C., Queralt, J., Busquets, M. A., Estelrich, J. 2016, *Int. J. Pharm.*, 515, 749.
27. Rodríguez-Burneo, N., Busquets, M. A., Estelrich, J. 2017, *Nanomaterials*, 7, 190.
28. Albanese, A., Tang, P.S., Chan, W.C.W. 2012, *Annu. Rev. Biomed. Eng.*, 14, 1
29. Wacker, B. K., Alford, S. K., Scott, E. A., Thakur, M-D., Longmore, G. D., Elbert, D.L. 2008, *Biophys J.* 94, 273.
30. Koning, G.A., Schiffelers, R.M., Wauben M.H, Kok, R.J., Mastrobattista, E., Molema, G., ten Hagen T.L., Storm G. 2006, *Arthritis Rheum.* 54, 1198.
31. Dubey, P.K., Mishra, V., Jain, S., Mahor, S., Vyas, S.P. 2004, *J Drug Target.* 12: 257.



Research Signpost
Trivandrum
Kerala, India

Recent Advances in Pharmaceutical Sciences VIII, 2018: 19-41 ISBN: 978-81-308-0579-5
Editors: Diego Muñoz-Torrero, Yolanda Cajal and Joan Maria Llobet

2. An overview on the modulation of the intestinal barrier and immune response by membrane vesicles secreted by the probiotic *Escherichia coli* Nissle 1917

Josefa Badia, Maria-José Fábrega, María-Alexandra Cañas
Laura Aguilera, Carina-Shianya Alvarez, Rosa Giménez and
Laura Baldomà

Secció de Bioquímica i Biologia Molecular, Departament de Bioquímica i Fisiologia
Facultat de Farmàcia i Ciències de l'Alimentació, Universitat de Barcelona
Institut de Biomedicina de la Universitat de Barcelona
Institut de Recerca Sant Joan de Deu (SJD) Barcelona, Spain

Abstract. Probiotic *Escherichia coli* Nissle 1917 (EcN) is a good colonizer of the human gut and its efficacy in the inflammatory process undergone in ulcerative colitis has been demonstrated. The probiotic action is mainly through the modulation of intestinal epithelial tight junctions and immune system. Here we review the role of outer membrane vesicles (OMVs) released by this probiotic strain on the modulation of intestinal homeostasis. EcN OMVs enter into host epithelial cells via clathrin-mediated endocytosis and are sorted to lysosomes via endocytic compartments. In cellular models of intestinal barrier, EcN OMVs stimulate the underlying immune system through the intestinal epithelium, triggering immune and defense responses. Thus, the use of probiotic derived OMVs could be a safe probiotic-derived strategy targeting intestinal inflammatory processes.

Correspondence/Reprint request: Dr. Josefa Badia, Departament de Bioquímica i Fisiologia, Universitat de Barcelona, E-08028 Barcelona, Spain. E-mail: josefabadia@ub.edu

Introduction

In the mammalian gut, bacteria are not in direct contact with the epithelium due to the mucin layer that covers the intestinal mucosa. In fact, a compact inner mucin layer, which is impenetrable to bacteria, physically separates microbiota and host epithelial cells. Thus, the crosstalk between microbiota and the host mainly relies on secreted factors that can go through the mucus layer, reach the epithelium and activate cell signalling pathways that modulate host immune and defence responses such as secretion of cytokines or antimicrobial peptides, mucus production or regulation of intercellular intestinal junctions [1,2]. Bacterial secreted factors can be released into the extracellular milieu as free-soluble compounds or included in membrane vesicles.

All bacteria, either commensal or pathogenic strains, have evolved different systems to contact and communicate with host cells. One strategy is the formation of membrane vesicles that can deliver the cargo to distant targets in the host. In fact, membrane vesicles are considered intercellular comunicasomes.

Here we give a view of the intestinal microbiota and especially in the vesicles released by Gram-negative bacteria, which are known as outer membrane vesicles (OMVs). We review the modulation of the intestinal barrier and the immune response provided by membrane vesicles secreted by the gram-negative probiotic *Escherichia coli* Nissle 1917.

1. Gut microbiota

The mammalian intestine is one of the most densely colonized ecosystems. The whole of the microorganisms that inhabit the intestine constitute the so-called intestinal microbiota, which is formed by between 500 and 1000 microbial species, mostly anaerobic and anaerobic facultative bacteria. Human gut microbiota constitutes a biomass of 1.5 kg shaped by 10^{14} microorganisms [3], thus outnumbering the total host cells by an estimated 10-fold. The microbiota has an enormous metabolic capacity and carries a repertory of genes that exceeds by more than 100 times the genetic information of the host. The concentration and the variety of microorganisms increase throughout the gastrointestinal tract, being the colon the most densely colonized section [4].

Gut microbiota plays important roles that are crucial for the function of the intestine and host survival. Therefore, it has been considered as an organ that acts synergistically with the host [5]. In this context, microbiota plays metabolic functions mainly associated with energy recovery, synthesis

of vitamins and fermentation of non-digestible compounds, which metabolism produces short chain fatty acids that have a positive influence on the differentiation and proliferation of the intestinal epithelium. Gut microbiota also provide important protective functions related with displacement of pathogens, either by competing for nutrients and specific receptors, or through expression of anti-microbial factors. Finally, gut microbiota has relevant structural functions that control the integrity of the intestinal barrier and it is essential for the development and normal function of the host immune system [6].

2. Gut microbiota-host communication

The communication between the microbiota and the host occurs at the intestinal mucosa, which is complex and structured in three components: the mucus layer, the epithelial cell barrier and the intestinal immune system.

The mucus layer that covers the gastrointestinal tract is organized in two layers at the colon level. The inner layer (50-200 μm thick) is firmly attached to the epithelium and consists of a compact structure formed by stacked mucin polymers in which bacteria cannot penetrate. The outer mucus layer is looser and is the habitat for commensal bacteria.

Epithelial cells that form a monolayer that separates the external environment from the host internal medium constitute the second layer of defence. This epithelium is mainly formed by enterocyte-type cells, which are the absorptive cells, and by other specialized cell types such as goblet cells, responsible for mucus secretion. M cells detect bacteria that have surpassed the internal mucus layer, phagocyte and translocate them to the lamina propria where a local immune response is triggered in order to eliminate the microorganism or induce tolerance. Paneth cells are specialized epithelial cells that secrete peptides with antimicrobial activity. This layer of epithelial cells constitutes a dynamic physical barrier. Adjacent cells in the monolayer are interconnected by different types of intercellular junctions; of special interest are the tight junctions (TJ), which regulate the permeability of the intestine helping to maintain a strict and regulated separation between the organism and the intestinal lumen. In addition, the intestinal epithelial cells must signal to the underlying immune system in response to luminal bacteria.

The third component of the intestinal mucosa is the immune system formed by the lymphoid tissue associated to the intestine. Specifically, the immune cells of the lamina propria coordinate the development of innate and adaptive responses that allow a state of tolerance to food antigens and

commensal microbiota and trigger specific mechanisms to eradicate pathogens [7].

The interaction between the microbiota, the intestinal epithelium and the host immune system is essential for host homeostasis. Changes in microbiota population can have harmful impact on human health. Many factors (infections, genetics, environment, diet, reduced physical activity) may lead to imbalances or shifts in microbiota composition, a concept known as dysbiosis. This condition has been linked to gastrointestinal disorders caused by bacterial or viral infections, and also to metabolic (obesity, insulin resistance, hepatic steatosis) and immunological diseases (allergies, autoimmune diseases or inflammatory diseases) [8,9].

3. Probiotics in gut homeostasis

The administration of probiotics is one of the approaches in the treatment of intestinal disorders, especially those associated with microbiota imbalance and homeostasis alteration. These approaches are aimed to restore the initial equilibrium and to regain the integrity of the intestinal barrier and the health status of the individual.

Probiotics are defined as “live microorganisms that, when administered in adequate amounts, confer a health benefit on the host” (WHO and FAO 2006). To be considered a probiotic, the strain should not have human pathogenic effects, be able to survive during the intestinal transit, be a good colonizer of the gut mucosa, diminish pathogen adherence to cell surface and invasion, and display antimicrobial properties against pathogens. Besides all these characteristics, the probiotic must be accompanied by beneficial effects on the host at different levels such as on the intestinal barrier function, intestinal immune system and on the microbiota itself [8]. Concerning intestinal barrier function, the action can be directed to several targets. One mechanism is the strengthening of the epithelial barrier through the regulation of the expression of TJ proteins or their redistribution inside the cell. Other mechanisms are related with the expression of molecules that interfere with pathogens such as adhesins that allow adhesion of the probiotic to intestinal mucosa diminishing pathogen adhesion by competitive exclusion, or secreting anti-microbial peptides that inhibit pathogen growth or survival. A probiotic may also modulate the host immune system.

However, it is important to note that not all these properties are found in all probiotics. Thus, each probiotic has individual mechanisms of action, which differ from those of other strains and confer its specific characteristics. This explains why a probiotic strain is useful to treat a specific pathology but not others. However, it has been proposed that some

mechanisms could be highly widespread among the probiotic genera while others are strain-specific.

Most of the widely used probiotics are Gram-positive bacteria from the genus *Lactibacillus* or *Bifidobacterium*. Besides, the Gram-negative strain *Escherichia coli* Nissle 1917 (EcN) is a well-studied probiotic used in the treatment of intestinal diseases.

3.1. *Escherichia coli* Nissle 1917 (EcN)

This Gram-negative bacterium belongs to the Enterobacteriaceae family and is included in the *E. coli* B2 phylogenetic subgroup. This strain was isolated by Alfred Nissle in 1917 from the stool of a soldier who survived a shigellosis outbreak during the First World War. It is currently commercialized as a probiotic for the treatment of dysbiosis and intestinal inflammatory bowel diseases in Germany with the trade name of Mutaflor® and in Italy as EcN®. The use of this probiotic has been particularly recommended for the prevention of diarrheal diseases caused by pathogens such as *Shigella*, *Salmonella* or *E. coli*, and for the treatment of ulcerative colitis. In fact, various clinical trials have proved its therapeutic benefits in inducing and maintaining remission of this inflammatory disease [10].

A number of studies have been carried out to characterize the properties of EcN, both at the phenotypic and genetic levels. This probiotic is a good colonizer of the human gut and positively affects gastrointestinal homeostasis and microbiota balance, as it promotes anti-inflammatory modulation of the immune response and reinforces the function of epithelial barrier through the positive regulation and redistribution of the TJ proteins. EcN has GRAS status (generally recognized as safe). Several factors contribute to its safety, such as the expression of a semi-rough lipopolysaccharide (LPS) with shortened O6 side chains that confers this probiotic sensitivity to serum. This probiotic does not produce known toxins, but several adhesins and fimbriae that allow this probiotic to effectively compete with pathogens for the binding sites in the host intestine. The EcN genome has been sequenced (genome size 5,441,200 bp) and is estimated to contain 5,324 coding sequences, being about 108 genes strain-specific [11,12]. Comparative genomic analyses indicate that EcN arises from of an uropathogenic ancestor like *E. coli* strain CFT073 and that through evolutionary processes has lost virulence factors and gained genes that confer to this strain the probiotic properties [13]. In this context, EcN expresses a wide repertoire of fitness factors that promote its competitiveness, a fact that can probably explain its success as a probiotic.

Within the fitness factors there are microcins, iron uptake systems, adhesins and proteases that help intestinal colonization [14,15]. EcN encodes six different iron transport systems that are advantageous for competing with other intestinal bacteria for the acquisition of iron within the gastrointestinal tract, in which this metal is limiting. In addition, this probiotic strain expresses several adhesins such as FimA, F1C and curli that help biofilm formation and contribute to EcN adhesion to intestinal mucosa and, therefore, the colonization and persistence in the intestinal tract [16].

Regarding the immunomodulatory effects, EcN modulates the host immune system by promoting a decrease in proinflammatory cytokines IL-2, TNF- α , IFN γ and an increase in anti-inflammatory cytokines like IL-10. This probiotic can reduce intestinal inflammation by downregulating expansion of newly recruited T cells into the intestinal mucosa. In this situation, resident activated intestinal T cells allow elimination of deleterious antigens, and hence contribute to maintaining immunological homeostasis [17]. On the other hand, the structural protein of the EcN flagellum, flagellin H1, is recognized by the immune receptor Toll-like receptor-5 (TLR5) on the epithelial host cell membrane. This interaction activates the downstream signaling pathway that triggers secretion of interleukin (IL) -8 (IL-8), a relevant cytokine that acts as a chemoattractant of neutrophils, ensuring the phagocytosis of pathogens *in situ*. Flagellin H1 also activates the host defense response to counteract adhesion and invasion of pathogens by increasing the synthesis of the inducible antimicrobial peptide β -defensin-2 (hBD-2) [18]. This antimicrobial peptide has a large spectrum of action being active against Gram-negative and Gram-positive bacteria, yeasts and virus. Additionally, EcN expresses on its cell surface a capsular polysaccharide, named K5 antigen, typical of pathogenic *E. coli* strains of the urinary tract and other strains causing extraintestinal infections. This capsule mediates the interaction of EcN with enterocytes and induces the expression of various chemokines such as the monocyte chemoattractant protein-1 (MCP-1), CCL5 (or RANTES) that recruits T cells, eosinophils and basophils, the macrophage inflammatory proteins 2-alpha and 2-beta (MIP- 2 α and MIP-2 β) and interferon- γ (IFN- γ). The loss of this capsular polysaccharide drastically reduces the level of chemokine induction after interaction with the host [19].

Within the modulatory effects, this probiotic is able to improve the intestinal epithelial barrier by strengthening TJs between adjacent epithelial cells. *In vivo* and *in vitro* studies have revealed that EcN promotes increased expression of the zonula occludens (ZO)-1 and ZO-2 proteins [20,21], although the microbial factors mediating these effects are not still known. More recently, it has been described that EcN mediates positive regulation of

the TJ protein claudin-14, and this effect has been attributed to the secreted TcpC protein [22].

The probiotic effect of EcN has been attributed to the combination of several properties that include particular fitness factors, interference factors and immunomodulatory properties [23]. However, despite the successful therapeutic applications of EcN the bacterial effectors and molecular mechanisms responsible for its beneficial effects are not always well-known.

4. Bacterial vesicles in host-microbiota cross-talk

OMVs are spherical membranous structures with an average diameter between 20 to 300 nm in size, which bud and detach from the cell during active growth. They contain a big range of bacterial molecules and compounds such as LPS, outer membrane proteins, periplasmic and cytosolic proteins, virulence factors, DNA, RNA and lipids. Thus, unlike other secretion systems, OMVs allow transfer of a diverse range of biochemically active molecules to proximal cells in a protected form. In the mammalian gut, OMVs are able to diffuse through the mucin layer, reach the intestinal epithelium and modulate its function and also control the innate and adaptive immune responses [24,25,26,27].

OMVs are released during all stages of bacterial growth in numerous media and conditions including natural environments such host fluids and tissues. They are originated from the outer membrane bacterial envelope, whose architecture is basic to understand vesicle biogenesis. The envelope of Gram-negative bacteria is formed by two membranes, the outer membrane and the cytoplasmic membrane, separated by the periplasmic space. These structures contain proteins that have key roles, such as nutrient acquisition, bacterial adhesion, secretion, signalling and protection against the external environment [28]. The mechanisms that lead to OMVs biogenesis are still poorly understood, although it is known that multiple processes seem to be involved, being destabilization of the membrane integrity a crucial factor [29]. All models proposed for OMVs biogenesis depend on an initial decoupling of the outer membrane from the peptidoglycan (PG) layer by disruption of the crosslinks between PG and the lipoproteins Pal and Lpp. This promotes the curvature of the outer membrane, leading to vesicle formation. Vesiculation can be also altered by factors such as temperature, nutrient availability, oxidation, quorum sensing and antibiotics [28]. During biogenesis, OMVs acquire a vast number of compounds, which are important for bacterial survival and for the interaction with the host [27]. However, the pathways by which OMVs include their cargo remain unknown [28,30].

Many studies carried out with Gram-negative pathogens showed that OMVs are internalized into host cells and contribute to virulence by delivering cytotoxic factors and mediators that interfere with the immune system [24,31,32]. Nowadays, microbiota-derived vesicles are seen as key players in signaling processes in the intestinal mucosa [33,34]. However, studies in this field are still limited, being the first reports focused on *Bacteroides fragilis* [35,36], a main Gram-negative group in the gastrointestinal tract of mammals. OMVs from this commensal promote immunomodulatory effects and ameliorate colitis in mouse models. The beneficial effects are in part mediated by the capsular polysaccharide A (PSA) through TLR-2, although in dendritic cells OMVs from this microbiota strain trigger changes in gene expression that are PSA-independent. Other studies reported the ability of *Akkermansia muciniphila* OMVs to protect the progression of induced colitis in mice [37]. Regarding Gram-positive bacteria, studies performed with *Bifidobacterium bifidum* LMG13195 showed that membrane vesicles from this probiotic activate the maturation of dendritic cells, triggering a regulatory T cells response [38].

5. OMVs released by the probiotic EcN modulate intestinal immune and defense responses

In the field of microbiota-derived vesicles, studies have been focused on OVMs released by the probiotic strain EcN and by commensal *E. coli* strains. Bacterial OMVs are isolated from culture supernatants and examined by transmission electron microscopy after negative staining (Fig. 1A).

5.1. Proteome of EcN OMVs

We approached proteomic analysis to identify the protein content of EcN OMVs [39]. This study was the first report of the vesicular proteome of a probiotic strain. By means of 1D SDS-PAGE and highly sensitive LC-MS/MS analysis, 192 EcN vesicular proteins were identified with high confidence in three independent experiments. In general, the identified proteins provide functions related with bacterial survival and interaction with the host, similarly to other bacterial vesicles [40]. Interestingly, of the 192 proteins, 18 were encoded by strain-linked genes and around 21% had not been previously described in bacterial vesicles. The EcN specific proteins are involved in the adhesion to the host tissues (fimbriae), immune modulation or bacterial survival in host niches (proteases, iron uptake

systems). Thus, these proteins may facilitate the colonization of the human gut. For instance, the presence of components of multiple iron uptake systems in EcN OMVs may allow the probiotic strain to outgrow commensal bacteria and compete with pathogenic strains that use similar siderophores for iron uptake. Concerning the identified proteases Pic and Sat, these proteins are typically associated to pathogens. Although the specific role in the probiotic strain has not been elucidated, it seems that they may act as fitness factors rather than virulence factors [41]. In this sense, Pic has been shown to promote intestinal colonization, hypersecretion of mucus and modulation of the host immune response [42].

In addition to the strain-related proteins, other identified proteins may contribute to the beneficial effects of this probiotic. These are proteins also found in OMVs isolated from Gram-negative pathogens (57 common proteins out of 192 total identified proteins). These common proteins may allow bacterial establishment and persistence in host tissues, which is an essential issue for the activity of both probiotic and pathogens. This common protein group contains fitness factors that allow bacterial survival in the host, including periplasmic proteins that help nutrient sensing (transport systems for amino acids, carbohydrates or inorganic ions), antimicrobial enzymes to kill competing bacteria (murein hydrolases), surface proteins that promote adhesion to host tissues, and factors able to modulate the host immune response (FlgE and FlgK). Interestingly, this common group is mainly formed by cytoplasmic proteins, most of them metabolic enzymes. They are moonlighting proteins that, depending on the cell location, can play different roles. Thus, in addition to the metabolic role, the secreted proteins play a function that contributes to gut colonization or modulation of the host immune response. A well-studied moonlighting protein is glyceraldehyde-3-phosphate dehydrogenase [43,44,45,46].

Regarding the proteins identified for the first time in bacterial vesicles, the *in silico* functional analysis revealed that they may also contribute to OMVs functions that are essential in the context of this probiotic strain. An example is the porin NanC, whose expression is induced by *N*-acetylneuraminic acid, one of the most abundant sialic acids on the eukaryote cell membrane. The ability to use sialic acids as carbon and nitrogen sources may help EcN to colonize and persist in the intestinal tract.

This proteomic study [39] revealed that EcN OMVs are equipped with a wide variety of proteins related with adhesion, immune modulation and bacterial survival in host niches. Therefore, these proteins may contribute to vesicle targeting to particular host tissues and mediate the probiotic beneficial effects on intestinal function.

5.2. Internalization of EcN OMVs by intestinal epithelial cells

Uptake of OMVs by epithelial host cells is mainly mediated by endocytosis. The endocytic pathway depends on the composition and cargo of the vesicles. The two main pathways involved in OMVs internalization are clathrin-mediated endocytosis and lipid raft-dependent endocytosis. These pathways create endosomal compartments with different surfaces that allow the delivery of vesicle components to various subcellular destinations.

Many studies dealing with internalization of bacterial OMVs have been carried out with vesicles from Gram-negative pathogens. However, regarding microbiota or probiotic-derived OMVs, contribution to this field is restricted to studies performed with the probiotic EcN [47]. In this study EcN OMVs were labelled with rhodamine isothiocyanate B-R18. Fluorescence of this fluorochrome is quenched when inserted in bilayer membranes at high concentration, but when vesicles are fused with the host cell, the fluorescence is emitted and can be monitored using a microplate fluorescence reader. In this case, the intensity of fluorescence emitted is proportional to the amount of internalized vesicles. Following this experimental approach, kinetics studies performed in several intestinal epithelial cells (Caco-2, HT-29, HT-29-MTX) incubated with rhodamine B-R18-labeled OMVs showed a time-dependent increase in fluorescence, consistent with internalization of EcN OMVs. The presence of intracellular vesicles was confirmed by confocal fluorescence microscopy (Fig. 1B).

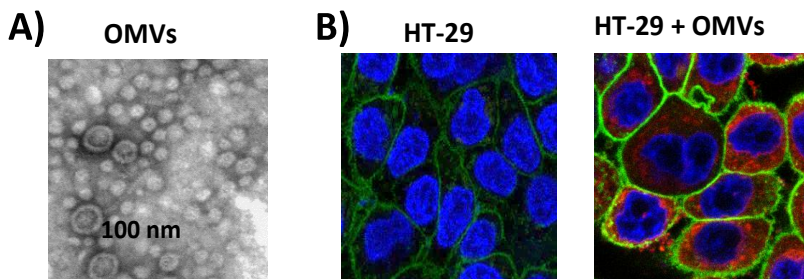


Figure 1. A) Image of EcN OMVs visualized by electron microscope after negative staining. B) Visualization of internalized EcN OMVs in HT-29 epithelial cells by fluorescence microscopy. Cell membrane was stained in green and nuclei in blue. Internalized rhodamine B-R-18 labeled OMVs were visualized in red. (Images have been provided by Alexandra Cañas).

Experiments performed in the presence of specific endocytosis inhibitors allowed the identification of the pathway responsible for the uptake of EcN OMVs. The inhibitors tested were the cholesterol-sequestering drugs nystatin and filipin III that disrupt lipid rafts, and chlorpromazine that inhibit clathrin-mediated endocytosis. OMVs entry was inhibited by chlorpromazine but not by nystatin or filipin III. Therefore, EcN OMVs are internalized by intestinal epithelial cells via clathrin-mediated endocytosis. It is well known that vesicles internalized through this pathway are sorted to lysosomal compartments. Accordingly, co-localization of EcN OMVs with clathrin and specific markers of endosomes and lysosomes was confirmed by confocal fluorescence microscopy [47]. No detection of OMVs in nuclei or mitochondria was observed, thus EcN vesicles are likely degraded inside lysosomes. In the acidic endo-lysosomal compartments some specific proteins or factors are dissociated from the vesicles and targeted to other subcellular locations to trigger specific actions and cell responses [48]. Although for EcN OMVs, the specific function and intracellular trafficking of vesicle-derived factors to other organelles have not been studied so far, flow cytometry analysis of phosphorylated γ H2AX in the nucleus of cells incubated with EcN OMVs showed that components released from internalized vesicles promote double strand breaks in the cell DNA. This effect on DNA was also confirmed by the formation of DNA tails in the Comet assay. The vesicle-associated factor responsible for this genotoxic activity has not been identified. Interestingly, the probiotic EcN produces colibactin, a non-ribosomal peptide-polyketide that induces double strand breaks in DNA. This peptide is synthesized by enzyme activities encoded in the *pks* island. Studies performed with an EcN mutant deficient in colibactin synthesis showed that, besides its genotoxic activity, colibactin is required for the *in vivo* anti-inflammatory effects of this probiotic [49]. Although the mechanism by which colibactin is delivered into the host cell remains unknown, the effects triggered by EcN OMVs on DNA suggest that colibactin could be delivered to mammalian cells by OMVs.

Despite EcN OMVs promote double strand breaks on the cell DNA, these vesicles do not reduce cell viability nor cause oxidative damage [47].

5.3. EcN OMVs reinforce the intestinal epithelial barrier

The intestinal epithelial layer forms a physical and biochemical barrier that maintains the segregation between host and intestinal microbiota. The function and integrity of this epithelial barrier depend on several factors, including the production of a mucin layer that covers the epithelial surface

and avoids the intimate contact with intestinal microbes, the secretion of antimicrobial peptides, and the formation of TJs that seal the paracellular space between adjacent epithelial cells. In addition, intestinal epithelial cells are essential to integrate microbial signals and coordinate the immune cell responses.

Recent studies have shown the ability of OMVs released by the probiotic EcN to reinforce the intestinal epithelial barrier by modulating the expression of genes encoding proteins relevant for the barrier function, particularly those involved in antimicrobial defense mechanisms [50] and the establishment of TJs [51].

Experiments performed with human colonic explants showed that EcN vesicles promote upregulation of the antimicrobial peptide hBD-2. Epithelial hBD-2 plays an important role in intestinal barrier function. Its expression is known to be induced by some probiotics, including EcN, as a mechanism involved in their beneficial action [52]. The induction of hBD-2 elicited by EcN OMVs might be attributed to flagella-associated proteins present in these vesicles [50]. In contrast, EcN OMVs do not significantly modify expression of β -defensin-1 (hBD-1), an antimicrobial peptide that acts as a component of host innate defenses at the intestinal surface. The lack of vesicle-mediated effects on hBD-1 is consistent with the non-regulated, high constitutive expression of this antimicrobial peptide in colon epithelial cells.

Regarding the modulation of mucus production, the probiotic EcN has been shown to upregulate the expression of several mucins in intestinal epithelial cell lines [53]. In the gut mucin-2 (MUC-2), which is secreted by goblet cells, is of special relevance since it is the main component of the intestinal mucus layer. However, up-regulation of MUC-2 by EcN seems not to be mediated by released OMVs [50].

Another mechanism by which microbiota, and especially probiotic strains, help to strengthen the integrity of the intestinal barrier is through the regulation of TJ proteins. TJs are multiprotein complexes that regulate the paracellular trafficking of macromolecules. They seal the adjacent epithelial cells in a selective permeable form and determine the apical and basolateral parts of the membrane and thus, cell polarity. TJs are formed by four types of transmembrane proteins: occludin, claudins, junctional adhesion molecules, and tricellulin. TJs also contain proteins ZO-1, ZO-2 and ZO-3, which bind to claudins and act as scaffolds anchoring the TJ transmembrane proteins to the actin cytoskeleton. Association of the ZO-proteins to TJ multiprotein complexes is regulated by phosphorylation

mechanisms. Specific kinases control the subcellular distribution of the TJ proteins and by end the strength of the epithelial barrier. Claudins constitute a large family of TJ proteins that regulate cell permeability and cohesion. In humans, this family includes 27 members. Some claudins have a sealing function, while others act as selective channels for small charged molecules. The pore- forming protein claudin-2 belongs to this last group and greatly contributes to the transepithelial water secretion. In fact, stimuli that raise claudin-2 levels result in increased barrier permeability.

Several *in vitro* and *in vivo* studies performed with live EcN bacteria showed that this probiotic positively modulates the intestinal epithelial barrier through the positive regulation and redistribution of TJ proteins ZO-1, ZO-2 and claudin-14 [20,21,22]. Upregulation of claudin-14 was attributed to the secreted protein TcpC [22]. These studies, however, did not reveal whether extracellular vesicles could mediate these effects. In addition, the TcpC secretion mechanism was unknown. With this information different experimental approaches were set up to assess the ability of EcN OMVs to strengthen the epithelial barrier in different epithelial cell lines [50]. To distinguish between TcpC and vesicle effects, a TcpC deficient mutant was derived from EcN, and OMVs were isolated from both the wild-type and the mutant EcN strains. The effect of OMVs on the epithelial barrier was confirmed by measuring the increase in transepithelial electrical resistance (TER) of T-84 cell monolayers at 24 h post-incubation. The vesicle-reinforcement effect was independent of TcpC expression. The positive TcpC activity on the TER was associated with the soluble secreted fraction. These results prove that TcpC is not secreted by OMVs.

The regulatory role of EcN OMVs on the expression of TJ proteins was analyzed measuring the mRNA (RT-qPCR) and protein levels (Western blot and confocal fluorescence microscopy) of ZO-1, ZO-2 and claudin-14 (known to be regulated by the probiotic EcN), and also the leaky protein claudin-2. EcN OMVs promote up-regulation of ZO-1 and claudin-14, and down-regulation of claudin-2. These effects are TcpC-independent (Fig. 2). Interestingly, soluble secreted TcpC also positively regulates the expression of ZO-1 and claudin-14, but this protein has no effect on the transcriptional regulation of claudin-2. Concerning ZO-2, results showed that vesicles released by this probiotic do not regulate its expression. Thus, the EcN-mediated upregulation of ZO-2 does not rely on secreted factors but probably depends on bacteria-associated components.

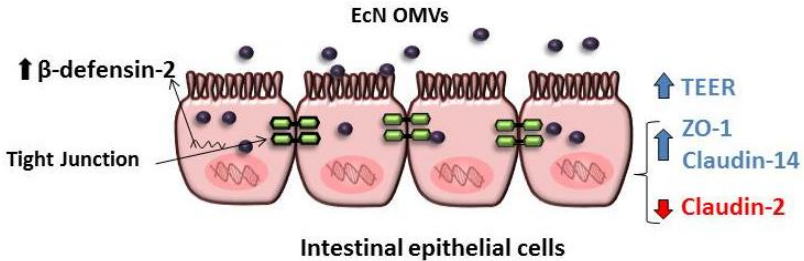


Figure 2. Modulation of the intestinal epithelial barrier by EcN OMVs in an intact epithelial barrier model: EcN OMVs reinforce the epithelial barrier through the increase of TER and positive regulation of the ZO-1 and claudin-14 proteins, as well as the negative regulation of claudin-2. In addition, EcN OMVs increase the expression of the antimicrobial peptide β -defensin-2.

Thus, contribution of EcN OMVs on the reinforcement of the intestinal epithelial barrier integrity, through several mechanisms, has been proved [51]. As stated, EcN OMVs directly modulate transcriptional regulation of TJ proteins, but also elicit additional responses that indirectly contribute to strengthen the epithelial barrier. In this sense, we have reported that OMVs released by this probiotic induce IL-22 expression in colonic explants [50]. This cytokine, mainly expressed by immune cells, targets epithelial cells and reinforces the intestinal barrier, thus limiting the access of microbial compounds and allergens to the systemic circulation.

5.4. Immunomodulatory role of EcN OMVs

As commented above, EcN is a good colonizer of the human gut and positively affects gastrointestinal homeostasis and microbiota balance. In addition to its beneficial effects on intestinal epithelial barrier, this probiotic modulates the host immune response towards an anti-inflammatory balance. The EcN-mediated effects have been mainly evidenced from a great number of *in vitro* and *in vivo* experiments performed with live probiotic suspensions [17,18,20,21,54]. Nonetheless, the bacterial factors that mediate these effects are not always known.

To define whether the immune modulation effects promoted by EcN are mediated through released OMVs, several *in vitro* and *ex vivo* cell models were set up to analyze the cytokine/chemokine response elicited by EcN OMVs in gut epithelial and immune cells [50].

- (i) Direct stimulation of peripheral blood mononuclear cells (PBMCs) was used as an *in vitro* model of intestinal inflammation and barrier disruption. Stimulation of these immune cells with EcN OMVs activates the expression and secretion of IL-10, MIP1 α , TNF- α , IL-6 and IL-8. In this model of inflamed barrier, bacterial lysates also trigger activation of these cytokines, even to a higher extent.
- (ii) Apical stimulation of Caco-2/PBMCs co-cultures in Transwell permeable supports. This *in vitro* model that mimics intact intestinal barrier allows evaluating the crosstalk between OMVs, intestinal epithelial cells and the underlying immune cells [55,56]. In this model, OMVs are not in direct contact with the immune cells. Therefore, upon apical stimulation OMVs are internalized by epithelial cells, and signaling between epithelial and immune cells is produced through the release of soluble mediators. Apical stimulation with EcN OMVs results in the activation of immunomodulatory responses in the underlying immunocompetent cells, leading to increased secretion of IL-10, MIP1 α , TNF- α , IL-6 and IL-8 in the basolateral compartment. In this model of intact intestinal barrier, bacterial lysates do not produce any activation effect. Parallel experiments performed in Caco-2 monolayers without underlying PBMCs showed that polarized Caco-2 cells are almost unresponsive to bacterial factors in the absence of crosstalk with immune cells. Overall results from this model indicate that released EcN OMVs can mediate the probiotic immunomodulatory effects in the intact intestinal mucosa. This mechanism may also apply to microbiota-derived vesicles.
- (iii) Stimulation of human colonic explants, an *ex vivo* model closer to the *in vivo* gut conditions. Results in this model confirmed the great potential of EcN OMVs to modulate the immune response in intact intestinal mucosa, being the expression profile for the cytokines analyzed similar to that from the *in vitro* co-culture model. The genes encoding IL-10, MIP1 α , TNF- α , IL-6 and IL-8 were upregulated in colonic explants incubated with EcN OMVs. In addition, vesicles from this probiotic diminished the expression of the pro-inflammatory cytokine IL-12.

The study on the immunomodulatory effects of EcN OMVs [50] proved the ability of probiotic vesicles to mediate signaling events to the immune system through the intestinal epithelial barrier. Thus, the beneficial effects of the probiotic EcN on gut homeostasis, especially modulation of the immune

response and barrier function, can be mediated by released OMVs. Our results with probiotic vesicles can be extrapolated to the microbiota-host crosstalk. Release of extracellular vesicles allows microbiota to communicate with intestinal mucosa cells, promoting the delivery of mediators that trigger host immune and defense responses.

6. OMVs in the treatment of intestinal inflammatory diseases

Inflammatory bowel diseases (IBD) are chronic gut inflammatory disorders that have an increasing incidence worldwide, particularly ulcerative colitis (UC) and Crohn's disease. They are multifactorial diseases that involve a dysregulated immune response against commensal gut microbes in genetically susceptible individuals with altered intestinal epithelial integrity [57]. Conventional IBD therapies including salicylates, corticoids, immunosuppressants and biological agents do not always yield good results [58]. As a common trait, IBD patients show an altered intestinal microbiota balance, a condition known as dysbiosis. For this reason several studies have evaluated the therapeutic effect of commensal and probiotic strains in clinical trials [59,60] or in animal models of colitis [35,37,61,62,63,64].

Concerning EcN, various clinical trials have evidenced its therapeutic benefits in inducing and maintaining remission of UC, showing similar anti-inflammatory effects as the standard treatment with aminosalicylate mesalazine [65,66]. Several mechanisms contribute to the therapeutic action of EcN against IBD, including the modulation of the host immune response toward an anti-inflammatory balance, the ability to reinforce the intestinal epithelial barrier [20,21,22], production of antimicrobial factors such as microcins and the induction of epithelial hBD-2 [18].

It has been reported that EcN OMVs could mediate the anti-inflammatory and barrier protection effects reported for this probiotic in experimental colitis [67]. In this study, oral administration of EcN OMVs was evaluated in the dextran sodium sulphate (DSS)-induced colitis mouse model. The experimental design included pre-treatment with EcN OMVs for ten days before DSS intake and a final five-day recovery period. The OMVs-treated group received EcN vesicles during all the experimental period (20 days). Administration of purified EcN OMVs significantly reduced DSS-induced weight loss and ameliorated clinical symptoms and histological damage. In addition, OMVs treatment counteracted the altered expression of cytokines and markers of intestinal

barrier function, thus proving the ability of EcN OMVs to ameliorate mucosal injury and gut inflammation.

Concerning microscopic analysis of colonic samples, the OMVs-treated mice showed preserved goblet cells replenished with their mucin content, and reduced mucosal infiltration areas, ulceration and oedema. Consistently, values for the colonic weight/length ratio were significantly smaller in this treated group than in the colitic control group. All these observations are consistent with an improvement in the mucosal barrier integrity in mice that received EcN OMVs.

The OMV-mediated anti-inflammatory effects were clearly evidenced by the improvement in the exacerbated immune response associated to colonic damage in DSS-treated mice. This treatment activates several cells of the innate immune response including epithelial cells, macrophages and dendritic cells, which leads to upregulated expression of pro-inflammatory cytokines such as IL-1 β , TNF- α , and IL-6, thus triggering an imbalance in T-regulatory cells and Th1/Th17 cell responses. This regulatory network facilitates sustained inflammation through activation of other cytokines such as IFN- γ , IL-12 and IL-17 and also reduction of the anti-inflammatory cytokine IL-10 [68]. This altered cytokine expression profile was counteracted by EcN OMVs treatment by increasing IL-10 expression and diminishing expression of the anti-inflammatory cytokines [67].

One of the first events in intestinal inflammation is the impairment of the epithelial barrier function. This alteration enables the access of luminal antigens that trigger the exacerbated immune response. Therefore, promotion of mucosal healing is fundamental to prevent intestinal inflammation. One mechanism used by EcN OMVs to protect the intestinal barrier in DSS-colitic mice is downregulation of MMP-9, a metalloprotease that disrupt gut epithelial TJs, thus leading to increased intestinal permeability [69]. In addition, this treatment preserves expression of the MMP-2, which displays an opposite role to MMP-9 [70].

Another factor that contributes to mucosal barrier function is the protein trefoil factor 3 (TFF-3). In conditions of intestinal inflammation, such as DSS-induced colitis, expression of TFF-3 is downregulated [71]. Interestingly, EcN OMVs were able to restore the mRNA levels of TFF-3 to values similar to those of healthy mice. Thus, upregulation of this peptide by EcN OMVs contributes to epithelial protection and repair, preserving the cell structure of the colonic mucosa in DSS-treated mice [67]. It is known that TFF-3 reinforces TJs by promoting the redistribution of ZO-1 from the cytosol to the intercellular junctions of intestinal epithelial cells, where

strongly interacts with occludin, without altering ZO-1 expression [72]. Although EcN OMVs upregulate ZO-1 expression in several intestinal epithelial cell lines [51] they do not compensate the reduced ZO-1 expression in the DSS-experimental colitis model. This may reflect that EcN OMVs activate different regulatory mechanisms in the presence of highly expressed inflammatory mediators, including those that modulate ZO-1 location at the TJ structures, such as TFF-3. In addition to the beneficial effects on epithelial barrier repair, upregulation of TFF-3 may also contribute to ameliorate the inflammatory response in DSS-treated mice, since overexpression of this peptide abolishes the IL-1 β mediated upregulation of certain pro-inflammatory cytokines [73].

Other markers of tissue damage and inflammation upregulated in DSS-induced colitis are cyclooxygenase-2 (COX-2) and inducible oxide nitric synthase (iNOS). These enzymes confer protection against tissue injury, inflammation and infection and are highly expressed at damaged sites. Although iNOS upregulation is part of the intestinal antibacterial response that results on nitric oxide (NO) production, excess NO has been associated with intestinal inflammation in IBD patients [74], being the infiltrating macrophages in intestinal mucosa the main source of upregulated iNOS [75,76]. In these conditions, high levels of NO may cause tissue injury and the mucosal lesions observed in both human IBD and mouse experimental colitis. In DSS-treated mice, administration of EcN OMVs downregulates the altered expression of both enzymes, thus contributing to mucosal healing [67].

Oral administration of OMVs isolated from the probiotic EcN significantly reduces colonic damage in colitic mice [67]. These vesicles mediate anti-inflammatory and barrier protection effects, similarly to what has been reported for this probiotic in experimental colitis. The components of EcN OMVs responsible for these effects remain unknown. The polyketide colibactin could be one of these mediators. It is known that colibactin is required for the *in vivo* anti-inflammatory effects of EcN [49]. Moreover, in the DSS-induced colitis mouse model, administration of an EcN mutant deficient in colibactin synthesis results in exacerbated colitis. Although the colibactin secretion mechanism has not been described so far, the anti-inflammatory effects of EcN OMVs in experimental colitis suggest that colibactin could be delivered to the intestinal mucosa, at least in part, through released vesicles. However, the contribution of other specific probiotic OMV-associated factors to the modulation of mucosal healing markers cannot be ruled out.

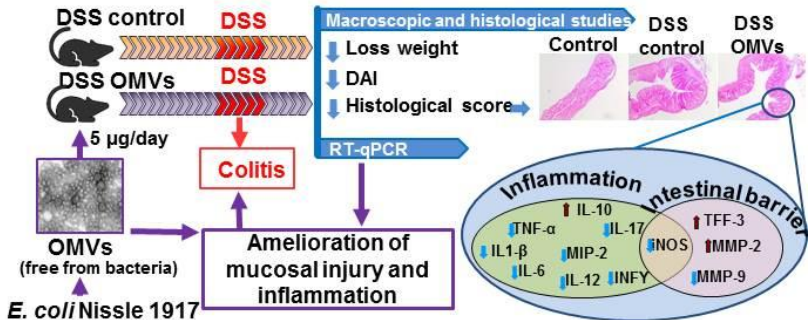


Figure 3. Antiinflammatory and barrier protection effects of EcN OMVs in DSS-induced experimental colitis in mice.

7. Concluding remarks

The influence of microbiota in human health is well known. Nowadays, microbiota imbalances (dysbiosis) have been associated with great variety of inflammatory and metabolic diseases. A therapeutic strategy to modulate microbiota composition is the administration of probiotics. This therapy is essentially an attempt to harness the beneficial effects of commensal microbiota. However, translation of probiotics or microbiota-based drugs to human healthcare requires knowledge of the molecular mechanisms involved in probiotic-host interactions. Moreover, although probiotics are Generally Regarded As Safe, some concerns about the potential risk associated with their use should be considered, especially in immunocompromised individuals and neonates.

Extracellular vesicles released by microbiota have a key role in bacteria-host cross-talk at the intestinal mucosa, as they act as a secretion and delivery pathway for selected bacterial proteins and active mediators directly to the host cells. Studies performed with the probiotic EcN prove the ability of the released vesicles to mediate signalling events to the immune system through the intestinal epithelial barrier, thus triggering appropriate host immune and defence responses. In addition, EcN OMVs mediates intestinal anti-inflammatory and barrier protective effects in the DSS experimental model of colitis.

Interestingly, isolated OMVs are free from bacteria and can elicit the same effect on gastrointestinal health as the probiotic itself. Thereby, EcN OMVs (either alone or in combination with secreted soluble factors) could represent a new therapeutic treatment with a high bio-safety level to

prevent and ameliorate inflammatory conditions associated with intestinal disorders. This potential formulation fits into the term postbiotic, a group of new potential treatments based on probiotic or microbiota products that is nowadays receiving great interest.

Acknowledgments

We thank Dr. F. J. Pérez-Cano for critical revision of the review.

References

1. Sánchez, B., Bressollier, P., Urdaci, M. C. 2008, *FEMS Immunol. Med. Microbiol.*, 54, 1.
2. Sánchez B, Urdaci MC, Margolles A. 2010, *Microbiology*. 156, 3232.
3. Moore, W. E., Holdeman, L.V. 1974, *Am. J. Clin. Nutr.*, 27, 1450.
4. Tiihonen, K., Ouwehand, A. C., Rautonen, N. 2010, *Ageing Res. Rev.*, 9, 107.
5. Scaldaferri, F., Gerardi, V., Lopetuso, L. R., Del Zompo, F., Mangiola, F., Bošković, I., Bruno, G., Petito, V., Laterza, L., Cammarota, G., Gaetani, E., Sgambato, A., Gasbarrini, A. 2013, *Biomed. Res. Int.*, 2013, 435268.
6. O'Hara, A. M., Shanahan, F. 2006, *EMBO reports*, 7, 688.
7. Bevins, C. L., Salzman, N. H. 2011, *Nat. Rev. Microbiol.*, 9, 356.
8. Ghoshal, U.C., Gwee, K. A., Holtmann, G., Li, Y., Park, S. L., Simadibrata, M., Sugano, K., Wu, K., Quigley, E. M. M., Cohen, H. 2018, *J. Gastroenterol. Hepatol.*, 33, 57.
9. Guinane, C. M., Cotter, P. D. 2013, *Therap. Adv. Gastroenterol.*, 6, 295.
10. Scaldaferri, F., Gerardi, V., Mangiola, F., Lopetuso, L. R., Pizzoferrato, M., Petito, V., Papa, A., Stojanovic, J., Poscia, A., Cammarota, G., Gasbarrini, A. 2016, *World J. Gastroenterol.*, 22, 5505.
11. Cress, B.F., Linhardt, R.J., Koffas, M.A.G. 2013, *Genome Announc.*, 1, e0004713.
12. Reister, M., Hoffmeier, K., Krezdorn, N., Rotter, B., Liang, C., Rund, S., Dandekar, T., Sonnenborn, U., Oelschlaeger, T.A. 2014, *Biotechnol.*, 187, 106.
13. Vejborg, R. M., Friis, C., Hancock, V., Schembri, M. A., Klemm, P. *Mol. Genet. Genomics*, 2010, 283, 469.
14. Grozdanov, L., Raasch, C., Schulze, J., Sonnenborn, U., Gottschalk, G., Hacker, J., Dobrindt, U. 2004, *J. Bacteriol.*, 186, 5432
15. Sun, J., Gunzer, F., Westendorf, A. M., Buer, J., Scharfe, M., Jarek, M., Gosling, F., Blocker, H., Ping, A. Z. 2005, *J. Biotechnol.*, 117, 147.
16. Lasaro, M. A., Salinger, N., Zhang, J., Wang, Y., Zhong, Z., Goulian, M., Zhu, J. 2009, *Microbiol.*, 75, 246.
17. Sturm, A., Rilling, K., Baumgart, D. C., Gargas, K., Abou-Ghazalé, T., Raupach, B., Eckert, J., Schumann, R. R., Enders, C., Sonnenborn, U., Wiedenmann, B., Dignass, A. U. 2005, *Infect. Immun.*, 73, 1452.

18. Schlee, M., Wehkamp, J., Altenhoefer, A., Oelschlaeger, T. A., Stange, E. F., Fellermann, K. 2007, *Infect. Immun.*, 75, 2399.
19. Hafez, M., Hayes, K., Goldrick, M., Warhurst, G., Grecis, R., Roberts, I.S. 2009, *Infect. Immun.*, 77, 2995.
20. Ukena, S.N., Singh, A., Dringenberg, U., Engelhardt, R., Seidler, U., Hansen, W., Bleich, A., Bruder, D., Franzke, A., Rogler, G., Suerbaum, S., Buer, J., Gunzer, F., Westendorf, A. M. 2007, *PLoS ONE*, 2, e1308.
21. Zyrek, A.A., Cichon, C., Helms, S., Enders, C., Sonnenborn, U., and Schmidt, M.A. 2007, *Cell. Microbiol.*, 9, 804.
22. Hering, N., Richter, J.F., Fromm, A., Wieser, A., Hartmann, S., Gunzel, D., Buckner, R., Fromm, M., Schulzke, J.D., and Troeger, H. 2014, *Mucosal Immunol.*, 7, 369.
23. Sonnenborn, U., Schulze, J. 2009, *Microb. Ecol. Health. Dis.*, 21, 122.
24. Ellis, T. N., Kuehn, M. J. 2010, *Microbio. Mol. Biol. Rev.*, 74, 81.
25. Donoghue, E. J. O, Krachler, A. M. 2016, *Cell Microbiol.*, 18, 1508.
26. Kuehn, M. J, Kesty, N. C. 2005, *Genes Develop.*, 1999, 2645.
27. Kulp, A., Kuehn, M. J. 2010, *Annu. Rev. Microbiol.*, 64, 163.
28. Schwechheimer, C., Kuehn, M. J. 2015, *Nat. Rev. Microbiol.*, 13, 605.
29. Pathirana, R. D., Kaparakis-Liaskos, M. 2016, *Cell. Microbiol.*, 18, 1518.
30. Kim, Y.S., Ho, S.B. 2010, *Curr. Gastroenterol. Rep.*, 12, 319.
31. Schertzer, J. W., Whiteley, M. 2013, *J. Mol. Microbiol. Biotechnol.*, 23, 118.
32. Chatterjee, D., Chaudhuri, K. 2013, *J. Biol. Chem.*, 288, 4299.
33. Kaparakis-Liaskos, M., Ferrero, R. L. 2015. *Nat. Rev. Immunol.*, 15, 375.
34. Olsen, I., Amano, A.J. 2015, *Oral Microbiol.*, 7, 27468.
35. Shen, Y, Giardino Torchia M. L., Lawson, G. W., Karp, C. L., Ashwell, J. D., Mazmanian, S. K. 2012, *Cell Host Microbe.*, 12, 509.
36. Stentz, R., Horn, N., Cross, K., Salt, L., Brearley, C., Livermore, D. M., Carding, S. R. 2015, *J. Antimicrob. Chemother.*, 70, 701.
37. Kang, C. S., Ban, M., Choi, E. J., Moon, H. G., Jeon, J. S., Kim, D. K., Park, S. K., Jeon, S. G., Roh, T. Y., Myung, S. J., Gho, Y. S., Kim, J. G., Kim, Y. K. 2013, *PLoS One*, 8, e76520.
38. López, P., González-Rodríguez, I., Sánchez, B., Gueimonde, M., Margolles, A., Suárez, A. 2012, *Vaccine*, 30, 825.
39. Aguilera, L., Toloza, L., Giménez, R., Odena, A., Oliveira, E., Aguilar J., Badia, J., Baldoma, L. 2014, *Proteomics*, 14, 222.
40. Lee, E.Y., Choi, D. S., Kim, K. P., Gho, Y. S. 2008, *Mass Spectrom. Rev.*, 27, 535.
41. Toloza, L., Giménez, R., Fábrega, M. J., Alvarez, C. S., Aguilera, L., Cañas, M. A., Martín-Venegas, R., Badia, J., Baldomà, L. 2015, *BMC Microbiol.*, 15, 250.
42. Navarro-Garcia, F., Gutierrez-Jimenez, J., Garcia-Tovar, C., Castro, L. A., Salazar-Gonzalez, H., Cordova, V. 2010, *Infect. Immun.*, 78, 4101.
43. Ferreira, E., Giménez, R., Cañas, M. A., Aguilera, L., Aguilar, J., Badia, J., Baldomà, L. 2015, *Int. J. Biochem. Cell Biol.*, 60, 202.
44. Ferreira, E., Giménez, R., Aguilera, L., Guzmán, K., Aguilar, J., Badia, J., Baldomà, L. 2013, *Res. Microbiol.*, 164, 145.

45. Aguilera, L., Ferreira, E., Giménez, R., Fernández, F. J., Taulés, M., Aguilar, J., Vega, M. C., Badia, J., Baldomà, L. 2012, *Int. J. Biochem. Cell Biol.*, 44, 955.
46. Egea, L., Aguilera, L., Giménez, R., Sorolla, M. A., Aguilar, J., Badía, J., Baldoma, L. 2007, *Int. J. Biochem. Cell Biol.*, 39, 1190.
47. Cañas, M. A., Giménez, R., Fábrega, M. J., Toloza, L., Baldomà, L., Badia, J. 2016, *PLoS ONE*, 11, e0160374
48. Bielaszewska, M., Rüter, C., Kunsmann, L., Greune, L., Bauwens, A., Zhang, W., Kuczius, T., Kim, K. S., Mellmann, A., Schmidt, M. A., Karch, H. 2013, *PLoS Pathog.*, 9, e1003797.
49. Olier, M., Marcq, I., Salvador-Cartier, C., Secher, T., Dobrindt, U., Boury, M., Bacquié, V., Pénary, M., Gaultier, E., Nougayrède, J. P., Fioramonti, J., Oswald, E. 2012, *Gut Microbes*, 3, 501.
50. Fábrega, M. J., Aguilera, L., Giménez, R., Varela, E., Cañas M. A., Antolín, M., Badía, J., Baldomà, L. 2016, *Front. Microbiol.*, 7, 705.
51. Alvarez, C. S., Badia, J., Bosch, M., Giménez, R., Baldomà, L. 2016, *Front Microbiol.*, 7, 1981.
52. Mündel, M., Schroeder, B. O., Zimmermann, K., Huber, H., Nuding, S., Beisner, J., Fellermann, K., Stange, E. F., Wehkamp, J. 2009, *Mucosal Immunol.*, 2, 166.
53. Hafez, M. M. 2012, *Probiotics Antimicrob. Proteins*, 4, 67.
54. Arribas, B., Rodríguez-Cabezas, M. E., Camuesco, D., Comalada, M., Bailón, E., Utrilla, P., Nieto, A., Concha, A., Zarzuelo, A., Gálvez, J. 2009, *Br. J. Pharmacol.*, 157, 1024.
55. Fang, H. W., Fang, S. B., Chiang-Chiau, J. S., Yeung, C. Y., Chan, W. T., Jiang, C. B., Cheng, M. L., Lee, H. C. 2010, *J. Med. Microbiol.*, 59, 573.
56. Pozo-Rubio, T., Mujico, J. R., Marcos, A., Puertollano, E., Nadal, I., Sanz, Y., Nova, E. 2011, *Br. J. Nutr.* 106, 1216.
57. Zhang, Y. Z., Li, Y. Y. 2014, *World J. Gastroenterol.*, 20, 91.
58. Ko, J. K., Auyeung, K. K. 2014, *Curr. Pharm.*, 20, 1082.
59. Fedorak, R. N. 2010, *Gastroenterol. Hepatol.*, 6, 688.
60. Wasilewski, A., Zielinska, M., Storr, M., and Fichna, J. 2015, *Inflamm. Bowel Dis.*, 21, 1674.
61. Ewaschuk, J. B., Diaz, H., Meddings, L., Diederichs, B., Dmytrash, A., Backer, J., Looijer-van Langen, M., Madsen, K. L. 2008, *Am. J. Physiol. Gastrointest. Liver Physiol.*, 295, G1025.
62. Garrido-Mesa, N., Utrilla, P., Comalada, M., Zorrilla, P., Garrido-Mesa, J., Zarzuelo, A., Rodríguez-Cabezas, M. E., Gálvez, J. 2011, *Biochem. Pharmacol.* 82, 1891.
63. Martín, R., Miquel, S., Chain, F., Natividad, J. M., Jury, J., Lu, J., Sokol, H., Theodorou, V., Bercik, P., Verdu, E. F., Langella, P., Bermúdez-Humarán, L. G. 2015, *BMC Microbiol.* 15, 67.
64. Souza, B. M., Preisser, T. M., Pereira, V. B., Zurita-Turk, M., de Castro, C. P., da Cunha, V. P., de Oliveira, R. P., Gomes-Santos, A. C., de Faria, A. M., Machado, D. C., Chatel, J. M., Azevedo, V. A., Langella, P., Miyoshi, A. 2016, *Microb. Cell Fact.*, 15, 150.

65. Losurdo, G., Iannone, A., Contaldo, A., Ierardi, E., Di Leo, A., Principi, M. 2015, *J. Gastrointestin. Liver Dis.*, 24, 499.
66. Floch, M. H., Walker, W.A., Madsen, K., Sanders, M. E., Macfarlane, G. T., Flint, H. J., Dieleman, L. A., Ringel, Y., Guandalini, S., Kelly, C. P., Brandt, L. J. 2011, *J. Clin. Gastroenterol.*, 45, S168.
67. Fábrega, M. J., Rodríguez-Nogales, A., Garrido-Mesa, J., Algieri, F., Badía, J., Giménez, R., Gálvez, J., Baldomà, L. 2017, *Front. Microbiol.*, 8,1274.
68. Neurath, M. F. 2014, *Nat. Rev. Immunol.*, 14, 329.
69. Nighot, P., Al-Sadi, R., Rawat, M., Guo, S., Watterson, D.M., Ma, T. 2015, *Am. J. Physiol. Gastrointest. Liver Physiol.*, 309, G988.
70. Garg, P., Vijay-Kumar, M., Wang, L., Gewirtz, A. T., Merlin, D., Sitaraman, S. V. 2009, *Am. J. Physiol. Gastrointest. Liver Physiol.*, 296, G175.
71. Lozano-Pérez, A. A., Ortiz-cullera, V., Zorrilla, P., Rodriguez-Cabezas, M. E., Cenis, J. L. 2014, *Int. J. Nanomed.*, 9, 4507.
72. Buda, A., Jepson, M. A., Pignatelli, M. 2012, *Cell Commun. Adhes.*, 19, 63.
73. Lin, N., Xu, L. F., Sun, M. 2013, *Biochem. Biophys. Res. Commun.*, 440, 143.
74. Kolios, G., Valatas, V., Ward, S. G. 2004, *Immunology*, 113, 427.
75. Rachmilewitz, D., Stamler, J. S., Bachwich, D., Karmeli, F., Ackerman, Z., Podolsky, D. K. 1995, *Gut*, 36,718–723.
76. Palatka, K., Serfozo, Z., Veréb, Z., Hargitay, Z., Lontay, B., Erdodi, F., Bánfalvi, G., Nemes, Z., Udvardy, M., Altorjay, I. 2005, *Scand. J. Gastroenterol.*, 40, 670.



Research Signpost
Trivandrum
Kerala, India

Recent Advances in Pharmaceutical Sciences VIII, 2018: 43-58 ISBN: 978-81-308-0579-5
Editors: Diego Muñoz-Torrero, Yolanda Cajal and Joan Maria Llobet

3. Development of hybrid compounds to tackle Alzheimer's disease

Francisco Javier Pérez-Areales and Diego Muñoz-Torrero

Laboratory of Pharmaceutical Chemistry (CSIC Associated Unit), Faculty of Pharmacy and Food Sciences, University of Barcelona, Av. Joan XXIII 27-31, E-08028 Barcelona, Spain
Institute of Biomedicine (IBUB), University of Barcelona, E-08028 Barcelona, Spain

Abstract. Alzheimer's disease (AD) is the main neurodegenerative disorder worldwide. Its pathogenesis involves a network where various mechanisms are interconnected. This complex pathological network makes it extremely challenging to find an efficacious treatment. Herein, we give an overview on the design of the so-called multi-target-directed ligands, i.e. compounds that concurrently hit several key pathogenic factors within the network, as a realistic option to tackle AD, with a particular emphasis on some structural classes of multitarget hybrids recently developed in our group.

Introduction

Alzheimer's disease (AD) is characterized by an inexorable progressive deterioration in cognitive ability and capacity for independent living [1]. AD is the most prevalent neurodegenerative disorder and one of the most important health-care problems in developed countries. Over 47 million people live with dementia worldwide, and this number is estimated to increase

Correspondence/Reprint request: Dr. Francisco Javier Pérez-Areales, Laboratory of Pharmaceutical Chemistry (CSIC Associated Unit), Faculty of Pharmacy and Food Sciences, and IBUB, University of Barcelona, Av. Joan XXIII 27-31, E-08028 Barcelona, Spain. E-mail: fjperezareales@gmail.com

to more than 131 million by 2050, as populations age. Dementia also has a huge economic impact, with the total estimated worldwide cost being US \$818 billion [2]. To aggravate this situation, current treatments against AD afford only temporary relief of the cognitive and functional symptoms, but do not prevent, halt, or delay disease progression.

During the past 40 years, intensive research efforts have aimed to decipher the mechanisms of AD progression. However, the etiology of AD is not yet completely understood, and the unique neuropathological clearly defined hallmarks are the senile plaques and neurofibrillary tangles (NFTs), which are mainly composed of aggregated β -amyloid peptide ($A\beta$) and hyperphosphorylated tau protein, respectively, together with a degeneration of the neurons and synapses [3,4]. The lack of success in discovering novel pharmaceuticals to tackle AD is very likely caused by the multifactorial nature of the disease, which involves various complex mechanisms where several key proteins and pathological pathways are interconnected in a robust network. Thus, we must conceive AD as a pathological network instead of a continuous process [5].

Considering the mechanistic complexity involved in the pathological network of AD, it is easy to understand why the classic medicinal chemistry paradigm of developing drugs based on the reductionist approach of “one molecule-one target” has met with very limited success, which highlights the need for a more comprehensive pharmacological strategy to obtain effective outcomes.

In this context, some pharmacological approaches are available for the treatment of multifactorial diseases, such as AD. The most commonly used in general pharmacotherapy, referred to as multiple-medication therapy (MMT), consists of combining several drugs with different action mechanisms. However, this approach might imply patient compliance and pharmacokinetics issues [6,7]. An alternative approach relies on the use of a multiple-compound medication (MCM), which implies the incorporation of different drugs into the same formulation in order to simplify dosing regimens and improve patient compliance [6,7].

Finally, a third strategy is based on the assumption that a single molecule may be able to hit multiple targets. This approach, the so-called multi-target-directed ligand therapy (MTDL, Fig. 1), shows advantages over the aforementioned strategies, such as easier pharmacokinetics, improved efficacy due to synergistic effects, improved safety by preventing the risk of drug-drug interactions, and easier development, among others [6,8,9]. MTDLs can be rationally designed through the molecular assembly of distinct pharmacophore moieties of known bioactive molecules, where each drug entity has conserved the potential to interact with its specific site on the target [9].

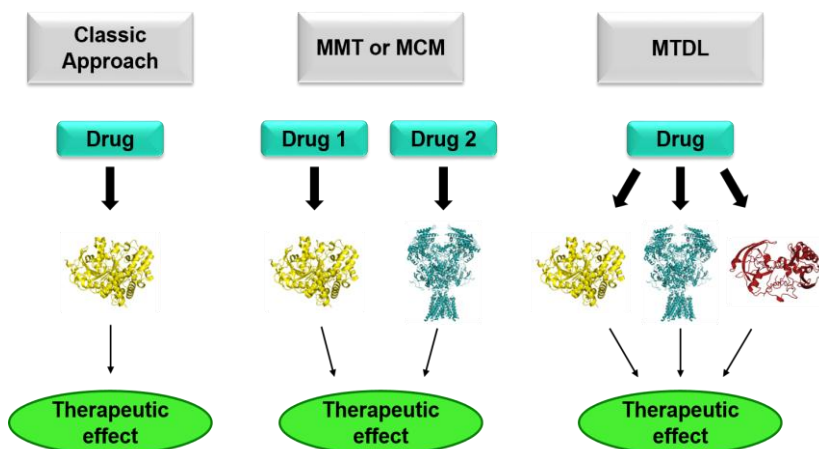


Figure 1. Different approaches to polypharmacological therapies against multifactorial diseases. Left: one-molecule-one-target strategy. Centre: multiple-medication therapy (MMT); in case of multiple-compound medication (MCM), both drugs are applied in the same pill. Right: multi-target-directed ligand (MTDL) approach.

In this chapter, we briefly review the design of hybrid molecules with the aim of combating AD, either by increasing the potency against a specific target, or by using a MTDL strategy in order to concurrently affect several targets within the AD network.

1. Increasing the potency against a key target, acetylcholinesterase

A common feature in AD patients is a cholinergic dysfunction, which is responsible for the clinical symptoms of the disease, which led to the postulation of the “cholinergic hypothesis of AD”. This hypothesis proposed that degeneration of cholinergic neurons and the associated loss of cholinergic neurotransmission contributed significantly to the deterioration in cognitive function, perception, comprehension, reasoning, and short-term memory, observed in patients with AD [10,11]. This abnormal acetylcholine (ACh) neurotransmission is caused by dysregulation at different levels of synapses, such as a decreased availability of ACh because of high-affinity choline uptake, reduced ACh release or reduced ACh synthesis [11,12].

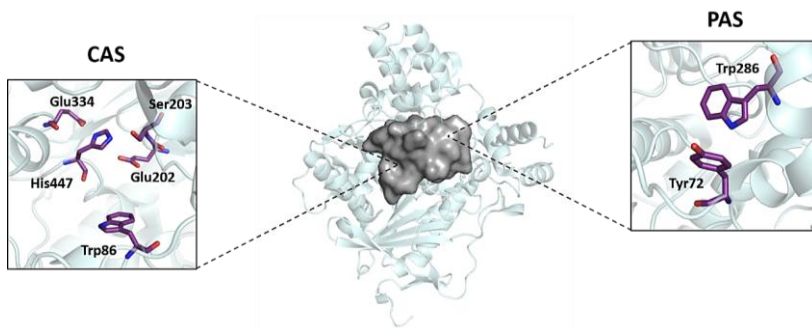


Figure 2. X-ray structure of *hAChE* (PDB ID: 3LII) with details of the CAS and the PAS.

At present, the most common therapeutic strategy aims at re-establishing the functional cholinergic neurotransmission by decreasing ACh metabolism through acetylcholinesterase inhibitors (AChEIs), which fit within the category of indirect cholinomimetic drugs [13]. Human AChE (*hAChE*) is the enzyme responsible for the hydrolysis of ACh, which takes place inside the catalytic anionic site (CAS) by means of the catalytic triad Ser203-His447-Glu334 (Fig. 2). A secondary binding site is the peripheral anionic site (PAS), which is located at the mouth of the narrow catalytic gorge and is responsible for the early binding and guiding of the substrate ACh towards the CAS [14,15].

The “cholinergic hypothesis” has led to four out of the five marketed anti-Alzheimer drugs, which act as AChEIs and are only symptomatic and effective for a limited time. The first approved drug of this group was tacrine (**1**, Fig. 3) [16,17], although it was withdrawn from the market due to hepatotoxicity issues [18].

1.1. Huprines as a new class of highly potent AChEIs

An example of how the inhibitory activity against AChE can be greatly increased by achieving a larger number of interactions within the CAS of the enzyme was reported by the group of Camps and Muñoz-Torrero with the development of huprines, a new class of compounds that turned out to be among the most potent reversible AChEIs described so far [19-21]. Huprines were designed by a conjunctive approach, using as templates two well-known CAS inhibitors, namely (–)-huperzine A (**2**, Fig. 3), an alkaloid isolated from *Huperzia serrata* with potent AChE inhibitory activity that is commercialized

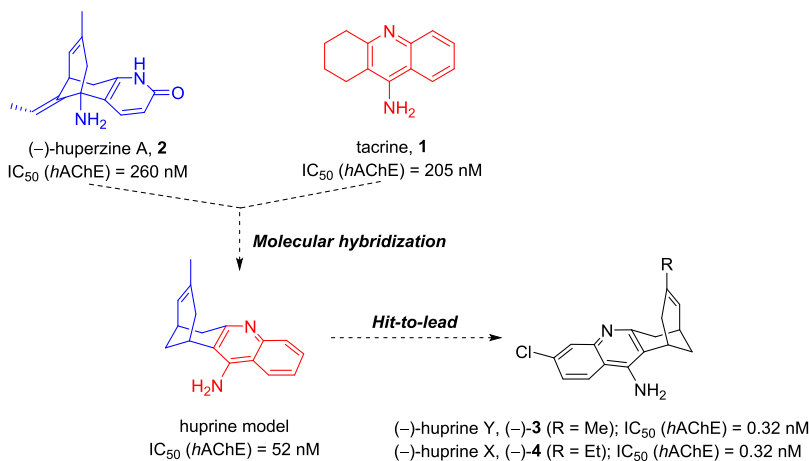


Figure 3. Design of huprines.

as a nutraceutical in the USA [21], and tacrine (**1**). More than thirty different huprines were designed, synthesized and pharmacologically tested. The most active huprines prepared to date are the so-called (-)-huprine Y, (-)-**3**, and (-)-huprine X, (-)-**4**, which are, in racemic form, up to 640- and 810-fold more potent *hAChE* inhibitors than the parent compounds tacrine and (-)-huperzine A, respectively [21]. X-Ray diffraction studies confirmed the extended binding of huprines within the CAS of AChE as compared with the binding mode of their parent compounds, which accounts in a great part for the higher AChE inhibitory potency of huprines, thereby confirming the success of the hybridization strategy [22].

1.2 Benzonaphthyridine–tacrine hybrids as novel AChEIs

As a further step to increase AChE inhibitory activity by enlarging the number of interactions with the enzyme, the so-called dual site binding consists of the simultaneous interaction of a compound with the two terminal binding sites within the catalytic gorge of AChE, i.e. with the CAS and the PAS. An attractive example of rational design of a dual binding site AChEI with a dramatic improvement of inhibitory potency is the development of the benzonaphthyridine–tacrine hybrid **9** [23]. This hybrid compound features a tacrine-based CAS interacting unit linked, by means of a tether of suitable length, to a previously developed PAS interacting unit.

Firstly, we carried out the design and synthesis of a PAS binding unit, structurally related to propidium (**5**, Fig. 4), a well-known PAS binding AChE inhibitor, which led to a pyrano[3,2-*c*]quinoline scaffold (**6**) [24]. Even though previous molecular dynamics (MD) simulations predicted that this structure would bind the PAS of AChE by means of π - π stacking interactions with residues Trp286 and Tyr72, compound **6** was found to be poorly active as AChEI ($IC_{50} > 10 \mu M$) [25]. Subsequent optimization of this PAS binding unit mainly involved the replacement of the oxygen atom at position 1 by a nitrogen. This structural modification should be accompanied by an increase in the basicity of the quinoline nitrogen atom, which, hence, should be protonated at physiological pH, thereby enabling additional cation- π interactions of the novel benzo[*h*][1,6]naphthyridine system (**7**, Fig. 4) at the PAS of AChE. MD simulations predicted an additional hydrogen bonding between the protonated pyridine nitrogen atom and the hydroxyl group of the PAS residue Tyr72 [26]. Compound **7** turned out to be a potent PAS AChEI ($IC_{50} = 65 \text{ nM}$), being 500-fold more potent than propidium and more than 150-fold more potent than the hit **6**.

Afterwards, we developed a hybrid (**9**) that featured the PAS binding pharmacophore of **7** and a unit of the well-known CAS binding ligand 6-chlorotacrine (**8**, an optimized derivative of tacrine, Fig. 5), a highly potent AChEI. Both moieties were connected through a 3-methylene linker, which was suggested by previous computational studies to be the most suitable to enable a dual site binding within AChE, thereby allowing the resulting hybrid to retain all the characteristic interactions of the parent compounds within the enzyme. Indeed, the 6-chlorotacrine fragment of the hybrid was predicted to be tightly bound at the CAS, with this moiety establishing cation- π interactions with Trp86 and Tyr337 and a hydrogen bond between

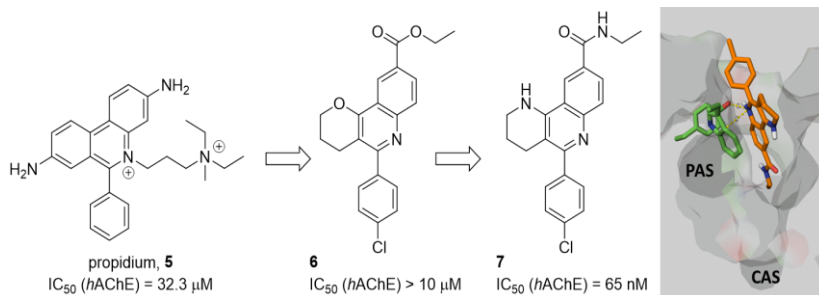


Figure 4. Left: optimization process of PAS AChEIs. Right: representation of the binding mode of compound **7** at the PAS of AChE [26].

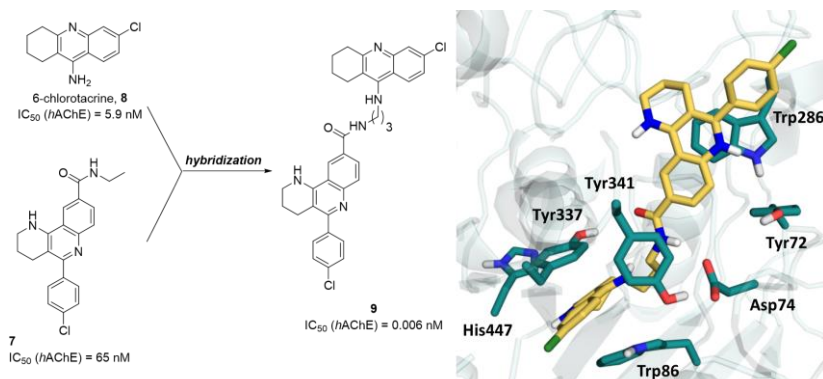


Figure 5. Left: design of hybrid **9**. Right: representation of the multi-site binding mode of hybrid **9** within AChE [23].

the protonated quinoline nitrogen with the carbonyl oxygen atom of His447. In turn, the benzo[*h*][1,6]naphthyridine moiety of the hybrid, whose quinoline nitrogen atom should be mostly protonated at physiological pH, was predicted to be firmly stacked against Trp286 at the PAS, establishing cation- π interactions. Remarkably, we found that an additional hydrogen bond could be formed between the amide group in the linker and Asp74. All this set of interactions along the catalytic gorge of AChE account for the extremely potent inhibitory activity of hybrid **9**, beyond our expectations, in the low picomolar range (IC_{50} = 6 pM), with this compound being 1000-fold more potent than the reference compound 6-chlorotacrine (IC_{50} = 5.9 nM) [23].

2. Huprine-based MTDLs against AD

Senile plaques and NFTs, mainly composed of aggregated A β and hyperphosphorylated tau protein, respectively, constitute two histopathological hallmarks clearly defined in AD patients. Consequently, both events have brought about the pertinent hypotheses about the origin of AD pathology. Firstly, the “amyloid hypothesis” postulates that AD is caused by an imbalance between A β production and clearance, resulting in increased amounts of A β , whose accumulation and aggregation into oligomers, and eventually fibrils and plaques, leads to neuronal damage and cell death [27]. The central event in the amyloid hypothesis is an alteration in the metabolism of the amyloid precursor protein (APP), which is directed

to an amyloidogenic pathway in AD patients, by which the sequential cleavage of APP through β -secretase (BACE1) and γ -secretase, affords a 39–43 amino acid polypeptide, A β , which is highly insoluble and shows strong tendency to aggregate [28]. In this regard, one of the most pursued targets in the search for new anti-Alzheimer drugs has been the modulation of A β production through BACE1 inhibitors [29]. BACE1 is an aspartic protease, whose active site contains two aspartate residues, Asp32 and Asp228, which are responsible for the initial cleavage of APP. The binding cleft is characterized for being partially covered by a highly flexible antiparallel hairpin-loop, referred to as the “flap”, which guides the entrance of the substrate into the catalytic site (Fig. 6) [30].

On the other hand, the “tau hypothesis” postulates that AD patients suffer from an increased kinase activity, which triggers tau hyperphosphorylation, and detachment of the resulting distorted protein from the microtubules, so that the axon disintegrates and the skeleton of the neuron is no longer maintained. Without the cytoskeleton, neurons degenerate, and connections between neurons are lost, what eventually leads to apoptosis due to the loss of function [31,32]. Moreover, defective tau protein has a strong tendency to aggregate, forming paired helical filaments (PHF) inside the neuron, whose abnormal accumulation results in NFTs formation. Tau aggregation occurs through a nucleation-dependent elongation mechanism [33]. In fact, tau may adopt stable seed structures, displaying prion-like characteristics [34,35]. Therefore, prevention of tau aggregation has emerged as another promising therapeutic approach.

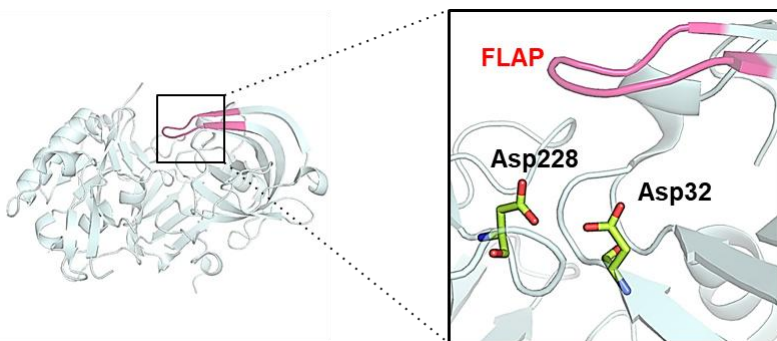


Figure 6. Structure of BACE1 (PDB ID: 1SGZ) with the details of the catalytic anionic dyad and the “flap”.

2.1. Rhein–huprine hybrids as a new class of anti-Alzheimer MTDLs

The multifactorial nature of AD led to the establishment of the MTDL strategy as a promising, realistic therapeutic approach. In this context, rhein–huprine hybrids were designed as a novel structural family of MTDLs. This class of compounds had its origin in the finding that compounds sharing a core structure of hydroxyanthraquinone displayed tau anti-aggregating properties *in vitro* with IC₅₀ values in the low micromolar range [36,37]. The structurally related compound rhein (**10**, Fig. 7, left) is a natural product found in the traditional Chinese herbal medicine rhubarb (*Rheum rhabarbarum*), which is well tolerated in humans [38]. We assumed that the hydroxyanthraquinone derivative rhein could also display tau anti-aggregating activity. Accordingly, the first generation of rhein–huprine hybrids was designed by connecting the hydroxyanthraquinone system of rhein and a moiety of the potent AChEI huprine Y (**3**) with a linker of suitable length. The lead compound of this family turned out to be the nonamethylene-linked hybrid (\pm)-**11** [39,40].

This family of hybrids was endowed with a very interesting *in vitro* and *in vivo* multi-target profile, especially the lead compound (\pm)-**11** (Fig. 7, right). Not unexpectedly, this compound displayed cholinergic activity through a potent inhibition of *human* AChE and butyrylcholinesterase (*h*BChE), and A β ₄₂ and tau anti-aggregating activity. But more surprisingly,

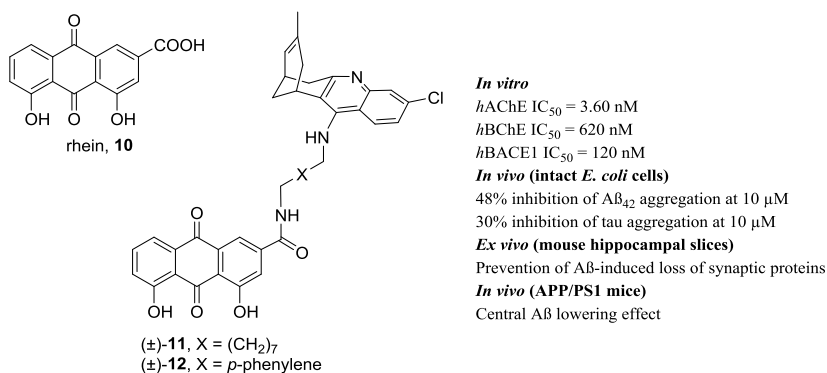


Figure 7. Left: rhein, **10**, the lead compound of the first generation of rhein–huprine hybrids, (\pm)-**11**, and the *p*-phenylene-linked analog (\pm)-**12**. Right: multi-target biological profile of the lead compound (\pm)-**11**.

the lead compound (\pm)-**11** was also found to be a potent inhibitor of *h*BACE1, which led to a significant A β lowering effect in a transgenic mouse model of AD (APP/PS1 mice) [39,40].

To shed light on the binding mode within *h*AChE, molecular modeling studies were carried out for the *p*-phenylene-linked rhein–huprine hybrid (\pm)-**12**, a less flexible analog of (\pm)-**11**, which was still a potent *h*AChEI, with an IC₅₀ value of 18 nM. These studies suggested that the potent inhibitory activity of these hybrids against *h*AChE arises from a dual site binding within the enzyme [40]. Likewise, a dual site binding was also predicted with regard to *h*BACE1 inhibition, with the huprine moiety interacting with the catalytic dyad and the rhein fragment interacting with an unexplored secondary binding site [40].

Of note, the huprine moiety, protonated at physiological pH, remains tightly bound to the catalytic site in both *h*AChE and *h*BACE1 by means of hydrogen bonding interaction with His447 and cation– π interactions with Trp86 and Tyr337 at the CAS of AChE, and a salt bridge with the catalytic dyad of BACE1. The basicity of the huprine moiety of these hybrids is therefore crucial for AChE and BACE1 inhibition, due to the need of being protonated at physiological pH to enable these strong interactions [40].

2.2. Second generation rhein–huprine hybrids

In general, compounds with high basicity suffer from low brain exposure as a result of poor permeation through biological membranes, particularly the blood-brain barrier (BBB), and high P-glycoprotein (P-gp)-mediated efflux liability [41,42]. Hence, tuning of drugs pK_a has been an approach widely adopted to increase drug concentrations in brain [41,43]. In this light, a second generation of rhein–huprine hybrids was envisaged in order to explore how modulation of their basicity would affect their multiple biological activities, while trying to improve their pharmacokinetic properties. In the case of BACE1 inhibitors, the optimal balance between the relevant properties of enzymatic potency and pharmacokinetics has been reported for compounds with pK_a values between 7 and 7.5 [44].

For the design of the novel hybrids, the lead compound **11** was used as a template. Structural modification of its huprine moiety, i.e. the replacement of the chlorobenzene ring by other aromatic rings, should modify the basicity of the pyridine nitrogen. The selection of the novel huprines was made on the basis of their calculated pK_a values by means of high-level quantum mechanical (QM) computations. In this way, we selected the 1,4-difluorohuprine **13a** (Fig. 8, left) and the thienohuprine **13b**, with reduced basicity compared with huprine Y (pK_a = 8.2, for the *N*-methylated

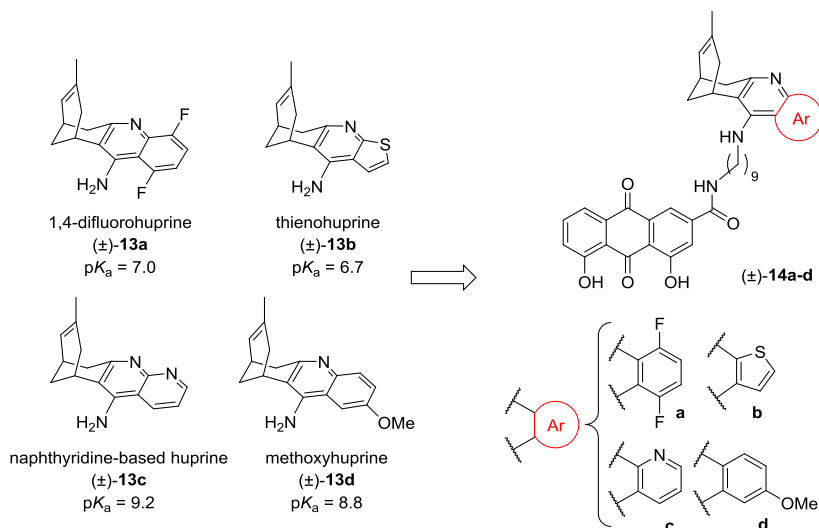


Figure 8. Left: selected modified huprines, (\pm)-**13a-d**, and their calculated pK_a values determined for the *N*-methylated derivatives by QM computations. Right: novel rhein–huprine hybrids, (\pm)-**14a-d**.

derivative of huprine Y), and the naphthyridine-based huprine **13c** [45] and the methoxyhuprine **13d**, which were predicted to be slightly more basic than huprine Y [46]. BACE1 localizes and is fully active in acidic endosomal compartments (pH 4.5–6.5) [47,48,49], where all the novel rhein–huprine hybrids, **14a-d** (Fig. 8, right), should be mostly in protonated form and therefore able to form a salt bridge with the aspartate residues of the catalytic dyad. On the other hand, AChE is located at physiological pH in synapses, where the most basic hybrids **14c** and **14d** should be mostly protonated, thereby retaining their AChE inhibitory activity, while the least basic hybrids **14a** and **14b** should predominate in the neutral form, with the consequent loss of hydrogen bond and cation– π interactions at the CAS of AChE.

It has been previously reported that replacement of the chlorobenzene ring of huprines by other aromatic systems is detrimental for the AChE inhibitory activity [20,21,45]. In agreement with these previous findings, all novel hybrids were clearly less potent than the lead compound **11**, but they still exhibited IC_{50} values in the submicromolar to low micromolar range, in most cases. As anticipated, the most potent second-generation hybrids were those of increased basicity, especially the naphthyridine derivative **14c**

(IC₅₀ = 180 nM), since they should retain their ability to bind at the CAS of AChE. The lower inhibitory potency of hybrid **14c** compared to the lead **11** was studied by means of QM computations and showed unfavorable secondary interactions due to the electrostatic repulsion between the lone pairs of the nitrogen atom at position 1 and of the His447 carbonyl oxygen [46]. Moreover, the decreased activity of **14c** might be ascribed to the absence of the chlorine atom present at position 3 of huprine Y, which fills a hydrophobic pocket near the CAS.

On the other hand, hybrids **14a** and **14b** displayed some *h*BACE1 inhibitory activity (22% inhibition at 1 μM, and 34% inhibition at 80 nM, respectively), whereas compounds **14c** and **14d** turned out to be essentially inactive. Again, this series of compounds was clearly less potent than the lead **11**, despite the fact that all novel second-generation rhein–huprine hybrids should be protonated at the acidic pH in endosomal compartments where BACE1 is located. According to QM calculations, unfavorable electrostatic interactions of the thiophene derivative **14b** with the carboxylate oxygens of the catalytic dyad of BACE1 might account for its lower potency compared with the lead compound **11** [46].

Furthermore, this second generation of rhein–huprine hybrids retained the Aβ₄₂ anti-aggregating activity, while displayed slightly increased tau anti-aggregating properties, compared with the lead compound **11**. A common feature of AD is the oxidative damage in cellular structures, which occurs after an overproduction of reactive oxygen species and a deficiency of the antioxidant systems. Thus, we also assessed the antioxidant capacity of this novel series of compounds because of the presence of phenolic groups in their structure, and since it had been previously reported that rhein as well as huprine Y and a class of huprine-based hybrids were endowed with antioxidant properties [50,51,52]. Very interestingly, all the novel hybrids turned out to be potent antioxidant agents, being 10–22-fold and 12–13-fold more potent than trolox in the ABTS^{•+} and DPPH assays, respectively, and slightly more potent than gallic acid [46]. Interestingly, using the PAMPA-BBB assay, all the hybrids were predicted to have good BBB permeability, a necessary requirement for all CNS drugs.

3. Conclusions

Novel approaches have to be explored to identify drugs that can efficiently treat AD. Focusing on the symptomatic treatment of AD by means of cholinomimetic agents, we have shown that molecular

hybridization is an effective strategy to derive extremely potent (subnanomolar or picomolar) AChEIs that display a wide array of interactions either at the CAS of the enzyme (e.g. huprines) or in a dual site manner, from the CAS to the PAS, all along the AChE catalytic gorge (e.g. benzonaphthyridine-chlorotracerine hybrids). More interestingly, molecular hybridization is an essential tool to design MTDLs, in a very promising approach to derive new drugs that are able to confront the complex pathological network of AD, and, hence, to modify the natural course of this devastating disease. Results from preclinical studies with animal models of AD support a disease-modifying effect for this kind of compounds (e.g. rhein-huprine hybrids).

Acknowledgements

This work was supported by Ministerio de Economía y Competitividad / FEDER (SAF2014-57094-R and SAF2017-82771-R) and Generalitat de Catalunya (GC) (2014SGR52 and 2017SGR106).

References

1. Prince, M., Bryce, R., Albanese, E., Wimo, A., Ribeiro, W., Ferri, C. P. 2013, *Alzheimer's & Dementia*, 9, 63.
2. Prince, M., Comas-Herrera, A., Knapp, M., Guerchet, M., Karagiannidou, M. 2016, *World Alzheimer Report 2016: Improving healthcare for people living with dementia. Alzheimer's Disease International*.
3. Blennow, K., de Leon, M. J., Zetterberg, H. 2006, *Lancet*, 368, 387.
4. Nelson, P., Alafuzoff, I., Bigio, E., Bouras, C., Braak, H., Cairns, N., Castellani, R., Crain, B., Davies, P. 2012, *J. Neuropathol. Exp. Neurol.*, 71, 362.
5. Anand, R., Gill, K. D., Mahdi, A. A. 2014, *Neuropharmacology*, 76, 27.
6. Cavalli, A., Bolognesi, M. L., Minarini, A., Rosini, M., Tumiatti, V., Recanatini, M., Melchiorre, C. 2008, *J. Med. Chem.*, 51, 347.
7. Schmitt, B., Bernhardt, T., Moeller, H.-J., Heuser, I., Frölich, L. 2004, *CNS Drugs*, 18, 827.
8. Morphy, R., Rankovic, Z. 2005, *J. Med. Chem.*, 48, 6523.
9. Muñoz-Torrero, D. 2013, *Curr. Med. Chem.*, 20, 1621.
10. Bartus, R., Dean, R., Beer, B., Lippa, A. 1982, *Science*, 217, 408.
11. Francis, P., Palmer, A., Snape, M., Wilcock, G. 1999, *J. Neurol. Neurosurg. Psychiatry*, 66, 137.
12. Benzi, G., Moretti, A. 1998, *Eur. J. Pharmacol.*, 346, 1.
13. Anand, P., Singh, B. 2013, *Arch. Pharm. Res.*, 36, 375.
14. Sussman, J. L., Harel, M., Frolow, F., Oefner, C., Goldman, A., Toker, L., Silman, I. 1991, *Science*, 253, 872.

15. Dvir, H., Silman, I., Harel, M., Rosenberry, T. L., Sussman, J. 2010, *Chem. Biol. Interact.*, 187, 10.
16. Davis, K., Thal, L. J., Gamzu, E. R., Davis, C. S., Woolson, R. F., Gracon, S. I., Drachman, D. A., Schneider, L. S., Whitehouse, P. J., Hoover, T. M., Morris, J. C., Kawas, C. H., Knopman, D. S., Earl, N. L., Kumar, V., Doody, R. S. 1992, *N. Engl. J. Med.*, 327, 1253.
17. Knapp, M., Knopman, D., Solomon, P., Pendlebury, W., Davis, C., Gracon, S. 1994, *JAMA*, 271, 985.
18. Camps, P., Muñoz-Torrero, D. 2002, *Mini Rev. Med. Chem.*, 2, 11.
19. Badia, A., Baños, J. E., Camps, P., Contreras, J., Görbig, D. M., Muñoz-Torrero, D., Simón, M., Vivas, N. M. 1998, *Bioorg. Med. Chem.*, 6, 427.
20. Camps, P., El Achab, R., Görbig, D., Morral, J., Muñoz-Torrero, D., Badia, A., Baños, J. E., Vivas, N. M., Barril, X., Orozco, M., Luque, F. J. 1999, *J. Med. Chem.*, 42, 3227.
21. Muñoz-Torrero, D., Camps, P. 2008, *Expert Opin. Drug Discov.*, 3, 65.
22. Dvir, H., Wong, D.M., Harel, M., Barril, X., Orozco, M., Luque, F. J., Muñoz-Torrero, D., Camps, P., Rosenberry, T. L., Silman, I., Sussman, J. L. 2002, *Biochemistry*, 41, 2970.
23. Di Pietro, O., Pérez-Areales, F. J., Juárez-Jiménez, J., Espargaró, A., Clos, M. V., Pérez, B., Lavilla, R., Sabaté, R., Luque, F. J., Muñoz-Torrero, D. 2014, *Eur. J. Med. Chem.*, 84, 107.
24. Camps, P., Formosa, X., Galdeano, C., Muñoz-Torrero, D., Ramírez, L., Gómez, E., Isambert, N., Lavilla, R., Badia, A., Clos, M. V., Bartolini, M., Mancini, F., Andrisano, V., Arce, M. P., Rodríguez-Franco, M. I., Huertas, O., Dafni, T., Luque, F. J. 2009, *J. Med. Chem.*, 52, 5365.
25. Camps, P., Formosa, X., Galdeano, C., Gómez, T., Muñoz-Torrero, D., Ramírez, L., Viayna, E., Gómez, E., Isambert, N., Lavilla, R., Badia, A., Clos, M. V., Bartolini, M., Mancini, F., Andrisano, V., Bidon-Chanal, A., Huertas, Ó., Dafni, T., Luque, F. J. 2010, *Chem. Biol. Interact.*, 187, 411.
26. Di Pietro, O., Viayna, E., Vicente-García, E., Bartolini, M., Ramón, R., Juárez-Jiménez, J., Clos, M. V., Pérez, B., Andrisano, V., Luque, F. J., Lavilla, R., Muñoz-Torrero, D. 2014, *Eur. J. Med. Chem.*, 73, 141.
27. Mawuenyega, K. G., Sigurdson, W., Ovod, V., Munsell, L., Kasten, T., Morris, J. C., Yarasheski, K. E., Bateman, R. J. 2010, *Science*, 330, 1774.
28. Kung, H. F. 2012, *ACS Med. Chem. Lett.*, 3, 265.
29. Ghosh, A., Osswald, H. 2014, *Chem. Soc. Rev.*, 43, 6765.
30. Hong, L., Tang, J. 2004, *Biochemistry*, 43, 4689.
31. Lee, V. M.-Y., Goedert, M., Trojanowski, J. Q. 2001, *Annu. Rev. Neurosci.*, 24, 1121.
32. Iqbal, K., Alonso, A. C., Chen, S., Chohan, M. O., El-Akkad, E., Gong, C.-X., Khatoun, S., Li, B., Liu, F., Rahman, A., Tanimukai, H., Grundke-Iqbal, I. 2005, *Biochim. Biophys. Acta*, 1739, 198.
33. Bergen, M. V., Friedhoff, P., Biernat, J., Heberle, J., Mandelkow, E.-M., Mandelkow, E. 2000, *Proc. Natl. Acad. Sci. U.S.A.*, 97, 5129.

34. Clavaguera, F., Hench, J., Lavenir, I., Schweighauser, G., Frank, S., Goedert, M., Tolnay, M. 2014, *Acta Neuropathol.*, 127, 299.
35. Sanders, D., Kaufman, S., DeVos, S., Sharma, A., Mirbaha, H., Li, A., Barker, S., Foley, A., Thorpe, J., Serpell, L., Miller, T., Grinberg, L., Seeley, W., Diamond, M. 2014, *Neuron*, 82, 1271.
36. Pickhardt, M., Gazova, Z., Bergen, M. V., Khlistunova, I., Wang, Y., Hascher, A., Mandelkow, E.-M., Biernat, J., Mandelkow, E. 2005, *J. Biol. Chem.*, 280, 3628.
37. Bulic, B., Pickhardt, M., Schmidt, B., Mandelkow, E.-M., Waldmann, H., Mandelkow, E. 2009, *Angew. Chem. Int. Ed.*, 48, 1740.
38. Yang, X., Sun, G., Yang, C., Wang, B. 2011, *Chem. Med. Chem.*, 6, 2294.
39. Serrano, F. G., Tapia-Rojas, C., Carvajal, F. J., Cisternas, P., Viayna, E., Sola, I., Muñoz-Torrero, D., Inestrosa, N. C. 2016, *Curr. Alzheimer Res.*, 13, 1017.
40. Viayna, E., Sola, I., Bartolini, M., De Simone, A., Tapia-Rojas, C., Serrano, F. G., Sabaté, R., Juárez-Jiménez, J., Pérez, B., Luque, F. J., Andrisano, V., Clos, M. V., Inestrosa, N. C., Muñoz-Torrero, D. 2014, *J. Med. Chem.*, 57, 2549.
41. Rankovic, Z. 2015, *J. Med. Chem.*, 58, 2584.
42. Ginman, T., Viklund, J., Malmström, J., Blid, J., Emond, R., Forsblom, R., Johansson, A., Kers, A., Lake, F., Sehgelmeble, F., Sterky, K. J., Bergh, M., Lindgren, A., Johansson, P., Jeppsson, F., Fälting, J., Gravenfors, Y., Rahm, F. 2013, *J. Med. Chem.*, 56, 4181.
43. Rombouts, F., Tresadern, G., Delgado, O., Martínez-Lamenca, C., Gool, M. V., García-Molina, A., Alonso de Diego, S., Oehlrich, D., Prokopcova, H., Alonso, J. M., Austin, N., Borghys, H., Brandt, S. V., Surkyn, M., De Cleyn, M., Vos, A., Alexander, R., Macdonald, G., Moechars, D., Gijsen, H., Trabanco, A. 2015, *J. Med. Chem.*, 58, 8216.
44. Lerchner, A., Machauer, R., Betschart, C., Veenstra, S., Rueeger, H., McCarthy, C., Tintelnot-Blomley, M., Jatton, A.-L., Rabe, S., Desrayaud, S., Enz, A., Staufenbiel, M., Paganetti, P., Rondeau, J.-M., Neumann, U. 2010, *Bioorg. Med. Chem. Lett.*, 20, 603.
45. Ronco, C., Sorin, G., Nachon, F., Foucault, R., Jean, L., Romieu, A., Renard, P.-Y. 2009, *Bioorg. Med. Chem.*, 17, 4523.
46. Pérez-Areales, F. J., Betari, N., Viayna, A., Pont, C., Espargaró, A., Bartolini, M., De Simone, A., Rinaldi Alvarenga, J. F., Pérez, B., Sabate, R., Lamuela-Raventós, R. M., Andrisano, V., Luque, F. J., Muñoz-Torrero, D. 2017, *Fut. Med. Chem.*, 9, 965.
47. Sorkin, A., von Zastrow, M. 2002, *Nat. Rev. Mol. Cell Biol.*, 3, 600.
48. Zhang, X., Song, W. 2013, *Alzheimers Res. Ther.*, 5, 46.
49. Hook, V., Toneff, T., Aaron, W., Yasothornsrikul, S., Bunday, R., Reisine, T. 2002, *J. Neurochem.*, 81, 237.
50. Pérez-Areales, F. J., Di Pietro, O., Espargaró, A., Vallverdú-Queralt, A., Galdeano, C., Ragusa, I. M., Viayna, E., Guillou, C., Clos, M. V., Pérez, B., Sabaté, R., Lamuela-Raventós, R. M., Luque, F. J., Muñoz-Torrero, D. 2014, *Bioorg. Med. Chem.*, 22, 5298.

51. Wang, Y., Fan, X., Tang, T., Fan, R., Zhang, C., Huang, Z., Peng, W., Gan, P., Xiong, X., Huang, W., Huang, X. 2016, *Sci Rep.*, 30, 37098.
52. Vargas, F., Díaz, Y., Carbonell, K. 2004, *Pharm. Biol.*, 42, 342.



Research Signpost
Trivandrum
Kerala, India

Recent Advances in Pharmaceutical Sciences VIII, 2018: 59-78 ISBN: 978-81-308-0579-5
Editors: Diego Muñoz-Torrero, Yolanda Cajal and Joan Maria Llobet

4. Study of the transport of substances across the blood-brain barrier with the 8D3 anti-transferrin receptor antibody

Itsaso Cabezón¹, Elisabet Augé¹, Antoni Camins², Jordi Vilaplana¹
and Carme Pelegrí¹

¹Secció de Fisiologia, Departament de Bioquímica i Fisiologia, Facultat de Farmàcia i Ciències de l'Alimentació, Universitat de Barcelona

²Departament de Farmacologia, Toxicologia i Química Terapèutica, Facultat de Farmàcia i Ciències de l'Alimentació, Universitat de Barcelona

Abstract. Numerous strategies have been proposed to overcome the blood-brain barrier (BBB) and efficiently deliver therapeutic agents to the brain. One of these strategies consists of linking the pharmacologically active substance to a molecular vector that acts as a molecular *Trojan Horse* and is capable of crossing the BBB using a receptor-mediated transcellular transport system of the brain capillary endothelial cells (BCECs). The transferrin receptor (TfR) is related to a transcytosis process in these cells, and the 8D3 monoclonal antibody (mAb), directed against the mouse TfR, is able to induce a receptor response. Thus, the 8D3 antibody could be a potential molecular *Trojan Horse* to transport pharmacologically active substances across the BBB. On these bases, a series of experiments were performed where the 8D3 antibody was conjugated to different cargoes, the resulting constructs were administered *in vivo* to mice, and the

Correspondence/Reprint request: Dra. Carme Pelegrí, Secció de Fisiologia, Departament de Bioquímica i Fisiologia, Facultat de Farmàcia i Ciències de l'Alimentació, Universitat de Barcelona, Av. Joan XXIII 27-31, 08028 Barcelona. E-mail: carmepelegri@ub.edu

distribution and intracellular mechanisms that these constructs undergo at the BBB were studied. Our results indicated a TfR-mediated and clathrin-dependent internalization process by which the 8D3-cargo constructs enters the BCEC. The resulting endocytic vesicles follow at least two different routes. On one hand, most vesicles enter intracellular processes of vesicular fusion and rearrangement in which the cargo is guided to late endosomes, multivesicular bodies or lysosomes. On the other hand, a small but not negligible percentage of the vesicles follow a different route in which they fuse with the abluminal membrane and open towards the basal lamina, indicating a potential route for the delivery of therapeutic substances. In this route, however, the 8D3-cargo remain fixed to the abluminal membrane, indicating that the 8D3 is maintained linked to the TfR, and the cargo does not go beyond the basal membrane. Altogether, different optimization approaches need to be developed for efficient drug delivery, but receptor-mediated transport (RMT) continues to be one of the most promising strategies to overcome the BBB.

Introduction

The blood-brain barrier (BBB) is a well-coordinated and highly selective barrier whose main function is to regulate brain homeostasis and the transport of endogenous and exogenous substances between the blood and the brain. It permits the selective brain uptake of nutrients and impedes the entrance of potentially harmful substances and pathogenic organisms into the brain [1-3]. Due to this restrictive nature of the BBB, the transport of therapeutics from the blood to the brain results extremely difficult, and has become a major pharmaceutical challenge in recent decades [1]. Only lipophilic molecules with a molecular mass under a 400-600 Da threshold are capable of crossing the BBB [1, 4]. Moreover, efflux transport systems such as P-glycoprotein, which are present in the brain capillary endothelial cells (BCECs), are able to export some of these small drugs back to the blood [5]. Hence, 98% of all small drugs and almost 100% of large molecule drugs are unable to cross the barrier [6].

Different strategies have been proposed to transport neurotherapeutics from the blood into the brain, including the utilization of the receptor-mediated transport (RMT) mechanisms present in the BCECs [1, 7]. The transferrin receptor (TfR), which is abundant in brain capillaries [7], has been extensively studied. Some monoclonal antibodies (mAbs) directed against this receptor have shown to be useful tools for studying TfR-mediated transcytosis across the BBB in rodents, and have been proposed as possible vectors or molecular *Trojan Horses* to transport substances across the BBB [8-14]. Some studies have concluded that anti-TfR mAbs accumulate in BCECs and do not cross the BBB, while other

studies, most of which have used the capillary depletion method or indirect outcome measures such as protein expression or enzymatic activity, have concluded that mAbs and/or their cargo are successfully transported across the BBB [8, 12, 14-16]. Thus, whether or not mAbs directed against the TfR undergo receptor-mediated transcytosis remains unclear (Figure 1).

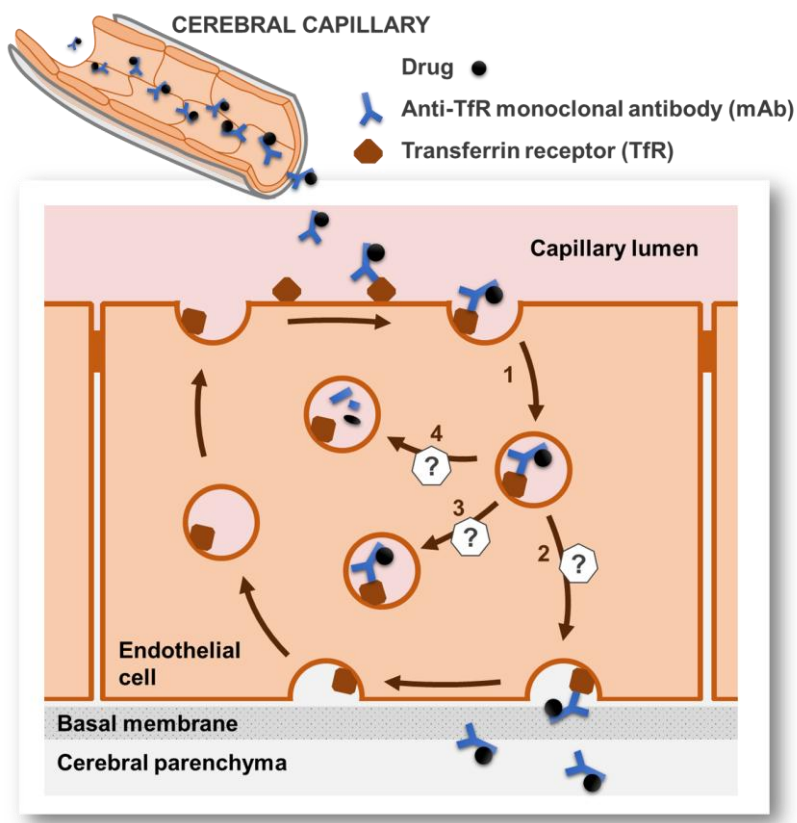


Figure 1. The proposed model for the transport of drugs across the BBB using RMT and anti-TfR mAbs includes: 1) the endocytosis of the drug-mAb/TfR on the luminal membrane and 2) the exocytosis of the mAb-drug on the basolateral membrane and receptor recycling. However, other possible destinations for the drug-mAb/TfR complex can be possible, as: 3) accumulation of the drug-mAb/receptor complex inside the BCEC, and 4) mAb and drug degradation.

The rat mAb 8D3, directed against the mouse TfR, has been proposed as a potential carrier candidate to transport substances across the mouse BBB. This mAb was first produced by Britta Engelhardt's research group in the Max Planck Institute (Bad Nauheim, Germany) [11], and some active substances that have been used as a cargo, seemed to achieve better results in crossing the BBB when attached to the 8D3 [14, 17-21]. However, the intracellular mechanisms the mAb or the mAb-cargo construct undergo inside BCECs still need to be elucidated.

The lack of more exhaustive analysis by means of microscopic techniques that allow the detection and direct localization of the mAb and / or cargo at a cellular and subcellular level, as well as the existing unknowledge regarding the cellular and intracellular processes that take part in the processing of these molecular *Trojan Horses* at the BBB level, have been the basis for the approach of this work.

In order to test the viability of the 8D3 as a potential carrier, a series of experiments were performed where the 8D3 antibody was conjugated to different cargoes, the resulting constructs were administered *in vivo* to mice, and the distribution and intracellular mechanisms that these constructs undergo at the BBB were studied.

1. The 8D3 antibody is able to recognize TfR and trigger the internalization of the cargo which is conjugated to [adapted from 22]

First of all, in order to test the reactivity of the 8D3 antibody for the TfR present in the luminal membrane of the BCECs, an immunohistochemical procedure was applied using 8D3 as the primary antibody on cryostat sections of mouse brain (male ICR-CD1). As expected, the staining permitted the visualization of brain capillaries (Figure 2A), where the BBB is present and the TfR is localized in the endothelial cells, but did not allow to visualize the vessels of the choroid plexus, in which the capillaries are fenestrated and the endothelial cells do not present TfR.

The second step was to test whether this antibody could be detected in brain capillaries after *in vivo* administration. For this purpose, a second group of animals underwent i.v. administration of 8D3 antibody in the caudal vein, and after 20 min of recirculation, brain samples were taken and localization of the 8D3 was determined via immunohistochemical techniques. The results showed that, in the same regions observed by direct immunohistochemistry, the brain capillaries contained the 8D3 antibody (Figure 2B1 and 2C1). They were stained with only the secondary antibody directed against 8D3, indicating that intravenously administered 8D3

antibody reaches and attaches to the BCECs. A simultaneous staining performed with laminin (a component of the basal membrane used to delimit the abluminal wall of the capillaries) showed that the laminin staining surrounded the 8D3 staining, suggesting that the antibody does not complete transcytosis, is unable to reach the cerebral parenchyma and remains inside the endothelial cell (Figure 2C3). It can also be observed that the 8D3 antibody presented a granular pattern (Figure 2C1 inset), which contrasted with the fine and smooth staining of the laminin (Figure 2C2 inset). This granular pattern suggested some endocytic process by which the antibody could have been internalized inside the BCEC.

After observing that the intravenously administered 8D3 antibody can be localized in the wall of the brain capillaries, our next goal was to develop an immunocomplex (IC) composed of the 8D3 antibody (molecular *Trojan Horse*) and Fab' fragments (that simulated a cargo) attached to the 8D3, and study the capacity of this antibody to transport the Fab' fragment across the BBB. A third group of animals received an i.v. injection of the 8D3-Fab' ICs in the optimal proportions established previously (1:4 weight/weight 8D3/Fab'). After different times of recirculation (2.5 h and 24 h, as 20 min seemed not enough to allow the mAb to cross the BBB),

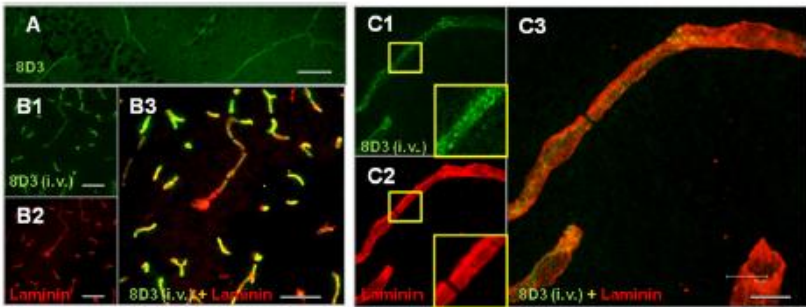


Figure 2. (A) Immunohistochemical labeling of mouse brain sections with the primary rat 8D3 MAb targeting murine TfR and the secondary AF488 anti-rat IgG (green color). (B and C) Brain sections from a representative mouse which received the 8D3 antibody intravenously. The sections were stained with an anti-laminin antibody as a primary, and both the AF555 (red color) and the AF488 anti-rat IgG (green color) as secondary antibodies to detect, respectively, the anti-laminin antibody and the administered 8D3. It can be observed that, after intravenous administration of 8D3, the antibody could be found in brain capillaries but not in parenchyma. The granular pattern of the 8D3 staining (C1 inset) contrasts with the uniform staining of the laminin (C2 inset). Scale bars: 10 μm . [adapted from 22].

brains were obtained in order to study the localization and colocalization of both components of the IC by immunohistochemistry. Using a fluorescence microscope, we observed that both components localized in the wall of the capillaries (Figure 3A1 and 3A2), with a clear granular pattern and high colocalization between the two stains (Figure 3A3), indicating that both components of the IC remain attached or at least where in the same endosomal compartment. The simultaneous staining with laminin (Figure 3B and C) demonstrated that both 8D3 and Fab' cargo get externally delimited by this marker. In control animals that received an i.v. injection of an IC formed by nonspecific rat IgG and Fab' fragments, also in a 1:4 ratio, neither

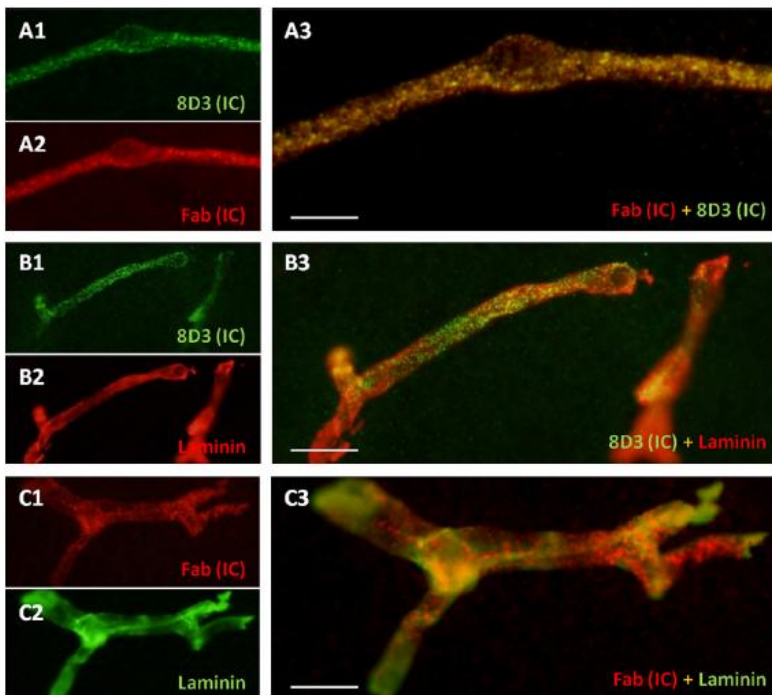


Figure 3. Localization of the components of the IC (8D3:Fab' 1:4) in brain capillaries of the hippocampus. (A) Localization of the 8D3 antibody with a secondary AF488 (green color) and of Fab' components with a secondary AF555 (red color). High colocalization (yellow color) of 8D3 and Fab' can be observed, and both components exhibit a granular pattern. (B and C) Simultaneous staining of laminin and 8D3 or Fab' components. 8D3 and Fab' seem to be localized inside the region delimited by the basal lamina. Scale bars: 10 μ m. [adapted from 22].

the IgG nor the Fab' staining was observed in brain sections, hence indicating that the IC is not retained in the BCECs if it does not include an antibody directed against the TfR.

In order to study the maintenance and stability of the IC in the wall of the blood vessels through the different recirculation times tested (2.5 h vs 24 h), we used the Fluorescence Resonance Energy Transfer (FRET) technique. As the ICs are formed by 8D3 rat IgG and goat anti-rat IgG Fab' fragments, they can be simultaneously immunostained with AF488 donkey anti-rat IgG and AF555 donkey anti-goat IgG. Microscope images of AF488 emission (green color) directly stimulated by its excitation frequency (blue color), were taken before and after bleaching AF555. When AF555 is bleached, it is incapable of capturing the emission of the AF488 that is emitted near to it (energy transfer), and thus, the detection of the donor emission is increased with respect to the initial conditions (Figure 4).

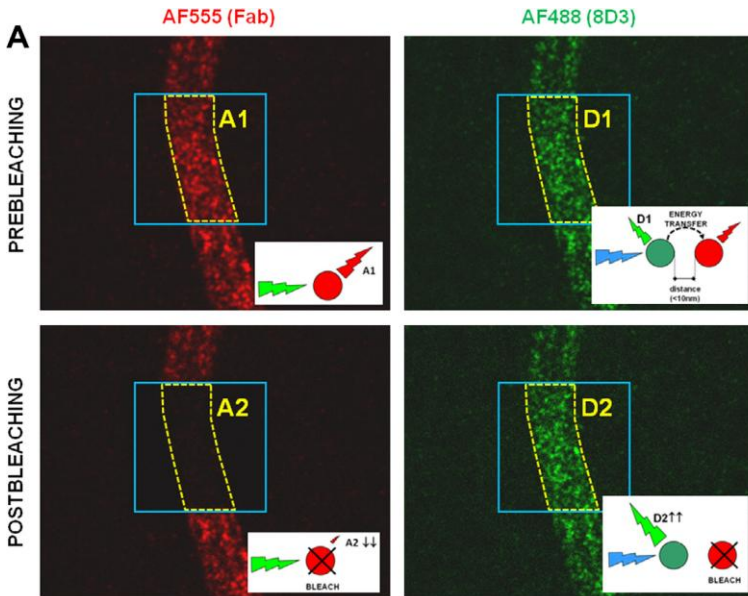


Figure 4. Process performed for one blood capillary using the FRET technique. When AF555 is bleached, it is incapable of capturing the green emission of the AF488 that is emitted near to it (energy transfer), and thus the observed donor emission (D2) after bleaching the AF555 is bigger than before bleaching (D1). A: acceptor emission, D: donor emission, 1: before bleaching, 2: after bleaching [adapted from 22].

Thus, by quantifying the increase of the detected donor emission, an indication of the number of molecules implicated in the energy transfer, i.e. molecules of AF488 and AF555 that are near one to the other, can be obtained. Statistical analysis indicated that the time of recirculation had a significant effect on the increase of the detected donor emission, being the increase higher in animals that were sacrificed 2.5 h after IC administration than in animals sacrificed 24 h later. As AF488 and AF555 stain respectively the 8D3 and the Fab' fragments, the increases also indicate the amount of 8D3 and Fab' fragments that persist attached on the original ICs. Thus, the colocalization of the fluorescent signals inside the endothelial cells decreased with time, indicating that ICs are processed and Fab' fragments probably separated from 8D3.

On the other hand, in order to directly visualize the 8D3 antibody and avoid the immunohistochemical processing, a fourth group of animals received an i.v. injection of 8D3 previously marked with fluorescein isothiocyanate (8D3^{FITC}). Likewise, another group of animals underwent i.v. administration of 8D3-Fab' ICs with FITC attached to Fab' (8D3-Fab'^{FITC}). Both 8D3^{FITC} (Figure 5) and 8D3-Fab'^{FITC} (data not shown) showed similar staining patterns in comparison with the anterior cases, being once again externally delimited by the laminin. However, a higher signal amplification was observed in the case of the 8D3-Fab'^{FITC} with respect to 8D3^{FITC}, probably due to a bigger amount of FITC per 8D3 molecule.

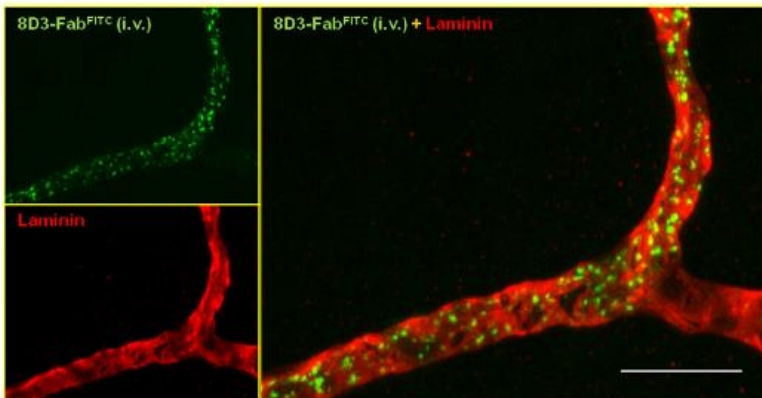


Figure 5. Localization of intravenously administered 8D3-Fab'^{FITC} (green color) and immunohistochemical staining with a primary antibody against laminin and secondary AF555 anti-rabbit IgG (red color) in brain capillaries of the hippocampus. The fluorescence of the administered IC is confined to the region delimited by laminin. Scale bar: 10 μ m [adapted from 22].

As concluding remarks, we observed that the 8D3 antibody, with or without a cargo attached, is able to bind the TfR present in the luminal membrane of the BCECs and gets retained in these cells, probably in intracellular vesicles. Inside these cells, some kind of IC processing is produced, and after 24 h of recirculation, there were less Fab' fragments near the 8D3 molecules than after 2.5 h of recirculation. In any case, the components of the IC were never observed beyond the basal membrane or reaching the brain parenchyma. Thus, nor the 8D3 neither the IC seem to have completed transcytosis. These results cast doubt on the transcytotic capacity of the 8D3 antibody, and contradict previous studies that advocate an efficient transcytosis. However, the highest magnification level the optical microscopy allows us to work with, is perhaps not enough to draw a reliable conclusion, and we cannot rule out that an undetectable amount of antibody could have crossed the BBB.

2. 8D3-cargo constructs at the BBB: Intracellular mechanisms and subcellular localization [adapted from 23]

In view of the results obtained, the next step to move along in the study of the 8D3 antibody was to monitor in a more precise way the antibody localization and clarify which intracellular processes take part at the BBB.

For this purpose, gold nanoparticles (AuNPs) were coated with the 8D3 antibody, and using transmission electron microscope (TEM) techniques, the passage of these AuNPs across the BBB and their dynamics inside BCECs after *in vivo* administration were studied in mice. AuNPs not only can be directly observed by TEM, but also can be considered as the cargo to be transported by the 8D3. To form the 8D3-AuNP conjugates, the 8D3 antibody was covalently attached to AuNPs measuring 20 nm in diameter. The 8D3:AuNP ratio for the conjugates was approximately of 30:1. The conjugate was intravenously administered to ICR-CD1 mice that were distributed into four different groups, each of them with a different time of recirculation (10 min, 30 min, 2.5 h and 24 h). Once the corresponding time had passed, animals were anesthetized and intracardially perfused with paraformaldehyde and glutaraldehyde, and brains were then removed and processed for TEM.

Image analysis permitted the study of the AuNP localization at a subcellular level and at the different times of recirculation. The localization patterns varied over time. At the shortest time of recirculation (10 min), the AuNPs were mostly attached to the lumen of the capillary, in clathrin-coated pits or internalized in endocytic vesicles of the endothelial cells that

contained one or few AuNPs inside. The 8D3-AuNP conjugates are individually internalized, as no clathrin-coated pits containing more than one AuNPs were observed. No AuNPs were observed in the brains of the control mice, which had been administered with intravenous non-specific IgG-AuNP conjugate, confirming that the internalization depended on the presence of the 8D3. At 30 min of recirculation, the percentage of AuNPs yet to be internalized had decreased, and some of the intracellular vesicles contained a higher number of AuNPs. At the highest times of recirculation (2.5 h and 24 h), almost a 100% of the AuNPs observed had already been internalized in the BCECs, and many of the AuNP-containing vesicles had a higher number of particles inside them (up to 23 AuNPs in two cases). Some of the AuNPs were found in the basal lamina of the endothelium, bordering the abluminal membrane of the BCECs, which would suggest that 8D3-AuNP complex had completed transcytosis but remained attached to the TfR. Most of these AuNPs were observed at 2.5 h of recirculation, being 4.6% the percent respect to the total number of the AuNPs observed at this time (Figure 6).

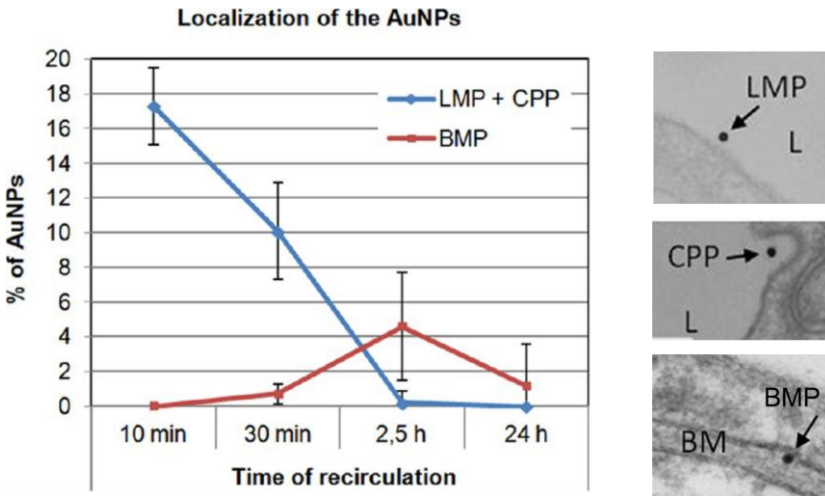


Figure 6. Percentage of AuNPs on the luminal surface [i.e. particles attached to the luminal membrane (LMP) and particles in clathrin-coated pits (CPP)] and basal membrane (BMP) for each recirculation time. Mean values and standard errors are shown. L: Lumen; BM: basal membrane. At 2.5 h of recirculation, all particles have been internalized, and the maximum percentage of particles that reach the basal membrane is obtained [adapted from 23].

Thus, at the shortest times of recirculation (10 min and 30 min), the predominant localization patterns were the lumen of the capillary, the clathrin-coated pits and the endocytic vesicles containing small amounts of AuNPs. Apart from the AuNPs that reach the basal lamina, the number of AuNPs per vesicle increased over time, so that at the longer times of recirculation, the vesicles containing high amounts of AuNPs was the main localization pattern (Figure 7).

The quantitative analysis performed with the data obtained permitted to establish and characterize a time-dependent trafficking pattern of endocytic internalization and endosomal processing of the conjugate at the BBB (Figure 8). The 8D3-AuNP conjugates are individually internalized within BCECs through a clathrin-dependent endocytosis process. The resulting AuNP-containing vesicles then follow at least two different routes. On one hand, most vesicles undergo intracellular processes of vesicular fusion and rearrangement in which the AuNPs end up accumulating in late endosomes, multivesicular bodies or lysosomes, which present a high AuNP content.

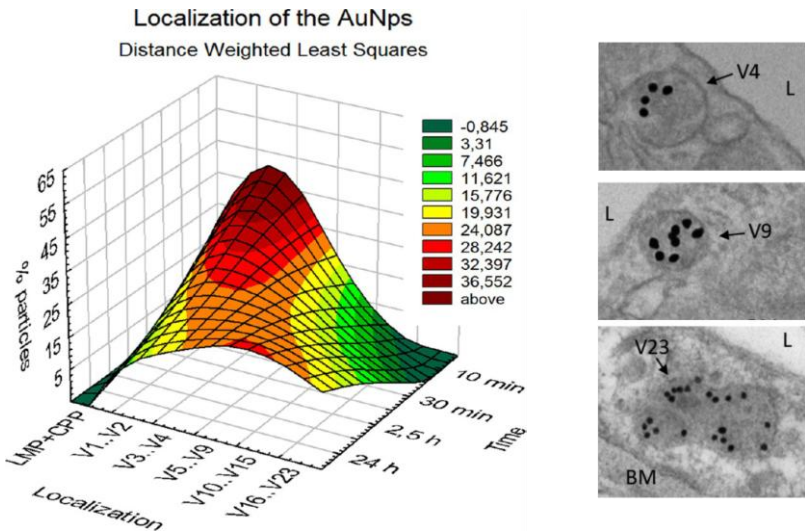


Figure 7. 3D contour graph obtained by adjusting, with distance weighted least-squares, the percentage of particles to the localization and the recirculation time. LMP: particles sited on luminal membrane; CPP: coated pit particles; V_i : vesicle containing i AuNPs. Particles sited on basal membrane are not plotted. L: Lumen; BM: basal membrane [adapted from 23].

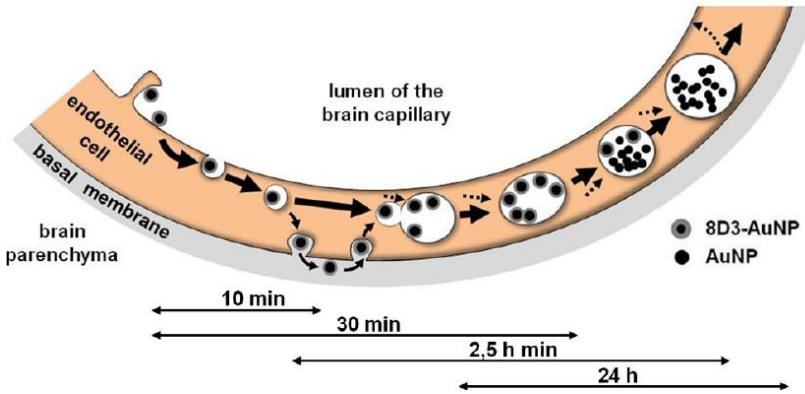


Figure 8. Deduced trafficking of the 8D3–AuNPs across the mouse BBB [adapted from 23].

On the other hand, a small percentage of vesicles (containing just one AuNP) follow a different route in which they fuse with the abluminal membrane and open to the basal lamina, which suggests an endosomal escape and transcytosis completion. However, the conjugates get retained in the basal lamina and do not reach the brain parenchyma.

Given the controversy regarding the possible use of anti-TfR antibodies to transport substances across the BBB, this study provided new information that may clarify some questions that are yet to be answered concerning the dynamics and intracellular processes the cargo undergo when coated with the 8D3 antibody. The results suggest that the 8D3 antibody may be a useful *Trojan Horse* to transport substances toward the BCECs. The 8D3 is able to drive the cargo to the brain capillaries and internalize it into the BCECs. This makes that a considerable amount of the intravenously administered cargo gets retained in the cerebral area instead of targeting another tissues or organs, and moreover, it makes the cargo to overcome the first barrier (the luminal membrane) reaching the inside of the endothelial cells. Although the cargo is mainly retained inside the BCEC, a small but not negligible percentage of particles escape from the conventional endosomal route, complete transcytosis and access the basal lamina, probably as a result of a different and uncommon endosomal sorting. This small percentage do not reach the brain parenchyma, perhaps due to the strong bond between the 8D3 and the TfR. Nevertheless, it should not be considered impossible for the cargo to reach the brain parenchyma once it has reached the basal lamina if

the linkage between the *Trojan Horse* and the transported cargo had properties that permitted the cargo to dissociate from the carrier.

3. Serial block-face scanning electron microscopy: A tool to three-dimensionally study the trafficking of mAb-cargo conjugates at the BBB [adapted from 25]

The results obtained by TEM provided relevant information at an ultrastructural level concerning the dynamics of the AuNPs when transported by the 8D3 antibody after *in vivo* administration. However, the two-dimensional (2D) image analysis entailed a series of limitations that we decided to overcome by carrying out a three-dimensional (3D) structural study that could give more insight into the transport of molecules across the BBB, and more knowledge on the trafficking of the AuNPs.

Serial block-face (SBF) imaging is a recently developed imaging technique that uses scanning electron microscopy (SEM) to acquire serial images and reconstruct large tissue regions in 3D [24]. In SBF-SEM, surface areas of the embedded tissue blocks are serially cut and removed with the built-in diamond knife in the SEM chamber between the cycles of SEM imaging. Because the consecutive areas of tissue are imaged with surface milling, this method generates largely pre-aligned images, which speeds up 3D reconstruction of the target structures. The objective of this work was first to determine whether the SBF-SEM resulted appropriate to reconstruct BBB segments and AuNP-containing endocytic vesicles, and if so, try to obtain additional information that would complement our previous 2D studies. This technique has been extensively used to explore the connectivity of the neural network, but only rarely to study the structure of the BBB, and no SBF-SEM data exist on the transport of molecules across this barrier.

To this end, we performed the same experimental design as for the 2D TEM study, but it was only reproduced at 2.5 h of recirculation (the time of recirculation where more diverse localization patterns were observed). After the mice brains were processed for SBF-SEM, the stained blocks were imaged using a Gatan 3View serial block-face imaging system installed on a FEI Quanta 250 FEG scanning electron microscope. The resulting datasets were assembled into volume files and aligned. 3D reconstruction of the desired structures was performed in image stacks using Imaris 8.0.2 and Imaris 7.2 software.

In a first attempt to perform a 3D reconstruction of the BBB and to observe the localization of the AuNPs, capillary segments (up to 10 μm long

along the z axis) from different brain samples were fully 3D rendered using low-magnification image stacks (10,000-25,000 \times). These image stacks were obtained using an incident electron beam with an energy of 2.3-2.4 kV and spot size 3, and a chamber pressure of 50 Pa was applied to scan across the samples at a pixel dwell time of 60 μ s. This level of magnification allowed us to identify the cellular components that form the neurovascular unit, such as BCECs, the basal lamina, pericytes, astrocytes, and three-dimensionally reconstruct them by manually tracing the area in each plane and surface rendering next (Figure 9). However, the AuNPs could not be clearly visualized, neither inside nor outside endocytic vesicles. This was due, on one hand, to the low resolution in the *x-y* plane, and on the other hand, due to the backscattered electron signal. Moreover, it must be pointed that the presence of bare resin in the lumen of the capillary caused electrical charging of the sample, and consequently, tissue deterioration or breakage.

Due to these technical problems, a second attempt with higher magnification imaging (>30,000 \times) of the capillary segments was considered, avoiding the inclusion of the whole lumen in the region of interest (ROI). We used an incident electron beam with an energy of 3.5 kV and spot size 3, and a chamber pressure of 50 Pa was applied to scan across the samples at a pixel dwell time of 60 μ s. At this level of magnification, BCEC segments and the basal lamina of the endothelium could be observed, as well as both the vesicles inside the BCECs and the AuNPs contained in them. The sequential images in the stack allowed us to 3D render structures such as the basal lamina or the vesicles located inside the BCECs by manually tracing the area in consecutive planes (Figure 10). Although the AuNPs were visible, due to their small size, it was impossible to 3D render them using this method; they are located in one or another section, but never in more than one, so it was impossible to reconstruct these particles in 3D by manually tracing the area across consecutive planes. Thus, a copy of the stack was preprocessed using the Fiji software to later replace the AuNPs in each section by 3D spheres of similar size (20 nm diameter) in Imaris. Since the AuNPs are the darkest structures in these images, they could be segmented with the Fiji software using a low threshold value. After segmentation, the resulting binary particles were split using a watershed to allow individual reconstruction. The final binary stack of images was loaded into Imaris as an additional channel of the original stack and the AuNPs were rendered as spheres in the final 3D reconstruction.

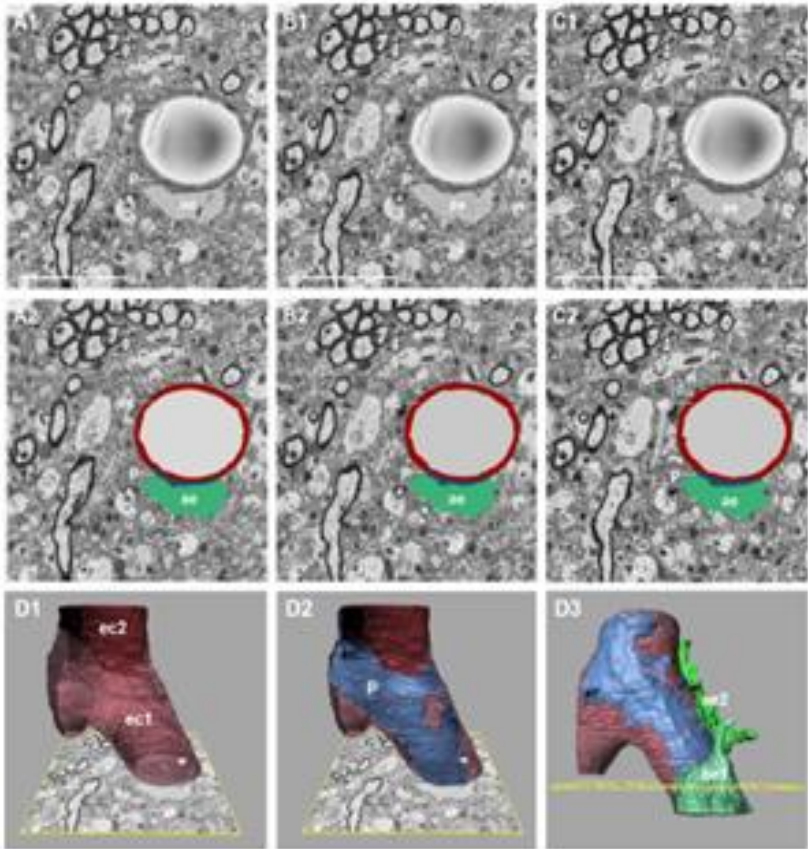


Figure 9. (A1-C1) Three selected serial images from an SBF-SEM low-magnification image stack. (A2-C2) Colored areas represent some of the structures that were selected and manually traced in A1-C1, respectively, for the subsequent 3D reconstruction. (D1-D3) Three snapshots of the video showing the 3D reconstruction: (D1) Two adjacent endothelial cells (ec1 and ec2) can be observed. Image B1 is superimposed on the reconstruction. (D2) A pericyte rendering is added to the reconstruction. (D3) The complete 3D reconstruction of the BBB segment, which includes the renderings of the two adjacent endothelial cells, the pericyte and two astrocytic endfeet (ae1 and ae2). Ec: endothelial cell; p: pericyte; ae: astrocytic endfeet. Scale bar: 5 μm [adapted from 25].

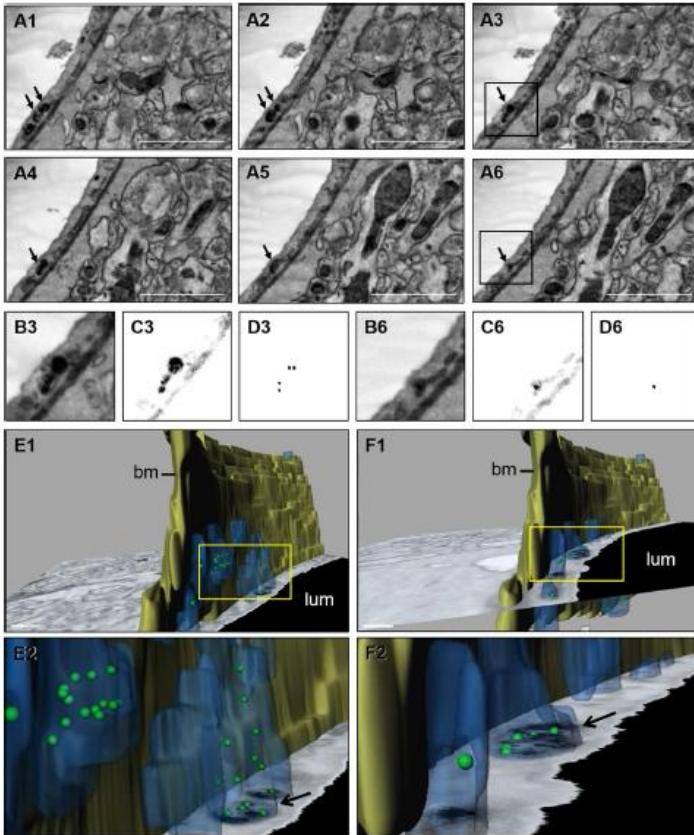


Figure 10. (A1-A6) Six selected serial images from an SBF-SEM high-magnification image stack. Arrows indicate the same vesicle sectioned on different planes. (B3-B6) Original insets from A3 and A6, respectively, in which the brightness and contrast have been modified to enhance visualization of the AuNPs. (D3 and D6) Images corresponding, respectively, to the insets from A3 and A6 that were obtained after applying the process of binarization, which permits to localize the AuNPs. (E1 and F1) Representative images of the 3D reconstruction of the SBF-SEM high-magnification image stack that contains images A1-A6. AuNPs are represented as green spheres. Blue regions are the endothelial vesicles. bm: basal lamina; lum: lumen of the capillary. (E2 and F2) Insets from E1 and F1, respectively. Arrow in E2 indicates some AuNPs that have lost the connection with the vesicular membrane, while in F2 it shows some ones in which the connection is maintained. Scale bar: 2 μm [adapted from 25].

Thus, this level of magnification and this strategy allowed for reliable 3D reconstructions in which the structures of the BBB, such as the basal lamina of the endothelium and the vesicles located in the BCECs, as well as the precise location of the AuNPs could be visualized simultaneously (Figure 10).

Regarding the shape of the vesicles, the 3D reconstruction allowed us to observe that although some of the AuNP-containing vesicles present a spherical or ellipsoidal form, they are often branched structures with irregular shapes, which sometimes even seem to merge with each other forming a complex endosomal network. As can be observed in Figure 10, some vesicles that show a spherical or ellipsoidal shape in a 2D plane can be considered part of a complex and irregular when subsequent sections are analyzed as a whole 3D structure.

We can conclude from this work that low-magnification imaging permits acquiring images of a large field of view and monitoring of relatively long capillary segments (more than 10 μm long), so that results appropriate for the identification and 3D reconstruction of cellular elements and some subcellular elements as nuclei. However, this resolution was too low for clear identification of the AuNPs. This led us to increase the level of magnification and re-establish the setting parameters for the SBF-SEM system. A higher accelerating voltage allowed the acquisition of higher magnification images, with sufficient resolution for AuNP visualization. We therefore achieved the goal of 3D reconstructing BBB segments and AuNP-containing vesicles, as well as precisely localizing the AuNPs within the cellular structures. We observed that the vesicles containing AuNPs are often branched structures with irregular shapes, which sometimes even seem to merge with each other forming a complex endosomal network. Moreover, we applied an innovative method by which the AuNPs were replaced by 3D spheres of similar size at the exact same coordinates inside the tissue volume.

4. Conclusion

Altogether, the different studies exposed in the present work, allowed us to clarify some doubtful aspects concerning the transport of drugs across the BBB using RMT and anti-TfR mAbs. These aspects, which are summarized in Figure 11, permit to conclude that:

1. The 8D3 antibody is capable of recognizing and binding to the TfR present in the luminal membrane of brain capillary endothelial cells following *in vivo* administration.
2. The 8D3 antibody is internalized inside the brain capillary endothelial cells after its binding to the TfR.
3. The 8D3 antibody is able to trigger the internalization of the cargo which is conjugated to, overcoming the first obstacle in the transport across the brain capillary endothelial cells.
4. The internalized cargo can vary in size and nature, ranging from proteins like the Fab' fragments of antibodies to larger particles like AuNPs measuring 20 nm in diameter.
5. The internalization of 8D3 and its cargo is produced by a clathrin-dependent endocytosis process.
6. Most of the resulting endocytic vesicles undergo a process of fusion, maturation and reorganization in which the 8D3-cargo complexes that are inside them progressively accumulate in endosomal networks of great complexity.
7. During the processing of these vesicles the interaction between TfR, 8D3 and/or cargo is lost.
8. Nonetheless, some endocytic vesicles containing the 8D3-cargo complexes complete transcytosis.
9. These vesicles fuse with the basolateral membrane and open up to the basal lamina.
10. When fused with the basolateral membrane, the 8D3-cargo complexes become exposed to the basal lamina.
11. Exposed 8D3-cargo complexes remain attached to the TfR and fail to go beyond the basal lamina.
12. In order to facilitate the cargo liberation to the brain parenchyma, it is necessary to modify and optimize the linkages between the 8D3 and the cargo and/or the linkage between the 8D3 and the TfR.
13. Although some improvements at the design level of the constructs are needed, the use of the RMT system and mAbs directed against transcytosis receptors is a strategy with great potential for transporting drugs through the BBB.

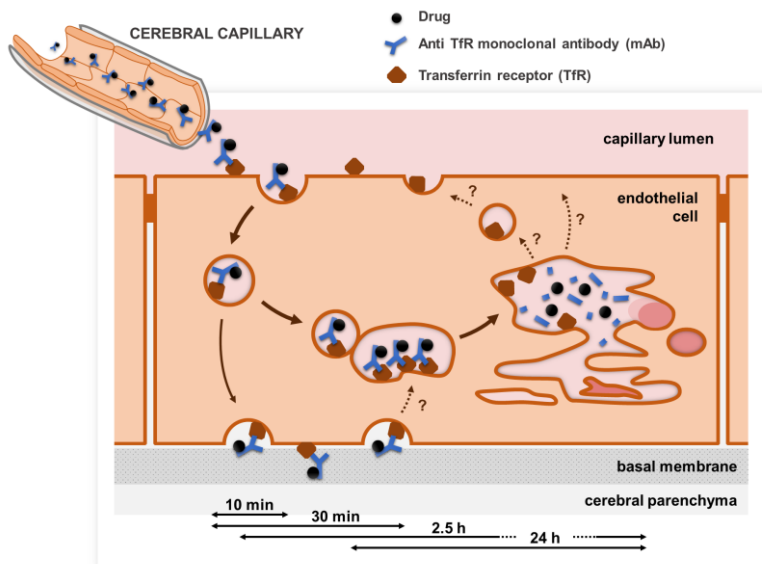


Figure 11. State of the art of both the transport of drugs across the BBB using anti-TfR mAbs and the possible destinations for the drug-mAb/TfR complexes.

Acknowledgements

This work is a summary of the doctorate thesis of Itsaso Cabezón, carried out in the Blood Brain Barrier Research Group from the Universitat de Barcelona (<http://hdl.handle.net/2445/110075>).

References

1. de Boer, A. G., Gaillard, P. J. 2007, *Annu. Rev. Pharmacol. Toxicol.*, 47, 323.
2. Correale, J., Villa, A. 2009, *Neurochem. Res.*, 34, 2067.
3. Chen, Y., Liu, L. 2012, *Adv. Drug Deliv. Rev.*, 64, 640.
4. Pardridge, W. M. 1998, *J. Neurochem.*, 70, 1781.
5. Begley, D. J. 1996, *J. Pharm. Pharmacol.*, 48, 136.
6. Pardridge, W. M. 2005, *NeuroRX*, 2, 3.
7. Scherrmann, J. M. 2002, *Vasc. Pharmacol.*, 38, 349.
8. Jefferies, W. A., Brandon, M. R., Hunt, S. V., Williams, A. F., Gatter, K. C., Mason, D. 1984, *Nature*, 312, 162.
9. Friden, P. M., Walus, L. R., Musso, G. F., Taylor, M. A., Malfroy, B., Starzyk, R. M. 1991, *Proc. Natl. Acad. Sci. U. S. A.*, 88, 4771.

10. Moss, T. 1996, *J. Comp. Neurol.*, 375, 675.
11. Kissel, K., Hamm, S., Schulz, M. 1998, *Histochem. Cell Biol.*, 110, 63.
12. Lee, H. J., Engelhardt, B., Lesley, J., Bickel, U., Pardridge, W. M. 2000, *J. Pharmacol. Exp. Ther.*, 292, 1048.
13. Moos, T., Morgan, E. H. 2001, *J. Neurochem.*, 79, 119.
14. Zhang, Y., Pardridge, W. M. 2005, *J. Pharmacol. Exp. Ther.*, 313, 1075.
15. Shi, N., Pardridge, W. M. 2000, *Proc. Natl. Acad. Sci. U. S. A.*, 97, 7567.
16. Alata, W., Paris-Robidas, S., Emond, V., Bourasset, F., Calon, F. 2014, *Mol. Pharmaceutics*, 11, 243.
17. Shi, N., Zhang, Y., Zhu, C., Boado, R. J., Pardridge, W. M. 2001, *Proc. Natl. Acad. Sci. U. S. A.*, 98, 12754.
18. Lee, H. J., Zhang, Y., Zhu, C., Duff, K., Pardridge, W. M. 2002, *J. Cereb. Blood Flow Metab.*, 22, 223.
19. Zhu, C., Zhang, Y., Zhang, Y. F., Li, J. Y., Boado, R. J., Pardridge, W. M. 2004, *J. Gene Med.*, 6, 906.
20. Rivest, V., Phivilay, A., Julien, C., Bélanger, S., Tremblay, C., Émond, V., Calon, F. 2007, *Pharm. Res.*, 24, 981.
21. Boado, R. J., Zhang, Y., Wang, Y., Pardridge, W. M. 2009, *Biotechnol. Bioeng.*, 102, 1251.
22. Manich, G., Cabezón, I., Del Valle, J., Duran-Vilaregut, J., Camins, A., Pallàs, M., Pelegrí, C., Vilaplana, J. 2013, *Eur. J. Pharm. Sci.*, 49, 556.
23. Cabezón, I., Manich, G., Martín-Venegas, R., Camins, A., Pelegrí, C., Vilaplana, J. 2015, *Mol. Pharmaceutics*, 12, 4137.
24. Ohno, N., Katoh, M., Saitoh, Y., Saitoh, S., Ohno, S. 2015, *Microscopy*, 64, 17.
25. Cabezón, I., Augé, E., Bosch, M., Beckett, A. J., Prior, I. A., Pelegrí, C., Vilaplana, J. 2017, *Histochem. Cell Biol.*, 148, 3.



Research Signpost
Trivandrum
Kerala, India

Recent Advances in Pharmaceutical Sciences VIII, 2018: 79-93 ISBN: 978-81-308-0579-5
Editors: Diego Muñoz-Torrero, Yolanda Cajal and Joan Maria Llobet

5. Evaluation of anti-inflammatory activity of food compounds using zebrafish

Cristina Arteaga*, Núria Boix, Marta Barenys, Joan M. Llobet
and Jesús Gómez-Catalán

Department of Pharmacology, Toxicology & Therapeutic Chemistry, INSA, Faculty of Pharmacy & Food Sciences, University of Barcelona. Av. de Joan XXIII, 27-31, 08028 Barcelona, Spain.

**Present address: Facultad de Ciencia e Ingeniería en Alimentos, Universidad Técnica de Ambato
Av. Los Chasquis y Río Payamino S/N Ambato, Ecuador*

Abstract. The principal aim of this work was to optimize and apply a zebrafish experimental model for the screening of anti-inflammatory substances present in the Mediterranean diet. The zebrafish is an organism widely used in various fields of experimental biology. The inflammation is easily inducible, reproducible and visualized in their early stages of development. Specifically, the migration of neutrophils to the injured caudal fin, one of the first steps of the inflammatory response, is quantitatively measured by image analysis. The anti-inflammatory effect of natural compounds can be evaluated as a decrease of migration. Adverse effects triggered by inflammation are mainly mediated by reactive oxygen species. The anti-oxidant activity of compounds was evaluated in zebrafish embryo measuring their protective effect against tert-butyl hydroperoxide toxicity. Several phenolic compounds have been assayed. Our results showed that the compounds with the greatest decrease on neutrophil migration were chlorogenic acid and cyanidin. The activity of these two polyphenols

Correspondence/Reprint request: Dr. Marta Barenys, Department of Pharmacology, Toxicology & Therapeutic Chemistry, Faculty of Pharmacy & Food Sciences, University of Barcelona. Av. de Joan XXIII, 27-31, 08028 Barcelona, Spain. E-mail: mbarenys@ub.edu

was quite similar to that observed with anti-inflammatory drugs (indomethacin, piroxicam) and NADPH oxidase inhibitor compounds (dibenzoidolium, apocynin). The anti-inflammatory and the anti-oxidant activity of the assayed polyphenols did not show a clear correlation.

Introduction

Nutrition is one of the main determinants of health. Multiple studies show that a balanced diet contributes to the prevention of numerous diseases. Specifically, the so-called "Mediterranean diet" has been associated with benefits in the prevention of many of the most prevalent chronic diseases in Western societies; it is known that the Mediterranean diet provides important dietary components such as carotenoids and phenolic compounds, which can contribute to reduce the risk of developing different pathologies [1].

Many of these chronic diseases (cardiovascular, metabolic, neurodegenerative) have an important component of inflammatory type in their etiology and pathological mechanism. Inflammation arises as a response of the body's immune system to cellular and tissue damage, and involves a cellular component and a chemical oxidative component. The cellular component involves the migration of leukocytes, mainly neutrophils, from the blood vessels to the injured tissue, attracted by several molecular factors liberated by the damaged cells and by the tissue resident macrophages. Once the leukocytes reach the site of the injury, a series of processes are triggered that include the formation of free radicals and the degradation of phospholipids to arachidonic acid (AA) by the action of phospholipases; arachidonic acid is metabolized by the cyclooxygenase or lipoxygenase pathway, thus producing prostaglandins, leukotrienes and thromboxane, inflammatory mediators necessary in the inflammation process [2]. Adverse effects of inflammation are mainly mediated by cytokines, proteases and oxygen species released by immune cells [3]. Therefore, the migration and activation of immune cells must be finely controlled because an excess of activity can cause additional tissue damage.

Neutrophils play a main role in the first steps of inflammation. They are the leading cells in host defense responses. The early recruitment is guided by tissue damage-associated molecular patterns (DAMPs) recognized by specific Toll-like receptors. One of these signal molecules is hydrogen peroxide generated by specific NADPH oxidases of injured epithelial cells. For more sustained recruitment, additional long-range

signals are activated, mainly chemokines of the CXCL8 family. These chemokines are produced both by immune cells (neutrophils, macrophages, T-cells) and tissue endothelial and epithelial cells. Lipids derived from arachidonic acid are also strong inducers of neutrophil chemotaxis.

Neutrophils are difficult cells to manipulate, therefore a series of techniques are used to understand their biology. Among the models used to investigate the biology of neutrophils are purified human neutrophils, neutrophil cell lines, murine models and zebrafish. In the zebrafish larvae it is possible to study the migration of neutrophils in response to a tissue injury in the whole organism environment [4].

Like mammals, teleost fishes possess several types of granulocytes and a separate lineage of macrophages. The most abundant granulocyte in the zebrafish is the neutrophil, which is characterized by having a segmented multi-lobed nucleus (2-3 lobes). This cell is similar to the human neutrophil, which also has a nucleus of multiple lobes and a heterophilic cytoplasm. As the neutrophil matures, so do its granules, expressing and accumulating several enzymes necessary for its function including myeloperoxidase. Polymorphonuclear neutrophils are the leukocyte dominant in zebrafish larvae at 4 days post fertilization (dpf), and in adult mammals [5].

Diet plays an important role in maintaining an optimal immune response, so that deficient intake can have negative consequences on the immune status and susceptibility of the organism to a wide variety of pathologies. The mechanisms implicated could be mediated by specific regulatory effects on the cellular response, or by an unspecific “antioxidant” action [6]. The present study is focused on investigating the application of a zebrafish larvae model for the screening of natural components present in the Mediterranean diet with possible anti-inflammatory activity. The zebrafish is an organism widely used in various fields of experimental biology. This animal model has multiple advantages such as high fecundity, small size, low maintenance cost, high throughput, rapid extra uterine development and the optical transparency of embryos and larvae. In addition, the exposure needs small amounts dissolved in the surrounding medium and compounds are absorbed through the gastrointestinal tract or through the skin, which allows a rapid evaluation of pharmacological or toxicological activity *in vivo* [7-10].

Two types of assays were developed and applied. In the first assay, the capacity of the substance to prevent the migration on neutrophils was measured. In the second assay, the *in vivo* “antioxidant” activity was evaluated measuring the protective effects against an oxidative stressor.

1. Material and methods

Obtaining zebrafish larvae

Adult wild type zebrafish were kept under standardized conditions. Eggs were collected cleaned and selected. Fertilized embryos were treated with standardized water, according to ISO 7346-1 and 7346-2 (2mM CaCl₂·2H₂O, 0.5mM MgSO₄·7H₂O, 0.75mM NaHCO₃, 0.07mM KCl). The fish were kept under controlled environmental conditions of 28°C.

Solutions

Natural compounds and anti-inflammatory drugs (Sigma Aldrich) were dissolved in dimethyl sulfoxide (DMSO). From the stock solution, serial dilutions were made in Danieau's 0.3X medium (17.4 mM NaCl, 0.23 mM KCl, 0.12 mM MgSO₄·7H₂O, 0.18 mM Ca(NO₃)₂, 1.5 mM HEPES, pH 6.5) that do not contain more than 1% (v / v) of DMSO if used in larvae or 0.1% if used in embryo experiments.

Neutrophil migration assay

The neutrophil migration assay is based on the model described by Cordero-Maldonado *et al.* (2013) [11]. Zebrafish larvae of 4 dpf previously depigmented with 0.2 mM N-phenylthiourea (PTU) were used. Inflammation was induced by means of an injury in the tail fin and potentiated with the addition of lipopolysaccharide (LPS) 10µg / mL to the medium. Exposure to compounds was carried out for eight hours. First a pre-exposure of one hour was carried out, before tail fin cutting. Subsequently, larvae were exposed to the compound and LPS during 7 hours. Larvae were anesthetized and stained with Leucognost pox kit (VWR) following the instructions of the manufacturer. Neutrophils were stained since all the mature cells of the neutrophilic line are positive for myeloperoxidase activity. The tests were carried out in triplicate with larvae coming from different spawn with a whole minimum of 20-25 larvae per compound. Each test was compared with its own negative control to correct the model variability.

Stained cells were observed in the area of the lesion. The area covered by the stained cells in a selected region of the tail was used as the quantitative measurement of migration. A Nikon eclipse TS100 microscope was used to capture the images with a 10X magnification. The analysis of images was done with the program ImageJ. It consisted of the following

phases: first a single image was obtained from three images captured with different focus planes. Then the contrast of the image was increased applying an exponential transformation. A threshold was applied to eliminate the background and saturate the selected signal. Finally, the integrated intensity in a standardized region of the zebrafish tail was measured as shown in Figure 1. Since the signal was saturated, the intensity measured was proportional to the stained area.

Antioxidant activity assay

The protective capacity against oxidative stress in the whole organism was evaluated in zebrafish embryos. Embryos were exposed from 2 to 26 hours post fertilization (hpf) to the assayed compound or to solvent control medium. Afterwards, the medium was changed and embryos were exposed to several concentrations of tert-butyl hydroperoxide (tBOOH) (26-50 hpf) to induce oxidative stress. At 50 hpf the medium was changed to standard Danieau's 0.3X medium (Fig. 2). At 50 and 72 hpf the lethality and the presence of malformations was assessed and quantified following the procedure previously described by Teixidó et al (2013) [12]. The percentage of lethality and of dysmorphogenesis was calculated per compound at every tested concentration, and the concentration-response curves for these effects were plotted. From these curves the concentration of tBOOH which produced mortality to 50% of the embryos (lethal concentration 50, LC50) and the concentration at which 50% of the embryos presented at least one dysmorphogenic feature (effective concentration 50 for dysmorphogenesis, EC50) were calculated. The protective activity of the compounds was evaluated measuring the shift to the right of the lethality-tBOOH concentration and malformation-tBOOH concentration curves relative to the solvent control. The tests were carried out in triplicate with embryos coming from different spawn with a whole minimum of 25-30 embryos per compound and tBOOH concentration.

Statistical analysis

The results were expressed as the mean \pm standard error of the mean (SEM). They were analyzed with the Graph Pad 7.02 Software Inc. program with a two-way ANOVA variance analysis and Bonferroni multiple comparison test. The results are shown as a percentage, where the controls correspond to 100% of neutrophil migration. In all cases, statistically significant differences are considered at three levels of significance, * $p < 0.05$; ** $p < 0.01$; *** $p < 0.001$.

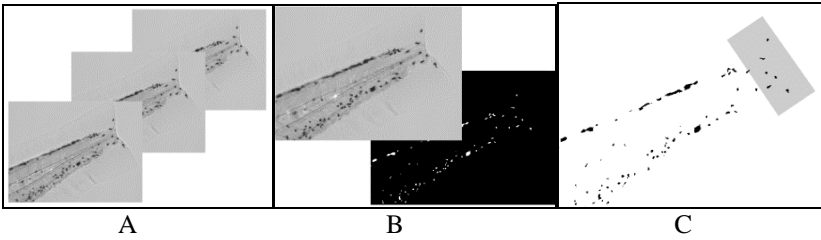


Figure 1. A) Images of zebrafish larvae showing cells with peroxidase positive staining captured with three different focus. B) Image before and after threshold application using ImageJ. C) Intensity integrated in a standardized area close to the fin tail.

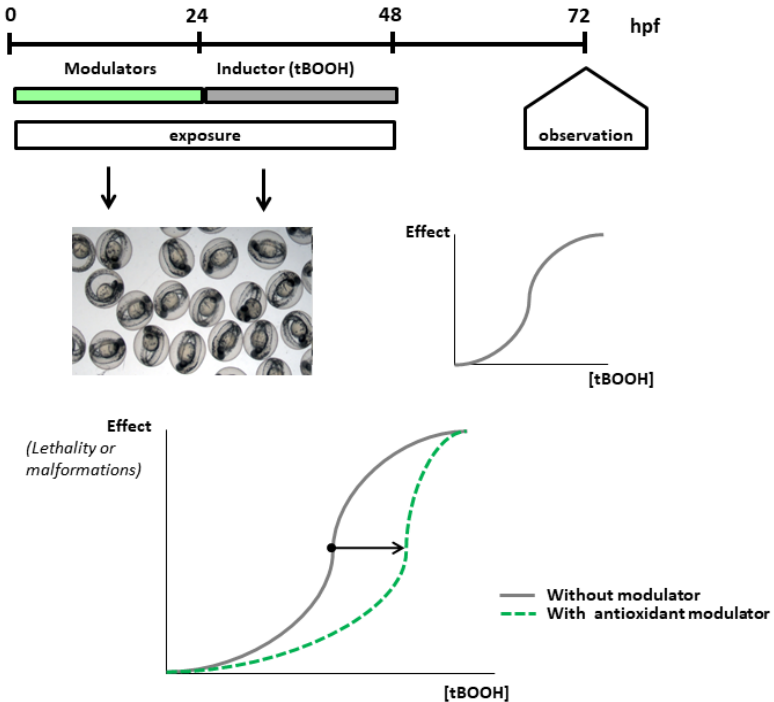


Figure 2. Experimental design of the antioxidant activity assay. Exposure to an antioxidant modulator protects from the toxicity induced by tBOOH. Shifts to the right of the effect (lethality or malformation index) vs concentration curve of tBOOH are observed.

Ethical statement

All procedures with zebrafish, larvae and embryos have been authorized by the Ethical Committee of Animal Experimentation of the University of Barcelona (protocol 7971 of the Department of Agriculture and Fishing of the Generalitat de Catalunya).

2. Results and discussion

Development and assessment of the methods

The capacity of the method to identify substances with anti-inflammatory activity was tested with some well-known positive controls, such as indomethacin and piroxicam, some non-anti-inflammatory products, such as doxepin and amantadine, and with inhibitors of NADPH oxidases such as dibenzoidolium (DPI) and apocynin (Fig. 3).

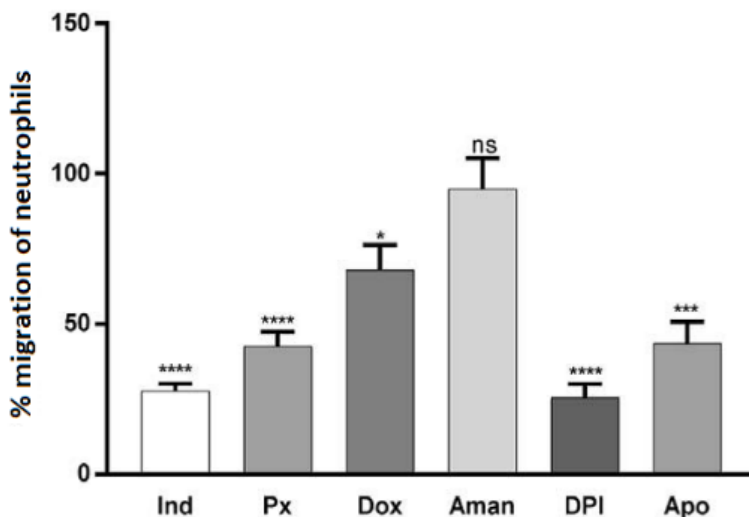


Figure 3. Migration of neutrophils, expressed in percentage of respective control (mean \pm SEM). Larvae exposed to different anti-inflammatory substances such as indomethacin 100 μ M (Ind), Piroxicam 5 μ M (Px), non-anti-inflammatory compounds such as doxepin 5 μ M (Dox), amantadine 10 μ M (Aman) and inhibitors of NADPH oxidases such as dibenzoidolium 100 μ M (DPI) and Apocynin 100 μ M (Apo).

Non-steroidal anti-inflammatory drugs (NSAIDs) inhibit both isoforms of the enzyme cyclooxygenase (COX). The COX-1 isoform is constantly expressed in most tissues, while COX-2 can be induced by various stimuli such as cytokines, prostaglandins and bacterial products such as lipopolysaccharide that contribute to the development of edema, fever and redness [13]. Our results of neutrophil migration in zebrafish larvae exposed to indomethacin and piroxicam show respectively 28% and 42% migration of neutrophils relative to the control.

Amantadine is an anti-viral drug generally used to treat and prevent influenza type A and without known anti-inflammatory activity. Treated larvae do not present significant differences with their control as the migration of neutrophils in this case represented 95%. The result is expected, since not being anti-inflammatory they have no effect on neutrophil migration. However, doxepin, which is an antidepressant drug, produced a moderate but significant inhibition of migration. Some studies suggest that doxepin has anti-inflammatory effects and is effective to treat atopic dermatitis [14].

The enzymes NADPH oxidases are dedicated exclusively to the production of reactive oxygen species (ROS). During phagocytosis, phagocytes activate NADPH oxidases to reduce molecular oxygen to superoxide anion, a precursor of microbicide reactive oxygen species (ROS). Previous studies suggest that after injury, cells in the wound margin of zebrafish larvae rapidly produce hydrogen peroxide (H_2O_2) that serves as an early paracrine signal to leukocytes [15, 16]. The test with DPI showed a significant inhibition of migration to 25% of controls. Apocynin, a phenolic compound isolated from the medicinal plant *Picrorhiza kurroa*, was also used, which also showed significant inhibition in neutrophil migration. Apocynin has been widely used to block the activity of NADPH oxidase *in vitro* [17, 18]. In our case, apocynin showed a 43% migration compared to controls.

These results suggest that the method could be applied for the identification of substances with potential anti-inflammatory activity. Significant inhibition of neutrophils migration was observed with substances acting at different molecular target (COX and NADPH oxidases) related with different chemotactic stimulus.

In order to validate the antioxidant activity assay, different compounds with well determined antioxidant activity were tested. A pre-exposure to N-acetylcysteine, N ω -Nitro L-arginine methyl ester hydrochloride (L-NAME), vitamin E, lipoic acid and quercetin resulted in significant shifts to the right hand of the lethality and malformation curves (results not shown).

Migration of neutrophils in zebrafish larvae exposed to food compounds

Tomato is among the most representative foods of the Mediterranean diet. Tomato derivatives, such as “sofrito” (fried tomato sauce, with onion, garlic, olive oil and some other vegetables), is characterized by containing a high variety of polyphenolic compounds [19]. We have assayed the activity of some of the major components, such as naringenin, oleuropein, rutin, cyanidin, chlorogenic acid and apigenin. The results showed that cyanidin and chlorogenic acid produce the greatest reduction of neutrophil migration (Fig. 4).

The putative protective effects of polyphenols on human health have been classically attributed to their antioxidant activity. Polyphenols can react directly with some reactive species. However it is now generally accepted that the direct scavenging of reactive radicals is not the main mechanism of action. A plethora of specific mechanisms have been described. Among

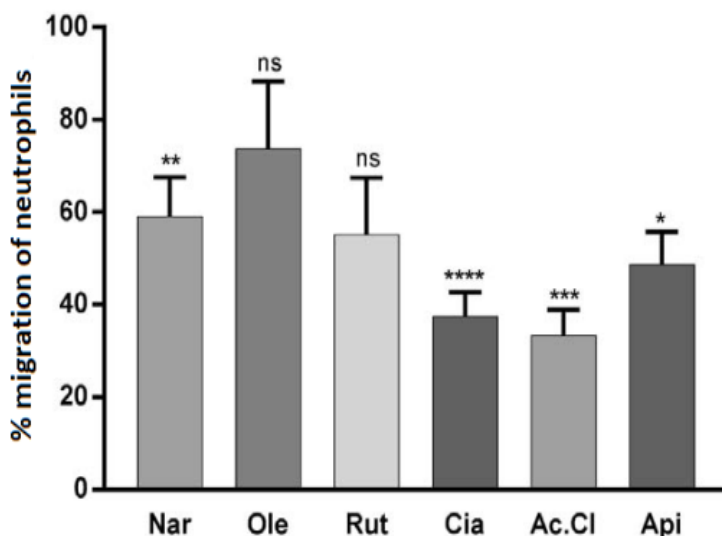


Figure 4. Neutrophil migration in larvae exposed to some polyphenols present in “sofrito”. Naringenin 20 μ M (Nar), Oleuropein 150 μ M (Ole), Rutin 20 μ M (Ru), Cyanidin 20 μ M (Cia), Chlorogenic acid 20 μ M (Ac.Cl) and Apigenin 20 μ M (Api). Data of each treated group is compared with its respective control and the percentage of migration is represented.

these mechanisms, several are directly related to potential anti-inflammatory effects. Inhibition of inflammasome activation and NF- κ B inflammatory pathway, stimulation of the Nrf2 signalling pathway, inhibition of NADPH oxidases and COX have been demonstrated for some specific polyphenols [3, 5, 20].

Cyanidin is a flavonoid that belongs to the anthocyanins group. Anthocyanins are water-soluble pigments present in many fruits and vegetables. Some studies demonstrated that oral administration to rats of cyanidin-3-glucoside (C3G) attenuates the inflammatory response through a decrease in the expression of inducible nitric oxide synthase (iNOS) and a suppression of pro inflammatory cytokine production [21].

Chlorogenic acid is a phenolic compound, very abundant in coffee, where it represents 98% of the total phenolic content (Martini *et al.*, 2016). Chlorogenic acid in addition to being present in raw coffee, is also found

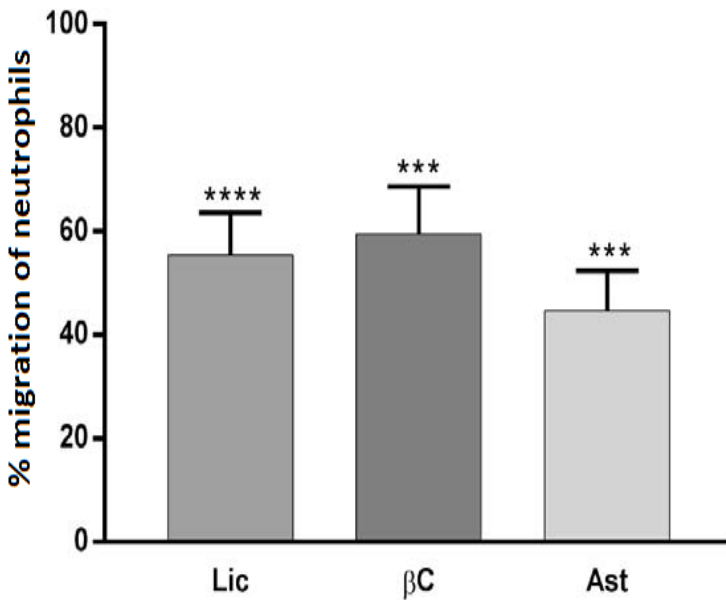


Figure 5. Neutrophil migration in larvae exposed to some carotenoid compounds present in “sofrito”: Lycopene 20 μ M (Lic), β -Carotene 25 μ M (β C) and Astaxanthin 20 μ M (Ast).

in many types of seeds and fruits such as sunflower seeds and blueberries. A lower content of chlorogenic acid has also been detected in potatoes, tomatoes, apples, pears and aubergines, but consumption of these sources represents 5 to 10% of the chlorogenic acid from the coffee source. Tajik et al, [22] showed that, in addition to its antioxidant and anti-inflammatory effects, chlorogenic acid is capable of exerting essential functions in the regulation of glucose and lipid metabolism, as well as in the disorders related to diabetes, cardiovascular disease, obesity and cancer.

Carotenoid compounds intake is high in the Mediterranean diet because they are present in multiple highly consumed foods as tomato and carrots. Two of the most abundant bioactive carotenoid pigments are lycopene and β -carotene. The strong antioxidant effects and other beneficial effects in vitro and in vivo of the carotenes are associated with their capacity to act as free radical scavengers. Carotenoids are pigments responsible for the color of fruits, flowers and leaves. Lycopene is lipophilic, red and is present in ripe tomatoes, the orange color of carrots is caused by β -carotene and the pink / red color is due to astaxanthin [23]. Most research on the health effects of tomato intake and tomato products is concentrated in lycopene; its health benefits have been studied especially in the prevention of chronic inflammatory diseases, cancer and cardiovascular problems [24, 25]. Our results (Fig. 5) show a moderate inhibitory activity on the neutrophil migration.

Antioxidant protective effects

In most of the cases, pre-exposure to the studied compounds produced a significant drift of the concentration-response curves of lethality and dysmorphogenesis to higher concentrations of tBOOH (Fig. 6; Table 1). The effect in lethality is in general more evident, in part by the higher variability of the morphologic effects.

It is surprising the lack of effect of resveratrol and EGCG, two of the most reputed health promoting polyphenols. These results could be explained by a limited bioavailability. However, previous results showed that polyphenols are well absorbed by zebrafish embryo from the water media [26]. On the contrary, the reason of the lack of effect could be an excessive concentration that could yield to a pro-oxidant effect.

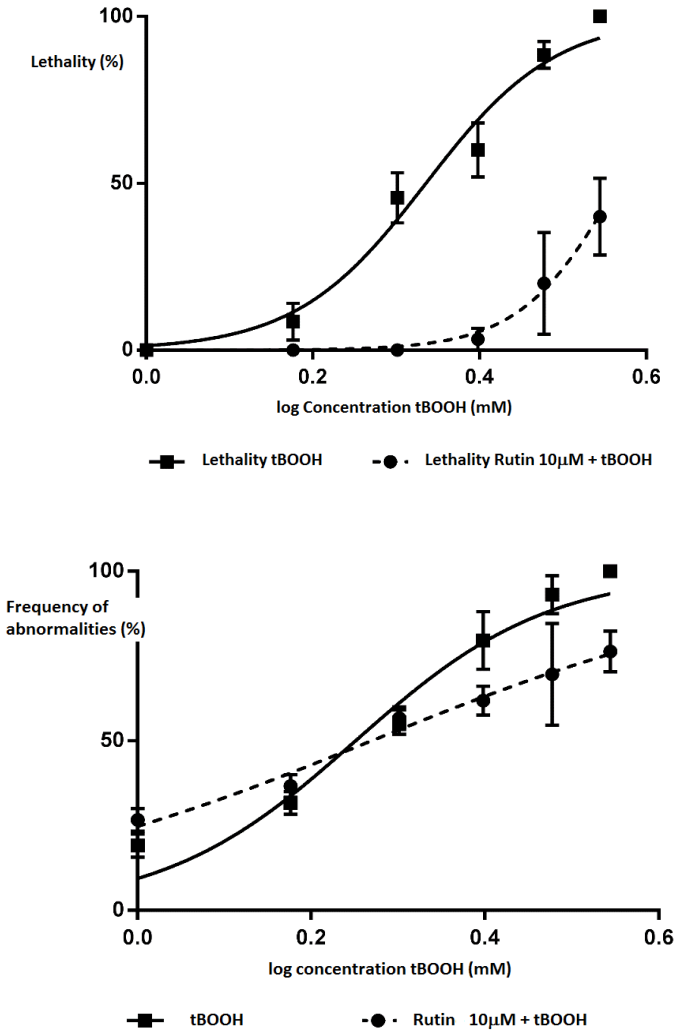


Figure 6. Concentration-response curves of lethality and dysmorphogenesis induced by tBOOH exposure in zebrafish embryo. In the case of pre-exposure to rutin 10 μM, the lethality curve shows a significant shift to the right side, indicating a protective anti-oxidant effect. The effect on dysmorphogenesis is less clear but a significant decrease of the slope is observed.

Table 1. Effect of some polyphenols on the lethality and morphologic abnormalities induced by tBOOH in zebrafish embryos. AOX: antioxidant protective effect; INC: the compound increases the adverse effect; NE: no significant effect observed.

Compound	Lethality			Morphologic abnormalities		
	LC ₅₀ tBOOH	LC ₅₀ tBOOH+ compound	Effect	EC ₅₀ tBOOH	EC ₅₀ tBOOH + compound	Effect
Naringenin 20 µM	2.17	3.48	AOX	1.78	1.80	NE
Oleuropein 15 µM	2.17	2.65	AOX	1.78	1.85	NE
Rutin 10 µM	2.17	3.68	AOX	1.78	1.86	AOX
Cyanidin 20 µM	2.17	3.23	AOX	1.78	1.54	INC
Clorogenic Ac. 20 µM	2.17	2.59	AOX	1.78	1.90	AOX
Apigenin 10 µM	2.17	3.35	AOX	1.78	2.00	AOX
Resveratrol 20 µM	2.71	2.61	NE	2.37	1.86	INC
Curcumin 10 µM	2.71	3.20	AOX	2.37	3.02	AOX
EGCG 20 µM	2.71	2.47	NE	2.37	2.69	NE

3. Conclusions

A method for the measurement of neutrophil migration in a whole organism in zebrafish larvae has been adapted and optimized. The method has been proven reliable and repetitive, although due to the variability of the individual response, the use of a large number of larvae and at least three replicates with different spawn are required. The quantification of migration, by means of image analysis, is reproducible and objective. By means of this established model, the anti-inflammatory activity of a selection of polyphenols and carotenoids of the Mediterranean diet has been studied.

A method for the assessment of antioxidant activity in a whole organism has been developed and applied to a series of natural polyphenols. The quantification of lethality and dysmorphogenesis is easy and reproducible. The protection against the *in vivo* effects of oxidative stress can be assessed independently of the actual mechanism of “antioxidants” action.

These methods can be applied to food extracts and can be useful as screening tests for the identification of fractions and individual compounds with potential anti-inflammatory and antioxidant activity. Additional work is necessary in order to assess the concentration-effect relationships of the anti-inflammatory and antioxidant activities of natural food compounds.

Acknowledgements

This research was funded by the Ministry of Economy AGL2013-49083-C3-1-R project, the FBG-300155 project and the scholarship granted by the Ecuadorian government through the SENESCYT (C. Arteaga).

References

1. Estruch, R. et al. 2013, *N. Engl. J. Med.*, 368, 1279
2. Kontogiorgis, C. A., Bompou, E.-M., Ntella, M., Vanden Berghe, W. 2010, *Anti-Inflammatory Anti-Allergy Agents Med. Chem.*, 9, 101.
3. Ahmed, A.U. 2011, *Front. Biol.*, 6: 274
4. Trede, N. S., Langenau, D. M., Traver, D., Look, A. T., Zon, L. I. 2004, *Immunity*, 20, 367.
5. Croft, K.D. 2016, *Arch. Biochem. Biophys.*, 595, 120.
6. de Oliveira, S., Rosowski, E.E., Huttenlocher, A. 2016, *Nature Rev. Immunol.*, 16, 378.
7. Goldsmith, P. 2004, *Curr. Opin. Pharmacol.*, 4, 504.
8. Lawrence, C. 2007, *Aquaculture*, 269, 1.
9. Lieschke, G. J., Oates, A. C., Crowhurst, M. O., Ward, A. C., Layton, J. E., 2001, *Blood*, 98, 3087.
10. Mathias, J. R., Perrin, B. J., Liu, T.-X., Kanki, J., Look, A. T., & Huttenlocher, A. 2006, *J. Leukocyte Biol.*, 80, 1281.
11. Cordero-Maldonado, M. L., Siverio-Mota, D., Vicet-Muro, L., Wilches-Arizábal, I. M., Esguerra, C. V., de Witte, P. A. M., & Crawford, A. D. 2013, *PLoS ONE*, 8, 1.
12. Teixidó, E., Piqué, E., Gómez-Catalán, J., Llobet, J.M. 2013, *Toxicol. In vitro*. 27, 469.
13. Rao, P. N. P., Knaus, E. E., Road, T. P., & Jolla, L. 2008, *J. Pharm. Pharm. Sci.*, 11, 81s.
14. Drake, L. A., Fallon, J. D., & Sober, A. 1994, *J. Am. Acad. Dermatol.*, 31, 613.
15. Pase, L., Nowell, C. J., & Lieschke, G. J. 2012, *Methods Enzymol.*, 506, 135.
16. Sumimoto, H. 2008, *FEBS J.*, 275, 3249.
17. S. Y. Kim, K.-A. Moon, H.-Y. Jo et al. 2012, *Immunol. Cell Biol.*, 90, 441.
18. Wind S1, Beuerlein K, Eucker T, Müller H, Scheurer P, Armitage ME, Ho H, Schmidt HH, Wingler K. 2010, *Br. J. Pharmacol.*, 161, 885.
19. Vallverdú-Queralt A1, de Alvarenga JF, Estruch R, Lamuela-Raventos RM. 2013, *Food Chem.*, 141, 3365.
20. Forman, H. J., Davies, K.J., Ursini, F. 2014, *Free Radic. Biol. Med.* 66, 24.
21. Tsuda, Takanori, Horio Fumihiko., Osawa, T. 2002, *J. Nutr. Sci. Vitaminol.*, 48, 305.
22. Tajik, N., Tajik, M., Mack, I., & Enck, P. 2017, *Eur. J. Nutr.*, 56, 2215.
23. Milani, A., Basirnejad, M., Shahbazi, S., & Bolhassani, A. 2016, *British J. Pharmacol.*, 174, 1290.

24. Story, E., Kopec, R., Schwartz, S., Harris, G. 2010, *Ann. Rev. Food Sci. Technol.*, 1, 1-24.
25. Palozza, P., Parrone, N., Catalano, a, & Simone, R. 2010, *Curr. Med. Chem.*, 17, 2547.
26. Vallverdú-Queralt, A.; Boix, N.; Piqué, E.; Gómez-Catalan, J.; Medina-Rejon, A.; Sasot, G.; Mercader-Martí, M.; Llobet J.M.; Lamuela-Raventos, R.M. 2015, *Food Chem.*, 181, 146.



Research Signpost
Trivandrum
Kerala, India

Recent Advances in Pharmaceutical Sciences VIII, 2018: 95-118 ISBN: 978-81-308-0579-5
Editors: Diego Muñoz-Torrero, Yolanda Cajal and Joan Maria Llobet

6. Biogeography of *Anisakis* (Anisakidae) and *Hysterothylacium* (Raphidascarididae) nematode species in consumed fish

X. Roca-Geronès, R. Fisa and I. Montoliu

Laboratory of Parasitology, Department of Biology, Health and Environment, Faculty of Pharmacy
and Food Sciences, University of Barcelona, Av. Joan XXIII, 27-31, 08028 Barcelona, Spain

Abstract. The presence of ascaridoid nematodes in commonly consumed fish constitutes an important health risk for humans as well as an economic problem for fisheries. Here, information is provided on the taxonomic status of the representative “anisakid-related” species of the families Anisakidae and Raphidascarididae. These parasites have a worldwide marine geographical distribution, mainly related to the presence of the vertebrate hosts involved in their life cycle. Morphological and molecular methods currently used for specific characterization of larval and adult nematode specimens are analysed and discussed. This study is focused on the taxonomy and parasite-host distribution of species of the genera *Anisakis* and *Hysterothylacium* from the North-East Atlantic Ocean and Mediterranean Sea regions.

1. Introduction

In the last four decades fish consumption has nearly doubled worldwide and global fish production, including aquaculture and wild-catch

Correspondence/Reprint request: Dr. Isabel Montoliu, Laboratory of Parasitology, Department of Biology, Health and Environment., Faculty of Pharmacy and Food Science, University of Barcelona, Av. Joan XXIII, 27-31, 08028 Barcelona, Spain. E-mail: montoliu@ub.edu

fisheries, has increased by many tons to meet the growing market demands [1]. Some of the most habitually consumed fish species are at risk of carrying zoonotic parasites, which can cause economic and sanitary problems [2]. In this context, anisakids that include fish in their life cycle have been ranked by the European Food Safety Authority [3] as a “biological hazard” of the highest importance in seafood products [2]. Species of the genera *Contracaecum* and particularly *Anisakis* and *Pseudoterranova* have been associated with the fishborne disease anisakiosis/anisakidosis, which produces both gastric and allergic reactions [4]. Other “anisakid-related” nematodes, such as *Hysterothylacium* species of the family Raphidascarididae, although considered non-pathogenic, are associated with allergic processes in humans [5] and human infection has also been reported [6]. Infection with *Hysterothylacium* can affect the growth rate and health of the fish hosts, making them more vulnerable to diseases and even resulting in mortalities [7,8].

Improving taxonomic descriptions for specific identification will shed light on the life cycle and geographical distribution of these nematodes, and help understand their epidemiological, biological and ecological patterns [9].

1.1. Taxonomical classification

The taxonomic status of fish-associated ascaridoid genera with zoonotical potential is as follows [10,11,12]:

Phylum:	Nematoda Rudolphi, 1808
Class:	Secernentea Chitwood, 1958
Order:	Ascaridida Skrjabin & Schultz, 1940
Superfamily:	Ascaridoidea Baird, 1853
Family:	Anisakidae Raillet & Henry, 1912
Subfamily:	Anisakinae Raillet & Henry, 1912
Genus:	<i>Anisakis</i> Dujardin, 1845
Genus:	<i>Pseudoterranova</i> Mozgovoi, 1951
Subfamily:	Contracaecinae Mozgovoi & Shakhmatova, 1971
Genus:	<i>Contracaecum</i> Raillet & Henry, 1912
Family:	Raphidascarididae Hartwich, 1954
Subfamily:	Raphidascaridinae Hartwich, 1954
Genus:	<i>Hysterothylacium</i> Ward & Magath, 1917

The evolutionary taxonomy of the superfamily Ascaridoidea is very uncertain, largely because of the great variation in morphological features and life cycle patterns among different species [10,13]. Most evolutionary hypotheses for ascaridoids were developed prior to the widespread use of

molecular techniques and cladistic analysis, and were typically based on the variation in one or a few key morphological structures or life history features [11].

In the last fifty years the systematics and classification of “anisakid-related” species has been much discussed. For example, some authors maintain that the four genera *Anisakis*, *Pseudoterranova*, *Contracaecum* and *Hysterothylacium* should be included in the family Anisakidae, with Anisakinae, Contracaecinae and Rhabdiascaridinae reduced to subfamilies [14,15,16,17,18], whereas others consider the subfamily Rhabdiascaridinae, which includes the *Hysterothylacium* species, to be an independent family taxon, the Rhabdiascarididae [10,11,12,19,20].

Despite these unresolved issues, no approach integrating both morphological and molecular tools has attempted to assess the specific classification of anisakid nematodes or the systematic importance of their features [12]. However, recent phylogenetic studies based on numerous representatives of anisakid nematodes have revealed three main clades that correspond to two subfamilies of Anisakidae, Anisakinae (which includes the *Anisakis* and *Pseudoterranova* genera among others) and Contracaecinae (which includes the *Contracaecum* among others), and one other clade corresponding to the family Rhabdiascarididae, which includes the *Hysterothylacium* genus [2,12].

The lack of available molecular and well-presented morphological data for “anisakid-related” nematodes makes it difficult to search for patterns that may resolve their phylogenetic lineages and shed light on their relationships [12].

1.2. Life cycle

Anisakid species mostly parasitize the digestive tract of marine mammals and use teleost fish as paratenic/transfer hosts for their infesting larvae. The most representative life cycle of these nematodes is that of *Anisakis simplex* represented in Fig. 1. The life cycle is as follows:

- L1 eggs are released into water through definitive host faeces, where the larval maturation process L1-L3 takes place in 20-27 days at 5-7°C.
- Immature L3 hatch and are consumed by the intermediate host, mostly euphasiid crustaceans, in which L3 evolve.
- Sea fish and cephalopods ingesting parasitized crustaceans act as paratenic/transfer hosts, harbouring the infesting L3.
- When final hosts feed on parasitized fish or cephalopods, L3 evolves into L4 and finally the adult form, the life cycle ending with egg production by the female.

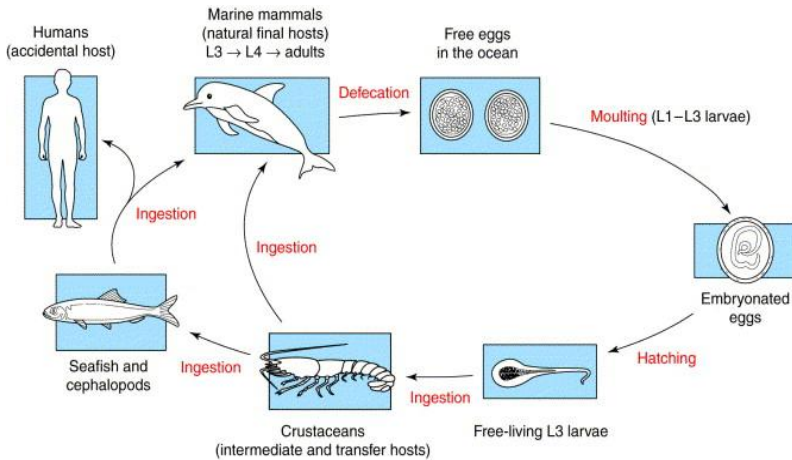


Figure 1. Life cycle of *Anisakis simplex* [4].

These hosts can also be infested by direct consumption of the intermediate crustacean host.

- Humans eating raw parasitized fish can act as an accidental host, in which L3 cannot develop to the adult stage.

In the life cycle of the rhabdiascarid *Hysterothylacium* cold-blood organisms like fish, mainly gadiform, act as definitive hosts [21]. Many species of this genus can evolve in marine and freshwater ecosystems in which fish occupying a low place in the food chain, such as anchovy or horse mackerel, usually act as intermediate/paratenic hosts, whereas large predatory fish are the definitive hosts, harbouring the adult forms [22,23].

1.3. Sanitary and commercial interest

The main food-borne zoonoses associated with the consumption of fishery products are mainly attributable to trematodes, cestodes and nematodes. Among the latter, anisakids are the most important parasites from a sanitary point of view, since they are capable of inducing anisakiosis/anisakidosis in humans [24]. Transmission occurs when humans eat raw or marinated fish parasitized with anisakid larvae L3. Most larvae are located in the visceral cavity but can also be present in the flesh surrounding this cavity and even deeper within the dorsal part of the fish, thus representing a major consumer health risk [2].

The disease can evolve with different symptomatology [25]. In gastric anisakidosis, larvae stick to the wall of the stomach and cause abdominal pain, nausea and vomiting 6-12 hours after ingestion. It usually remits spontaneously but sometimes mechanical extraction by endoscopy is necessary. Intestinal anisakidosis occurs when larvae stick to the thin intestinal wall, which usually happens 48-72 hours after ingestion and can provoke serious inflammatory reactions, sometimes requiring surgical extraction. Gastric and intestinal symptoms can be combined in gastro-intestinal anisakidosis.

Anisakidosis can also be manifested by allergic reactions, usually provoking urticaria or angioedema, and in some severe cases causing anaphylactic shock [25]. Some *Anisakis* species may cause a combination of gastric and allergic anisakidosis known as gastro-allergic anisakidosis [2,25].

This fishborne pathology can be an important public health problem in countries where raw fish is habitually consumed, as occurs on the Eastern coast of Asia. The aetiological agents in 90% of documented clinical cases worldwide are *Anisakis simplex* (*sensu stricto*), *Anisakis pegreffii* and *Pseudoterranova decipiens* [26]. Nevertheless, studies on the zoonotic potential of these nematodes should be extended, since human cases of anisakidosis are most likely underreported, probably due to unspecific symptoms associated with acute and chronic infections [2].

Furthermore, “anisakid-related” nematodes can entail economic losses for the fish industry, involving both wild and farmed fish [2]. When present in fish intended for consumption, these parasites have a considerable quality-reducing effect due to their unappealing appearance [27], so heavily infected fish have no commercial value [28].

1.4. Identification methods

Accurate identification at the species level is very important to understand epidemiological, biological, and ecological patterns [2,18]. Morphological methods are useful but are often insufficient for specific identification. New molecular methods have provided solid information for the specific identification of anisakids in the last decades [9].

Morphological criteria

Species identification in Anisakidae and Rhabdiascarididae has traditionally been complicated due to a lack of differentiating morphological features, particularly in larval stages. In adult worms, the morphological characters

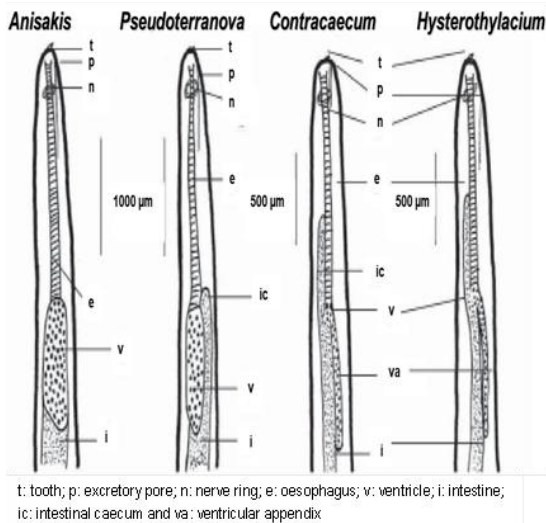


Figure 2. Main morphological differences at the genus level of third stage larvae L3 in “anisakid-related” nematodes [21].

with taxonomic interest are the ventriculus shape; the form of lips; the length and shape of spicules and postanal papillae in males; and the position of the vulva in females [29,30]. The main morphological taxonomic characters of third stage larvae L3 are the structures of the anterior part of digestive tract (oesophagus, ventricle, ventricle appendix intestinal caecum); the anatomical oral tooth; the position of the excretory pore; the distance of the nerve ring to the apical end (Fig. 2), and the caudal morphology, mainly the presence/absence of a caudal spine or mucron [21,31,32]. *Hysterothylacium* species are usually found in fish as fourth stage larvae L4, which can be characterized and differentiated mainly by the presence of labia, the absence of a tooth, and the presence of a cluster of spines at the caudal end [33].

Molecular methods

The first molecular method used in the study of anisakid genetics was Multilocus Allozyme Electrophoresis (MAE) (19-24 enzyme loci), which revealed the existence of high genetic heterogeneity within *Anisakis*, *Pseudoterranova* and *Contraecaecum* and increased the diversity of species included in these genera. This technique allowed the genetic characterization of several anisakid species: it estimated their genetic differentiation, established their genetic relationships and identified their larval stages without morphological characters [9].

The introduction of polymerase chain reaction (PCR) methods confirmed the taxonomic characterisation obtained through allozyme markers. Among these methods the most used are PCR-RFLP (Restriction Length Polymorphism), a polymorphism study of restriction fragments in the PCR products of the ITS-DNA region (Fig. 3) [34]; PCR-SSCP (Single Strand Conformational Polymorphism), a conformational analysis of simple chain polymorphism of PCR-amplified DNA of ITS regions; direct sequencing of PCR-amplified DNA of the 28S region (LSU) and the complete internal transcribed spacer (ITS-1, 5.8S, ITS-2) of ribosomal DNA; and PCR and sequencing of cytochromoxidase b (mtDNA *cytb*) and mitochondrial cytochromoxidase 2 (mtDNA *cox2*) [9]. In recent years the analysis and sequencing of the partial gene of the small subunit of the mitochondrial ribosomal RNA gene (*rrnS*) and the elongation factor EF1 α -1 of the nuclear DNA gene have also been used after PCR for differentiation [35,36].

The advantage of these PCR techniques is they allow the use of alcohol- or formalin-preserved specimens, whereas MAE is limited to frozen or fresh individuals. Moreover, PCR-DNA methods have also facilitated the study of phylogenetic relationships between anisakid species based on the evolutionary lineage concept and have confirmed the existence of sibling species by establishing their taxonomic status [9].

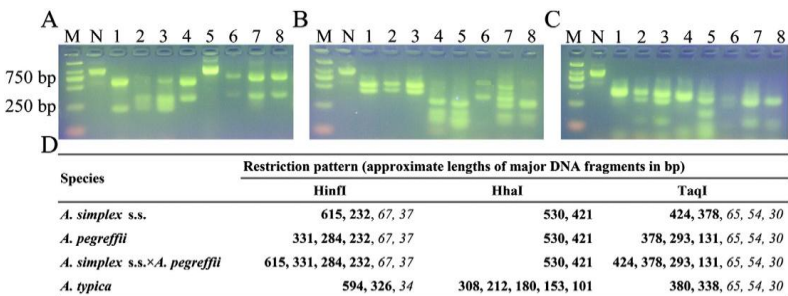


Figure 3. Molecular identification of *Anisakis* and *Hysterothylacium* larvae by PCR-RFLP with *Hinfi* (A), *HhaI* (B) and *TaqI* (C) restriction enzymes of the ITS PCR products and fragment sizes (D). Fragments in bold might be visible in the gel, while fragments in italics might not. M: the 2000 bp DNA ladder marker; N: ITS PCR products; Pattern 1: *A. simplex* (s.s.); Pattern 2: *A. pegreffii*; Pattern 3: Recombinant genotype of *A. simplex* (s.s.) and *A. pegreffii*; Pattern 4: *A. typica*; Pattern 5: *Hysterothylacium* spp.; Pattern 6: *H. aduncum*; Pattern 7: *H. fabri*; and Pattern 8: *H. amoyense* [34].

The description of morphospecies, or species complexes, based on previously recognized cosmopolitan species (*sensu lato*), has solved one of the major problems in the systematics of anisakid nematodes, namely the occurrence of parallelism and convergence of morphological features. This can confound the systematic value of morphological criteria and is often associated with a high genetic and ecological divergence between the species [9].

Genetic/molecular markers used to characterize anisakid species have allowed intermediate/paratenic host fish species and definitive host pinnipeds and cetaceans from different geographical marine regions to be screened and identified [2]. Genetic data can also provide information on ecological and evolutionary aspects, such as host preference and host–parasite co-evolutionary adaptations, including host–parasite co-phylogenetic processes [2].

2. Parasite and host geographical distribution

According to a report by the European Food Safety Authority (EFSA) (European Food Safety Authority, Panel on Biological Hazards (BIOHAZ), 2010), no maritime area can be considered free from anisakids. The geographical distribution of different anisakid species, as well as raphidascaridids, depends on the distribution of their definitive hosts. As a wide range of crustaceans, fish and cephalopods can act as intermediary or parathenic hosts, the definitive hosts have more influence on the species distribution [9].

2.1. Family Anisakidae

Most documented and studied species of Anisakidae are included in *Anisakis*, *Pseudoterranova* and *Contracaecum* genera. *Anisakis* species are distributed around the world, parasitizing cetaceans, mainly whales and dolphins. *Pseudoterranova* and *Contracaecum* species usually have pinnipeds as definitive hosts, which tend to live in cold waters and are usually found in the most northern and southern waters of the planet [9].

Genus *Anisakis*

Up to nine different species of the genus *Anisakis* have been described morphologically and molecularly worldwide (Table 1). All these species are characterized by distinct diagnostic genetic markers, possess distinct gene pools and are reproductively isolated [2].

A. simplex (*sensu lato*) is a complex of three sibling species including *A. simplex* (*s.s.*), *A. pegreffii* and *A. berlandi* (= *A. simplex* sp. C), which are morphologically non-differentiable [35]. These species parasitize cetaceans, mainly delphinids: the two first are distributed worldwide and the latter are

Table 1. *Anisakis* species and their geographical distribution based on definitive and paratenic host sampling (following [9]).

<i>Anisakis</i> species	Geographical distribution
<i>A. simplex</i> (<i>s.s.</i>)*	North and North-East Atlantic; Bering Sea; South Africa; North-East and North West Pacific
<i>A. pegreffii</i> *	Mediterranean Sea; North-East Atlantic; South West Atlantic; North West Pacific; New Zealand and South Africa
<i>A. berlandi</i> *	North-East and South Pacific; South Africa and New Zealand
<i>A. ziphidarum</i> **	Central Atlantic; South Africa and Mediterranean Sea
<i>A. nascettii</i> **	Central Atlantic; Iberian Atlantic coasts; South Africa and New Zealand
<i>A. physeteris</i>	Mediterranean Sea; Central and North East Atlantic
<i>A. brevispiculata</i>	South Africa; Central Atlantic and Iberian Atlantic coasts
<i>A. paggiae</i>	South Africa; Central Atlantic and North-East Atlantic
<i>A. typica</i>	Central and South West Atlantic; Mediterranean Sea; China Sea and Somali coast

*Sibling species of the complex *A. simplex* (*sensu lato*); **sibling species

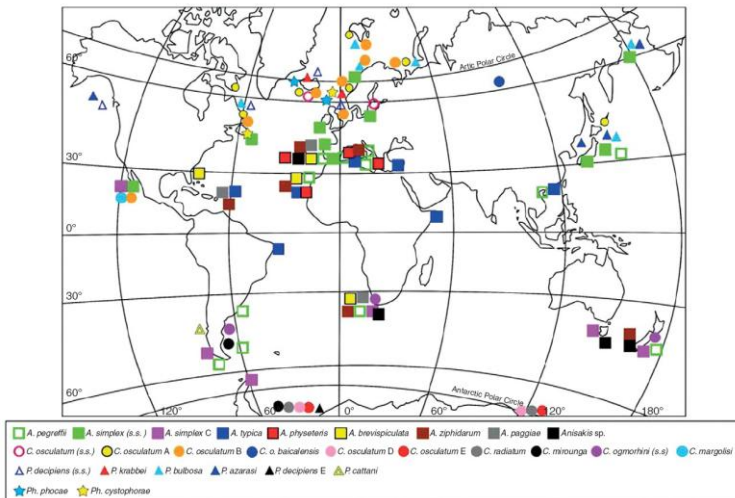


Figure 4. Geographical distribution of *Anisakis*, *Pseudoterranova*, *Contracaecum* and *Phocascaris* species based on definitive and intermediate/paratenic host sampling [9].

more focalized (Fig. 4) [9]. *A. simplex* (*s.s.*) has also been recorded in other cetacean families like Balaenopteridae, Monodontidae and Phocoenidae, and *A. pegreffii* in the family Neobalaenidae. *A. ziphiidarum* and *A. nascettii* are sibling species detected in Ziphiidae cetaceans, mainly in warm waters and the southern hemisphere, respectively. *A. physeteris* is a parasite of the kogiid sperm whale and is typical of Mediterranean and European Atlantic waters. *A. brevispiculata* and *A. paggiae* have been detected in the pygmy sperm whale in North Atlantic and South African marine waters, and *A. typica* in delphinids from warm waters like the Caribbean Sea [9].

Genus *Pseudoterranova*

Eight distinct species of the genus *Pseudoterranova*, parasitizing a wide range of pinnipeds worldwide, have been molecularly recognised [37]. Adults of *P. decipiens* (*sensu lato*), which are in fact a complex of six biological species, are worldwide-distributed parasites of phocid and otariid seals. *P. decipiens* (*s.s.*) has been documented from a wide range of Phocidae species and also some Otariidae, mainly in waters of the northern hemisphere (Fig. 4). *P. krabbei* is typical of the North-East Atlantic and has been recorded in Phocidae species. *P. bulbosa* is habitually found in the bearded seal and has been registered mainly in northern waters. *P. azarasi* parasitizes a wide range of pinnipeds, including sea lions and seals, mainly from northern waters but has also been documented in Japan. *P. cattani* is also a parasite of sea lions but mainly from South Pacific regions. Finally, *P. decipiens E* is a typical parasite of weddell seals and has been reported from the Antarctica [9]. The other two recognised species of *Pseudoterranova* are *P. kogiae* from the pygmy sperm whale, *Kogia breviceps* and *P. ceticola* from the dwarf sperm whale, *K. sima*.

Genus *Contracaecum*

The genus *Contracaecum* comprises at least 50 different species that parasitize mostly pinnipeds and fish-eating birds in their adult form (Fig. 4). The most studied and documented species are those within the *C. osculatum* and *C. ogmorhini* complexes. The former includes five sibling species that usually parasitize Phocidae: *C. osculatum A*, *C. osculatum B* and *C. osculatum* (*s.s.*), documented in Arctic hosts; and *C. osculatum D* and *C. osculatum E*, documented in Antarctic hosts (Fig. 4). The *C. ogmorhini* complex includes two sibling species that mainly parasitize otariid pinnipeds: *C. ogmorhini* (*s.s.*), documented in the Austral region, and

C. margolisi from the Boreal area. Other *Contracaecum* species are *C. osculatum baicalensis*, molecularly differentiated from the *C. osculatum* complex and endemic to the freshwater Lake Baikal (Russia), *C. radiatum*, documented in Antarctic waters, and *C. mirounga*, registered in Antarctic and sub-Antarctic areas [9].

Clustering methods based on allozyme markers showed that the *Phocanema* species, *P. phocae* and *P. cystophorae* (Fig. 4), despite morphological differences with *Contracaecum* species, form a clade with the *Contracaecum* species parasitizing seals, suggesting an evolutionary hypothesis for the systematic status of these species [9].

2.2. Family Raphidascarididae

The family Raphidascarididae includes numerous genera (~13) and their species are distributed worldwide, as are their definitive hosts, which constitute a wide range of marine and freshwater fish species. *Hysterothylacium*, *Raphidascaroides* and *Raphidascaris* are the genera comprising most species, *Hysterothylacium* being the most prevalent in many marine ecosystems [8,17,38].

Genus *Hysterothylacium*

The genus *Hysterothylacium*, currently consisting of ~67 species, is considered one of the largest of the fish-parasitising ascaridoid genera, with worldwide distribution [33,39]. *Hysterothylacium* species have been documented in an extensive range of marine and freshwater fish, which act as paratenic or definitive hosts [17].

Among the five most widely distributed species, *H. aduncum* has been detected in many geographical areas, including the Mediterranean Sea, North-East Atlantic, North-East Pacific and the Yellow Sea, as well as Antarctic waters and New Zealand coasts. *H. corrugatum* has been recorded along North American Atlantic coasts and also the coasts of Ecuador. *H. cornutum* has been reported in the Adriatic Sea as well as the North Atlantic and Pacific Oceans. *H. fortalezae* is found in the Mediterranean Sea, the Brazilian Atlantic coasts and the Gulf of Mexico. *H. reliquens* has been registered in Brazil, Canada and Central America Atlantic coasts, Colombian Pacific coasts and the Persian Gulf. Finally, *H. zenish* has been detected from the East and South China Sea to the Java Sea, the North-East Australian shelf and Namibia coasts [40].

The genetic study of *Hysterothylacium* species is still ongoing and their taxonomical status is not clear. Martín-Sánchez *et al.* [41] suggest *H. fabri*, frequently detected in the Mediterranean Sea, is a complex of three sibling species. As more work is carried out analysing the possible existence of sibling species, the distribution of identified species may change.

3. *Anisakis* spp.

3.1. Morphological and molecular specific identification

To date, nine species belonging to the genus *Anisakis* have been identified worldwide [35]. The need to correctly identify *Anisakis* species is especially important at the larval level because they are the causative agents of anisakidosis, mainly *A. simplex* (*s.s.*) and *A. pegreffii*. Morphological taxonomy of *Anisakis* species has traditionally relied on adult specimens, but in the absence of these forms third stage larvae can be distinguished in the morphological types I and II, following the criteria of Berland [31], which is based mainly on the length of the ventricle and the presence/absence of a spine or mucron at the caudal end. *Anisakis* type I, characterized by a long ventricle and the presence of a mucron, includes the *A. simplex* (*s.l.*) complex, with an oblique ventricle-intestine union, and the species *A. ziphidarum*, *A. nascettii* and *A. typica*, with a blunt ventricle-intestine union (Table 2). Species included in type II are *A. physeteris*, *A. brevispiculata* and *A. paggiae*, whose larvae lack a mucron and have a short ventricle; they also tend to be bigger than species of type I.

In many cases these morphological differences are insufficient for species identification, and molecular approaches are needed. Discriminatory morphometric analysis of the main morphological characters of larvae of non-differentiable species of the *A. simplex* complex, *A. simplex* (*s.s.*) and *A. pegreffii*, has been suggested as a possible method of species differentiation [42]. Ventricle length and the oesophagus/ventricle length ratio have been proposed as discriminating parameters in both L3 and L4, after measuring the total body length, the maximum body width, the distance of the nerve ring from the anterior end, the length of the oesophagus, the ventricle length and width, the ratio between the oesophagus and ventricle length, the tail length and the mucron. More morphometric studies of the two sibling species larvae from different geographical areas are required to find more discriminatory functions of morphological parameters.

Table 2. Morphological differences of L3 of *Anisakis* species, related to larval type and cladistic classification.

Species	Main larval morphological differences	Larval type (Berland, 1961) [31]	Cladistics (Mattiucci <i>et al.</i> 2017) [2]
<i>A. simplex</i> (s.s.)* <i>A. pegreffii</i> * <i>A. berlandi</i> *	Presence of mucron, long ventricle. Oblique ventricle-intestine union	I	First clade
<i>A. ziphidarum</i> ** <i>A. nascettii</i> **	Presence of mucron, long ventricle. Blunt ventricle-intestine union	I	Second clade
<i>A. typica</i>	Presence of mucron, long ventricle. Blunt ventricle-intestine union	I	Fourth clade
<i>A. physeteris</i> <i>A. brevispiculata</i> <i>A. paggiae</i>	Absence of mucron, short ventricle	II	Third clade

*Sibling species of the complex *A. simplex* (*sensu lato*); **sibling species

3.2. Presence of *Anisakis* species in vertebrate hosts from the North-East Atlantic Ocean and Mediterranean Sea

Regarding fish consumption and anisakidosis risk in the Iberian Peninsula, two marine geographical areas are of interest, the North-East Atlantic Ocean, corresponding to FAO (Food and Agriculture Organization) zones 27.8 and 27.9, and the Mediterranean Sea, corresponding to FAO zone 37. Focusing on the *Anisakis* species distribution in these two maritime zones, *A. simplex* (s.s.) and *A. pegreffii* are the most detected species, and also the most associated with human cases of anisakidosis. *A. simplex* (s.s.) is the most documented species in the North-East Atlantic, its southern limit being the Spanish Atlantic coast near Gibraltar and the Alboran Sea, and the northern limit the Arctic Sea. This species has not been detected in the Mediterranean although it has been registered in the Alboran Sea, oceanographically considered part of the Atlantic Ocean. On the other hand, *A. pegreffii* is widely distributed in the Mediterranean Sea and is also present, but with less prevalence, in the North-East Atlantic. *A. pegreffii* shares a southern limit with *A. simplex* (s.s.) of the Spanish coasts, whereas its northern limit is the Bay of Biscay, although it has been detected in some migratory fish species from more northern waters [2].

Several cetacean species have been documented as definitive hosts for *A. simplex* (s.s.) and *A. pegreffii* (see Table 3). Although both sibling species

Table 3. List of definitive hosts recorded for the species *A. simplex* (s.s.) and *A. pegreffii* from the North-East Atlantic and Mediterranean Sea (modified from [2,9]).

Definitive host	<i>A. simplex</i> (s.s.)	<i>A. pegreffii</i>
Cetaceans		
Balenopteridae		
<i>Balaenoptera acutorostrata</i>	NEA	-
Delphinidae		
<i>Delphinus delphis</i>	NEA	M
<i>Globicephala melaena</i>	NEA	NEA, M
<i>Lagenorhynchus albirostris</i>	NEA	-
<i>Stenella coeruleoalba</i>	NEA	M
<i>Tursiops truncatus</i>	-	M
Phocoenidae		
<i>Phocoena phocoena</i>	NEA	-

NEA: North-East Atlantic; M: Mediterranean Sea

can share the same definitive hosts, in the North-East Atlantic *A. pegreffii* has only been documented in one cetacean species, *Globicephala melaena*, while in the Mediterranean it has been reported in other species like *Delphinus delphis* and *Stenella coeruleoalba*, which are also hosts of *A. simplex* (s.s.) in the North-East Atlantic [2].

A. simplex (s.s.) and *A. pegreffii* share and even co-infect a wide range of teleost fish species of several families, which act as paratenic hosts (see Table 4). Some of these species are habitually consumed fish such as hake (*Merluccius merluccius*), horse mackerel (*Trachurus trachurus*), blue whiting (*Micromesistius poutassou*), cod (*Gadus morhua*), anchovy (*Engraulis encrasicolus*), Atlantic mackerel (*Scomber scombrus*) and squid (e.g. *Todarodes sagittatus*) [2]. *A. simplex* (s.s.) has also been recorded in three squid species of the family Ommastrephidae [2].

In sympatric areas where the sibling species *A. simplex* (s.s.) and *A. pegreffii* share cetacean and fish hosts, hybrid specimens between these species have been reported [43,44,45,46]. However, the large recovery of larval hybrid forms in fish and the rare observation of hybrid adults in marine mammals has induced controversy in the taxonomical interpretation of these hybrids, becoming an important unresolved issue in *Anisakis* taxonomy [36,47,48].

Table 4. List of paratenic/fish hosts recorded for the species *A. simplex* (s.s.) and *A. pegerffii* from the North-East Atlantic and Mediterranean Sea [2,9].

Fish species	<i>A. simplex</i> (s.s.)	<i>A. pegerffii</i>	Fish species	<i>A. simplex</i> (s.s.)	<i>A. pegerffii</i>
Belontiidae			Muraenidae		
<i>Belone belone</i>	NEA	NEA	<i>Muraena helena</i>	-	M
Bothidae			Phycidae		
<i>Arroglossus laterna</i>	NEA	-	<i>Physic physic</i>	-	M
<i>Arroglossus imperialis</i>	-	NEA	Pleuronectidae		
Carangidae			<i>Pleuronectes platessa</i>	NEA	-
<i>Trachurus trachurus</i>	NEA	NEA, M	Schophthalmidae		
Citharidae			<i>Lepidorhombus boschi</i>	NEA	NEA, M
<i>Citharus linguatula</i>	NEA	NEA	Scombridae		
Clupeidae			<i>Scomber scombrus</i>	NEA	NEA, M
<i>Merluccius merluccius</i>	NEA	-	<i>Trachurus trachurus</i>	-	M
<i>Clupea harengus</i>	NEA	-	Scorpaenidae		
Congridae			<i>Scorpaena scorpa</i>	NEA	NEA
<i>Conger conger</i>	NEA	M	Sebastidae		
Engraulidae			<i>Helicolenus dactylopterus</i>	-	M
<i>Engraulis encrasicolus</i>	-	M	Soleidae		
Gadidae			<i>Dicologlossa cuneata</i>	-	NEA
<i>Boreogadus saida</i>	NEA	-	<i>Scophthalmus mediterraneus</i>	-	NEA
<i>Gadus morhua</i>	NEA	-	Sparidae		
<i>Melanogrammus aeglefinus</i>	NEA	-	<i>Spondylitoxoma cantharus</i>	NEA	-
<i>Micromesistius pontassou</i>	NEA	NEA, M	Sternopychidae		
<i>Pollachius virens</i>	NEA	-	<i>Manrolucus muelleri</i>	NEA	-
<i>Trisopterus luscus</i>	NEA	-	Trachichthyidae		
Hexagrammidae			<i>Haplostethus mediterraneus</i>	-	M
<i>Pleuragrammus auratus</i>	NEA	-	Trachinidae		
Lophidae			<i>Echiichthys vipera</i>	-	M
<i>Lophius piscatorius</i>	NEA	M	Trichiuridae		
Lotidae			<i>Lepidopus caudatus</i>	-	M
<i>Brosme brosme</i>	NEA	-	<i>Trichurus leporus</i>	-	M
<i>Molva idypterygia</i>	NEA	-	Triglidae		
Merlucciidae			<i>Euirigla gurnardus</i>	NEA	-
<i>Dicentrarchus labrax</i>	NEA	-	Xiphidae		
<i>Merluccius merluccius</i>	NEA	NEA, M	<i>Xiphias gladius</i>	NEA	M

NEA: North-East Atlantic; M: Mediterranean Sea

Regarding other *Anisakis* species, according to Mattiucci's review, three species have been detected in the North-East Atlantic and the Mediterranean [2,9]. *A. physeteris* has been documented in the North-East Atlantic from the sperm whale *Physeter macrocephalus* (Physeteridae) and in the Mediterranean Sea from *Physeter catodon*. *A. typica* has been registered in the Mediterranean delphinid *Stenella coeruleoalba*, and *A. paggiae*, although not recorded in the North-East Atlantic, has been associated with Kogiid whales (*Kogia breviceps* and *K. sima*) from this area, due to the presence of larvae in the deep-sea fish *Anoplogaster cornuta*, which supports an oceanic deep-water life cycle for this species [49]. These three *Anisakis* species have also been detected in different paratenic/fish hosts from the same zones: *A. physeteris* in *Trachurus trachurus*, *Merluccius merluccius*, *Phycis phycis*, *Phycis blenoides*, *Scomber scombrus* and *Xiphias gladius*; *A. typica* in *Trachurus trachurus*, *Merluccius merluccius*, *Phycis phycis* and *Scomber scombrus*; and *A. paggiae* in *Merluccius merluccius* [2,9].

4. *Hysterothylacium* spp.

4.1. Morphological and molecular specific identification

Hysterothylacium species are potential zoonotic parasites and are the most common species of Raphidascarididae, having been reported in a wide range of fish [13,50]. The study of adult worms in their fish final hosts is essential for a correct specific identity, but is not always available.

Morphological larval type description is based on the main morphological parameters: the presence/absence of a tooth for L3 or labia morphology for L4, the position of the excretory pore, the ventricular appendix, the intestinal caecum and the morphology of the tail, with the presence/absence of a mucron or a cluster of spines (also called a cactus) as shown in Fig. 6. Morphometric analysis of these parameters is also important for the larval classification [33].

The attempt to characterize and classify these larvae has been extensive in marine teleost fish from the South Pacific (Australia and New Caledonia) and the Persian Gulf. Up to sixteen different larval morphotypes have been described in these areas, most of them with both a morphological and molecular characterization [33,51,52]. Shamsi et al. [33] proposed a key to differentiate the several morphotypes present in Australian waters. This key needs to be extended to include the new morphotypes described in other regions.

Each larval morphotype cannot be associated with a single species because sometimes the same morphotype presents different genotypes [33],

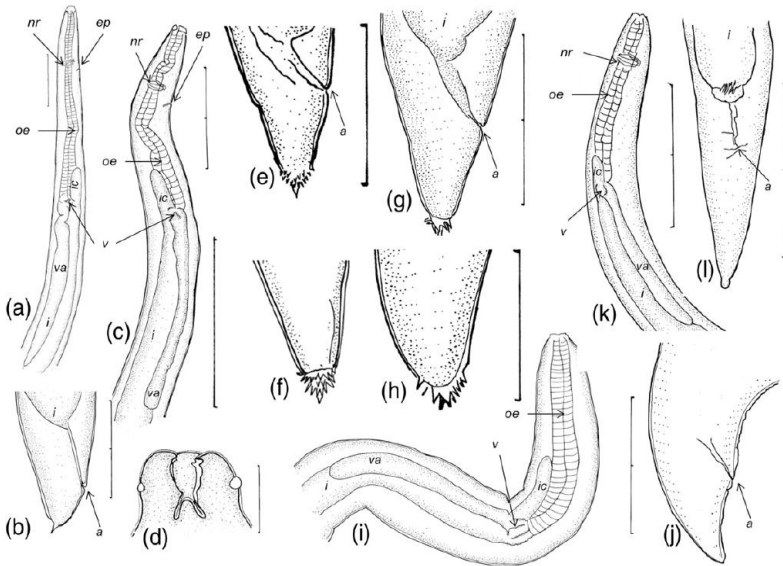


Figure 6. *Hysterothylacium* morphotypes. Larval type III: a) and b) anterior and posterior ends, respectively (scale-bars=0.4 and 0.2 mm, respectively). Larval type IV: c) anterior end (scale-bar=0.4 mm), d) labia (scale-bar=0.3 mm) and e–h) posterior ends (scale-bar=0.2 mm in e and f and 0.1 mm in g and h). Larval type V: i) and j) anterior and posterior ends (scale-bars=0.2 mm). Larval type VI: k) and l) anterior and posterior ends (scale-bars=0.4 and 0.2 mm, respectively), excretory pore was not visible in this specimen (modified from [33]).

meaning that different species can have similar larval morphology. Moreover, larvae can exhibit rather uniform morphology, which is completely different from their adult forms [18]. A comparison between larval morphology and genetics is needed to specifically identify larval morphotypes, the sequencing of ITS-1 and ITS-2 of rDNA after PCR amplification of these regions being the most used molecular method for this purpose [18,33].

Studies on *Hysterothylacium* morphotypes from fishes in different European marine waters are scarce. In this area *Hysterothylacium* larvae are usually identified based solely on morphological parameters and very few studies compare the larval morphology with a proper molecular analysis [38,53]. Therefore, more studies are needed to ascertain the possible morphotypes present in European marine waters.

4.2. Presence of *Hysterothylacium* species in vertebrate hosts from the North-East Atlantic Ocean and Mediterranean Sea

Within *Hysterothylacium* species in Mediterranean and North-East Atlantic regions, *H. aduncum* is the most frequently reported in a wide range of teleost fish [22,54]. However, *H. fabri* is typically reported in many Mediterranean fish species, sometimes with a higher prevalence than *H. aduncum* [38,41,55]. As mentioned in section 2.2, while *H. aduncum* has been detected worldwide, for example, in the North-East Pacific and the Yellow Sea as well as Antarctica and New Zealand waters, *H. fabri* has only been documented in the South and East China Sea [40].

H. aduncum and *H. fabri* specimens from the Mediterranean and the North-East Atlantic have been mostly detected in their larval forms (see Table 5) and very few studies have documented their adult form in final fish hosts in these regions. Sanmartin-Duran et al. [56] detected adult specimens of *H. aduncum* in *Scophthalmus maximus* and *Conger conger*, while Mackenzie et al. [54] and Carreras-Aubets et al. [57] reported the adult form in *Trachurus trachurus* and *Mullus barbatus*, respectively. Adult forms of *H. fabri* have been documented [58] in *Mullus surmulentus*.

Other *Hysterothylacium* species, including *H. corrugatum*, *H. incurvum* and *H. petteri*, have been recorded in swordfish (*Xiphias gladius*) from the Mediterranean Ionic and Tyrrhenian Sea, and the North-East Atlantic Ocean [35]. Moreover, some authors have also found *H. auctum* in the Baltic Sea [68], and Gibson [69] lists 13 different *Hysterothylacium* species in European marine waters, including *H. aduncum* and *H. fabri* but without specifying the region. Regarding the Mediterranean Sea, Bruce et al. [39] detected *H. fortalezae*, without specifying the region, *H. cornutum* and *H. increscens* in the Adriatic Sea, *H. bifidalatum* in the Algerian part of the Mediterranean and *H. rhacodes* in the East Mediterranean.

5. Conclusion

The present review highlights the importance of improving taxonomic descriptions of “anisakid-related” nematode species. Accurate species identification and knowledge of their geographical distribution would shed light on the epidemiological, biological and ecological patterns of these parasites, which are of sanitary and commercial concern. Among Anisakidae, *Anisakis* spp. are the main causative agents of anisakidosis and the most widely detected in cetacean definitive hosts worldwide, while *Pseudoterranova* and *Contracaecum* species have a more reduced distribution, mainly in the most northern and southern areas of the planet, pinnipeds being their main definitive hosts.

Table 5. List of intermediate fish hosts recorded for the species *H. aduncum* and *H. fabri* from the North-East Atlantic and Mediterranean Sea [55,56,58,59,60,61,62,63,64,65,66,67].

Fish species	<i>H. aduncum</i>	<i>H. fabri</i>	Fish species	<i>H. aduncum</i>	<i>H. fabri</i>
Carangidae			Pomatomidae		
<i>Trachurus mediterraneus</i>	M	M	<i>Pomatomus saltatrix</i>	M	-
<i>Trachurus trachurus</i>	NEA, M	-	Schophthalmidae		
Clupeidae			<i>Lepidorhombus whiffiagonis</i>	NEA	-
<i>Alosa alosa</i>	NEA	-	<i>Lepidorhombus boscii</i>	NEA	-
<i>Alosa fallax</i>	NEA	-	<i>Scophthalmus maximus</i>	NEA	-
<i>Sardina pilchardus</i>	M	-	Serranidae		
Congridae			<i>Serranus scriba</i>	-	M
<i>Conger conger</i>	NEA	-	Scorpaenidae		
Engraulidae			<i>Scorpaena porcus</i>	-	M
<i>Engraulis encrasicolus</i>	NEA, M	-	<i>Scorpaena scrofa</i>	-	M
Gadidae			Soleidae		
<i>Micromesistius pontassou</i>	NEA, M	-	<i>Microchirus variegatus</i>	NEA	-
Labridae			<i>Solea solea</i>	M	-
<i>Symphodus tinca</i>	-	M	Sparidae		
Merlucciidae			<i>Sparus aurata</i>	M	-
<i>Merluccius merluccius</i>	M	M	<i>Diplodus vulgaris</i>	M	-
Mullidae			<i>Pagellus erythrinus</i>	M	M
<i>Mullus barbatus</i>	M	M	<i>Boops boops</i>	M	-
<i>Mullus surmulentus</i>	M	M	Triglidae		
Phycidae			<i>Trigla lucerna</i>	NEA	-
<i>Phycis phycis</i>	M	M			
<i>Phycis blennioides</i>	M	M			

NEA: North-East Atlantic; M: Mediterranean Sea

Classification of the genus *Hysterothylacium* at the family level remains controversial, and its inclusion in the family Raphidascarididae is not unanimously accepted. In their larval stages, *A. simplex* (*s.l.*) and *H. aduncum* are the most frequently detected species in a wide range of commonly consumed fish from European and Spanish marine waters, including the North-East Atlantic and Mediterranean. Specific identification of these nematodes at larval stages, combining morphological and molecular methods, is crucial from an epidemiological point of view, due to the existence of morphologically non-differentiable sibling species, such as *A. simplex* (*s.s.*) and *A. pegreffii*, both of sanitary importance. The detection of hybrids of these two species needs to be followed up by genetic characterization studies to ascertain if they are viable hybrids giving rise to hybrid adults. Although molecular methods are effective in many cases, morphological knowledge of larvae and adults is still important for correct identification. It is therefore necessary to undertake studies on *Hysterothylacium* morphotypes in fish from marine European waters for which data remain quite scarce.

Acknowledgements

The authors are grateful to Dr. Shokoofeh Shamsi for her advice, contributions and exhaustive knowledge. This work was supported by the Generalitat de Catalunya 2014 SGR Project (1241).

References

1. FAO/WHO 2014, Multicriteria-based ranking for risk management of foodborne parasites. Report of a Joint FAO/WHO Expert Meeting. September 3–7, 2012, FAO Headquarters, Rome.
2. Mattiucci, S., Cipriani, P., Paoletti, M., Levsen, A., Nascetti, G. 2017, *J. Helminthol.*, 91, 422.
3. European Food Safety Authority, Panel on Biological Hazards (BIOHAZ) 2010, *EFSA J.*, 8, 1543.
4. Audicana, M.T., Ansotegui, I. J., Fernández de Corres, L., Kennedy, M.W. 2002, *Trends Parasitol.*, 18, 20.
5. Valero, A., Terrados, S., Díaz, V., Reguera, V., Lozano, J. 2003, *J. Investig. Allergol. Clin. Immunol.*, 13, 94.
6. Yagi, K., Nagasawa, K., Ishikura, H., Nakagawa, A., Sato, N., Kikuchi, K., Ishikura, H. 1996, *Jpn. J. Parasitol.*, 45, 12.
7. Balbuena, J.A., Karlsbakk, E., Kvenseth, A.M., Saksvik, M., Nylund, A. 2000, *J. Parasitol.*, 86, 1271.
8. Li, L., Gibson, D.I., Zhang, L.P. 2016, *Syst. Parasitol.*, 93, 1.

9. Mattiucci, S., Nascetti, G. 2008, *Adv. Parasitol.*, 66, 47.
10. Fagerholm, H.P. 1991, *Syst. Parasitol.*, 19, 215.
11. Nadler, S.A., Hudspeth, D.S. 2000, *J. Parasitol.*, 86, 380.
12. Pereira, F.B., Luque, J.L. 2017, *Parasitol. Int.*, 66, 898.
13. Anderson, R.C. 2000, *Nematode parasites of vertebrates. Their development and transmission*, CABI Publishing, Wallingford.
14. Hartwich, G., 1974, *Keys to the Nematode Parasites of Vertebrates*, Anderson, R.C., Chabaud, A.G., Willmott, S. (Eds.), CAB publishing, Wallingford, 1.
15. Gibson, D.I., 1983, *Concepts in Nematode Systematics*, Stone, A.R., Platt, H.M., Khalil, L.F. (Eds.), Academic Press, New York, 321.
16. Gibbons, L.M. 2010, *Keys to the nematode Parasites of Vertebrates: supplementary volume*, CABI Publishing, Wallingford.
17. Moravec, F., 1994, *Parasitic nematodes of freshwater fishes of Europe*, Academia, Praha.
18. Pantoja, C.S., Pereira, F.B., Santos, C.P., Luque, J.L. 2016, *Parasitol. Res.*, 115, 4353.
19. Nadler, S.A., Carreno, R.A., Mejía-Madrid, H., Ullberg, J., Pagan, C., Houston, R., Hugot, J.P. 2007, *Parasitol.*, 134, 1421.
20. Park, J., Sultana, T., Lee, S., Kang, S., Kim, H.K., Min, G., Eom, K.S., Nadler, S.A. 2011, *BMC Genomics*, 12, 392.
21. Rello, F.J., Adroher, F.J., Valero, A. 2004, *An. Real Acad. Cienc. Vet. And. Orient. Andalucía Orient.*, 17, 173.
22. De Liberato, C., Bossù, T., Scaramozzino, P., Nicolini, G., Ceddia, P., Mallozzi, S., Cavallero, S., D'Amelio, S. 2013, *J. Food Prot.*, 76, 1643.
23. Deardorff, T.L., Overstreet, R.M. 1981, *Proc. Helm. Soc. Wash.*, 48, 113.
24. Chai, J.Y., Murrell, K.D., Lymbery, A.J. 2005, *Int. J. Parasitol.*, 35, 1233.
25. Audicana, M.T., Del Pozo Gil, M.D., Daschner, A. 2007, *Tratado de alergología e inmunología Clínica*, Pelaez, A., Dávila, I. (Eds.), SEAIC, Madrid. 1681.
26. D'amico, P., Malandra, R., Costanzo, F., Castigliero, L., Guidi, A., Gianfaldoni, D., Armani, A. 2014, *Food Res. Int.*, 64, 348.
27. Karl, H., Levse, A. 2011, 22, 1634.
28. Aspholm, P.E. 1995, *Fish. Res.*, 23, 375.
29. Davey, J.T. 1971, *J. Helminthol.*, 45, 51.
30. Petter, A., Maillard, C. 1987, *Bull. Mus. Natl. Hist. Nat. Paris*, 4, 773.
31. Berland, B. 1961, *Sarsia*, 2, 1.
32. Petter, A.J., Maillard, C. 1988, *Bull. Mus. Natl. Hist. Nat. Paris*, 4, 347.
33. Shamsi, S., Gasser, R., Beveridge, I. 2013, *Parasitol. Int.*, 62, 320.
34. Kong, Q., Fan, L., Zhang, J., Akao, N., Dong, K., Lou, D., Ding, J., Tong, Q., Zheng, B., Chen, R., Ohta, N., Lu, S. 2015, *Int. J. Food Microbiol.*, 199, 1.
35. Mattiucci, S., Cipriani, P., Webb, S.C., Paoletti, M., Marcer, F., Bellisario, B., Gibson, D.I., Nascetti, G. 2014, *J. Parasitol.*, 100, 199.
36. Mattiucci, S., Acerra, V., Paoletti, M., Cipriani, P., Levsen, A., Webb, S.C., Canestrelli, D., Nascetti, G. 2016, *Parasitol.*, 143, 998.

37. Timi, J.T., Paoletti, M., Cimmaruta, R., Lanfranchi, A.L., Alarcos, A.J., Garbin, L., George-Nascimento, M., Rodríguez, D.H., Giardino, G. V., Mattiucci, S. 2014, *Vet. Parasitol.*, 199, 59.
38. Pekmezci, G.Z., Yardimci, B., Onuk, E.E., Umur, S. 2014, *Parasitol. Int.*, 63, 127.
39. Bruce, N.L., Adlard, R.D., Cannon, L.R.G. 1994, *Invert. Taxon.*, 8, 583.
40. <http://www.marinespecies.org> (last access 12/03/18).
41. Martín-Sánchez, J., Díaz, M., Artacho, M.E., Valero, A. 2003, *Parasitol. Res.*, 89, 214.
42. Quiazon, K.M.A., Yoshinaga, T., Ogawa, K., Yukami, R. 2008, *Parasitol. Int.*, 57, 483.
43. Umehara, A., Kawakami, Y., Matsui, T., Araki, J., Uchida, A. 2006, *Parasitol. Int.*, 55, 267.
44. Meloni, M., Angelucci, G., Merella, P., Siddi, R., Deiana, C., Orrù, G., Salati, F. 2011, *J. Parasitol.*, 97, 908.
45. Cavallero, S., Ligas, A., Bruschi, F., D'Amelio, S. 2012, *Vet. Parasitol.*, 187, 563.
46. Costa, A., Cammilleri, G., Graci, S., Buscemi, M.D., Vazzana, M., Principato, D., Giangrosso, G., Ferrantelli, V. 2016, *Parasitol. Int.*, 65, 696.
47. Abattouy, N., Valero, A., Lozano, J., Barón, S.D., Romero, C., Martín-Sánchez, J. 2016, *Parasite Epidemiol. Control*, 1, 169.
48. Mladineo, I., Bušelić, I., Hrabar, J., Vrbatović, A., Radonić, I. 2017, *Mol. Biochem. Parasitol.*, 212, 46.
49. Klimpel, S., Kuhn, T., Busch, M.W., Karl, H., Palm, H.W. 2011, *Polar Biol.*, 34, 899.
50. Klimpel, S., Seehagen, A., Palm, H.W., Rosenthal, H., 2001, Deep-water metazoan fish parasites of the world. Logos Verlag Berlin.
51. Cannon, L.R.G. 1977, *Int. J. Parasitol.*, 7, 233.
52. Ghadam, M., Banaii, M., Mohammed, E.T., Suthar, J., Shamsi, S. 2018, *J. Helminthol.*, 92, 116.
53. Vardić Smrzlić, I., Valić, D., Kapetanović, D., Kurtović, B., Teskeredžić, E. 2012, *Parasitol. Res.*, 111, 2385.
54. MacKenzie, K., Campbell, N., Mattiucci, S., Ramos, P., Pinto, A.L., Abaunza, P. 2008, *Fish. Res.*, 89, 136.
55. Ternengo, S., Levron, C., Mouillot, D., Marchand, B. 2009, *Parasitol. Res.*, 104, 1279.
56. Sanmartín-Duran, M., Quinteiro, P., Ubeira, F. 1989, *Dis. Aquat. Org.*, 7, 75.
57. Carreras-Aubets, M., Montero, F.E., Kostadinova, A., Carrassón, M. 2012, *Mar. Pollut. Bull.*, 64, 1853.
58. Arculeo, M., Hristovski, N., Riggio, S. 1997, *Ital. J. Zool.*, 64, 283.
59. Valero, A., Martín-Sánchez, J., Reyes-Muelas, E., Adroher, F.J. 2000, *J. Helminthol.*, 74, 361.
60. Farjallah, S., Slimane, B.B., Blel, H., Amor, N., Said, K. 2006, *Parasitol. Res.*, 100, 11.

61. Valero, A., Paniagua, M.I., Hierro, I., Díaz, V., Valderrama, M.J., Benítez, R., Adroher, F.J. 2006, *Parasitol. Int.*, 55, 1.
62. Keser, R., Bray, R.A., Oguz, M.C., Çelen, S., Erdogan, S., Doguturk, S., Aklanoglu, G., Marti, B. 2007, *Helminthologia*, 44,217.
63. Rello, F.J., Adroher, F.J., Valero, A. 2009, *Int. J. Food Microbiol.*, 129, 277.
64. Rello, F.J., Adroher, F.J., Valero, A. 2008, *Parasitol. Res.*, 104, 117.
65. Amor, N., Farjallah, S., Merella, P., Said, K., Slimane, B. 2011, *Parasitol. Res.*, 109, 1429.
66. Bao, M., Roura, A., Mota, M., Nachón, D.J., Antunes, C., Cobo, F., Pascual, S. 2015, *Parasitol. Res.*, 114, 3721.
67. Keskin, E., Koyuncu, C.E., Genc, E. 2015, *Parasitol. Int.*, 64, 222.
68. Szostakowska, B., Myjak, P., Kur, J., Sywula, T. 2001, *Acta Parasitol.*, 46, 194.
69. Gibson, D.I., 2001, European register of marine species: a check-list of the marine species in Europe and a bibliography of guides to their identification, Costello, M.J., Emblow, C.S., White, R.J. (Eds.), Muséum national d'histoire naturelle, Paris, 174.



Research Signpost
Trivandrum
Kerala, India

Recent Advances in Pharmaceutical Sciences VIII, 2018: 119-136 ISBN: 978-81-308-0579-5
Editors: Diego Muñoz-Torrero, Yolanda Cajal and Joan Maria Llobet

7. High performance thin-layer chromatography (HPTLC) in the quality control of herbal products

Salvador Cañiguer¹, Débora Arruda Frommenwiler^{1,2}, Eike Reich²
and Roser Vila¹

¹Unitat de Farmacologia, Farmacognòsia i Terapèutica, Facultat de Farmàcia i Ciències de l'Alimentació, Universitat de Barcelona, Av. Joan XXIII, 27-31 08028 Barcelona, Spain; ²CAMAG AG, Sonnenmattstrasse 11, 4132 Muttenz, Switzerland

Abstract. The introduction of high performance thin-layer chromatography (HPTLC) for quality control of herbal products, using standardised methodology and system suitability tests for the qualification of the plates, has improved reproducibility. The use of intensity markers implemented by the Ph. Eur. improved the description and interpretation of the chromatograms. Quantitative information can be retrieved from the electronic images of the chromatograms and used for *comprehensive HPTLC fingerprinting*: a single HPTLC analysis gives information on identity, purity and content of an herbal drug/preparation/product, simplifying the quality control.

Correspondence/Reprint request: Prof. Salvador Cañiguer, Unitat de Farmacologia, Farmacognòsia i Terapèutica, Facultat de Farmàcia i Ciències de l'Alimentació, Universitat de Barcelona, Av. Joan XXIII, 27-31, 08028 Barcelona, Spain. E-mail: s.caniguer@ub.edu

Introduction

Herbal products are those that contain herbal drugs, herbal drug preparations or their combinations as active ingredients.

According to the European Pharmacopoeia (Ph. Eur.) [1], herbal drugs are mainly whole, fragmented or broken plants or parts of plants in an unprocessed state, usually in dried form but sometimes fresh. The word “plant” is here used in the broader sense to also include algae, fungi and lichens. Certain exudates that have not been subjected to a specific treatment are also considered to be herbal drugs.

Herbal drug preparations (or herbal preparations) are homogeneous products obtained by subjecting herbal drugs to treatments such as extraction, distillation, expression, fractionation, purification, concentration or fermentation. They include, for example, extracts, essential oils, expressed juices, processed exudates, and herbal drugs that have been subjected to size reduction for specific applications, for example herbal drugs cut for herbal teas or powdered for encapsulation [1].

In most of the cases herbal products reach the market as medicines or as dietary supplements, depending on the region and the regulatory framework applied, which have different quality requirements. However, the quality of herbal drugs and herbal preparations is the basis for the reproducibility of the safety and the efficacy, and should be taken into account in all steps of the production process. The chemical complexity of herbal drugs and preparations, its variability inherent to its natural origin, the limited knowledge of the chemical constituents responsible of the therapeutic activity, and the possibility of adulterations and contaminations, make the quality control a challenging process [2].

The main objectives of quality control are to certify the identity of the herbal drug/preparation/product analysed, its purity concerning possible adulterations, falsifications and contaminants, and the strength/content of active principles or markers. Quality specifications published in Pharmacopoeias, which include analytical methods plus criteria of acceptance, are mandatory for medicinal products and can also be followed for dietary supplements [3].

Identification of herbal drugs and detection of possible adulterations rely in macroscopical and microscopical examinations and the analysis by thin-layer chromatography (TLC) or high performance thin-layer chromatography (HPTLC). In the case of herbal preparations, such as extracts, TLC/HPTLC are the preferred techniques and, sometimes, other chromatographic techniques, like gas chromatography (GC) in the case of essential oils, are used. Content/strength determination is done mainly by

high performance liquid chromatography (HPLC) and in certain cases by GC or spectrophotometry.

Although TLC was very early included in the Pharmacopoeias for the analysis of herbal drugs and preparations, significant improvements have been achieved by the introduction of HPTLC and the standardisation of the methodology. The objective of the present chapter is to introduce to the reader the new opportunities opened by these improvements that allow a deeper exploitation of HPTLC in the field of quality control of herbals.

1. High performance thin-layer chromatography

High performance thin-layer chromatography (HPTLC) is a planar chromatographic technique resulting from the evolution of the classical thin-layer chromatography (TLC), but it goes far beyond the old TLC performed on HPTLC plates [4]. Indeed, HPTLC and TLC share the same basic principles involved in the separation, which results from the interaction of the constituents of the sample with a planar stationary phase, the liquid mobile phase and the gas phase produced in the chromatographic chamber. Also, they share advantages such as visual results, parallel analysis of samples, single use of the plate, rapid results, flexibility and the possibility of multiple detection. Some technical differences between HPTLC and TLC, concerning the plate, solvent consumption, duration of development and sensitivity are shown in Fig. 1.

Beyond this differences and similarities, HPTLC is a new concept, which primary focuses are reproducibility and separation power. It uses well-defined methods, with optimized and standardized parameters, that pass a validation process, and give reliable analytical results with good intra- and inter-laboratory reproducibility. Instrumentation for HPTLC can be simple to sophisticated and allows obtaining traceable digital images and a deeper exploitation of the data contained in these images. Moreover, HPTLC is GMP friendly [4,5].

Well described sample preparation, well defined layout of the plate and volume of application, as well as fully specified chromatographic conditions and detection system(s), including not only the composition of the mobile phase, but the relative humidity, the use of a saturated, an unsaturated or a pre-conditioned chamber, the developing distance, etc. are necessary for reproducible results. The use of a method-specific system suitability test (SST) on each plate is a key point in order to qualify the developed plate, rely on each single analysis and compare analyses done on different plates.

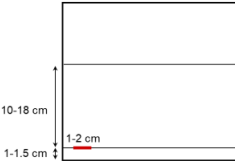
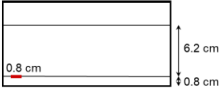
	TLC	HPTLC
		
Plate size	20 x 20 cm	10 x 20 cm or 10 x 10 cm
Average particle size	10 -15 μm	5 -7 μm
Particle size distribution	Wide	Narrow
Layer thickness	250 μm	100-200 μm
Application volume	10-20 (-50) μL	2-10 μL
Number of samples/plate	max. 12	max. 15
Development duration	30-200 min	10-30 min
Solvent consumption	50 mL	10-35 mL
Limit detection:		
Absorbance	100 - 1000 ng	10 - 100 ng
Fluorescence	1 - 100 ng	0.1 - 10 ng

Figure 1. Some differential characteristics of TLC and HPTLC.

2. Quality of herbal medicinal products, HPTLC and Pharmacopoeia

The active ingredients (herbal drugs and herbal preparations, such as extracts or essential oils) of the herbal medicinal products must fulfill the quality requirements established in the corresponding regulations, including the related Pharmacopoeia. The objective of these specifications is to demonstrate identity, purity and content of active principles or markers [2,3].

TLC and, more recently, HPTLC has been traditionally used for proving identity of herbal drugs and extracts, as well as for the investigation of the presence of possible adulterations or falsifications, which is a key part of establishing the purity. In addition, HPTLC is also used, to a lesser extent, for the quantification of active principles or markers. The use of TLC/HPTLC for checking the identity and purity is mainly based on the visual observation of the chromatographic fingerprint, this is the sequence of zones of the chromatogram of the sample, taking in account the number, position (R_F) and color/fluorescence of the zones in one or more detection modes.

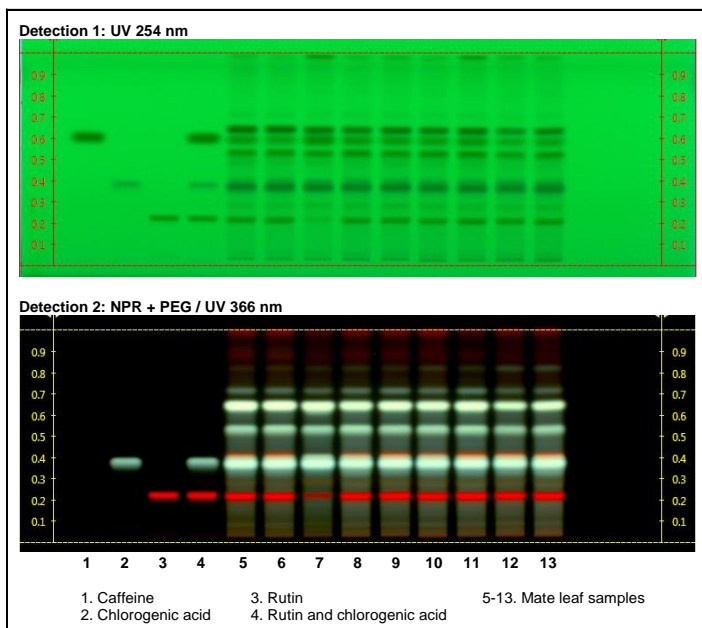


Figure 2. HPTLC chromatograms for identification of mate leaf (*Ilex paraguariensis* A.St.-Hil.) A single analysis with two subsequent detections allows the detection of caffeine, under UV 254 nm, and polyphenols (caffeoylquinic acids and flavonoids), under 366 nm after derivatisation with NPR and PEG. Developing solvent: toluene, water, anhydrous formic acid, ethyl formate, (3:6:8:60 V/V/V/V). Plate: HPTLC silicagel 60 F₂₅₄. NPR: Natural product reagent, PEG: Polyethylen glycol 400.

The possibility of multiple detection gives flexibility to TLC/HPTLC and allows detecting compounds of different phytochemical groups in a single analysis. Figure 2 shows, as example, the case of mate leaf (*Ilex paraguariensis* A.St.-Hil.), the characteristic constituents of which are caffeine and polyphenols, particularly caffeoylquinic acids and flavonoids [6]. In a single HPTLC analysis of the samples extracted with methanol, two detections are used sequentially: first, the observation of the developed plate under UV light at 254 nm, allowing the detection of caffeine by comparison to a reference substance on a separate track, followed by a second detection using natural product reagent (NPR) and polyethylen glycol 400 (PEG) and observation under UV light at 366 nm. This second detection system cannot show the presence of caffeine, but detects a series of zones due to caffeoylquinic acids and flavonoids characteristic of mate leaf.

HPTLC is also very useful for discriminating close taxa that can be used as adulteration or falsification of the desired species. Recently, an optimized HPTLC method has been described that distinguishes the roots of 28 different *Angelica* taxa and related species belonging to the Apiaceae family, including those traditionally used in Europe (e.g. *Angelica archangelica* L., *Levisticum officinale* W.D.J.Koc) and those traditionally used in Asian countries such as *Angelica acutiloba* (Siebold & Zucc.) Kitag., *A. dahurica* (Hoffm.) Benth. & Hook.f. ex Franch. & Sav., *A. gigas* Nakai, *A. pubescens* Maxim., *A. sinensis* (Oliv.) Diels, *Ligusticum sinensis* Oliv., and *Ligusticum chuanxiong* S.H.Qiu, Y.Q.Zeng, K.Y.Pan, Y.C.Tang & J.M.Xu. [7].

Lavender flower (*Lavandula angustifolia* Mill.) is an herbal drug used mainly as sedative [8], whereas lavandin (*Lavandula × intermedia* Emeric ex Loisel.) is a hybrid between *L. angustifolia* Mill. and *L. latifolia* Medik., used for the production of essential oils as ingredients of industrial perfume and fragrance materials. The essential oils of both lavender flower and lavandin flower are characterized by a high content of linalool and linalyl acetate. Lavandin has higher biomass and oil yield, but the oil is considered of lower quality due to the higher content of 1,8-cineol and camphor [1,9].

The presence of a purple zone in lavandin flower, absent in lavender flower, allow an easy differentiation of both species by the HPTLC analysis of their toluene extracts, as it is shown in Fig. 3. In addition, the analysis clearly discriminates old lavender flowers from the herbal drug harvested in the current year.

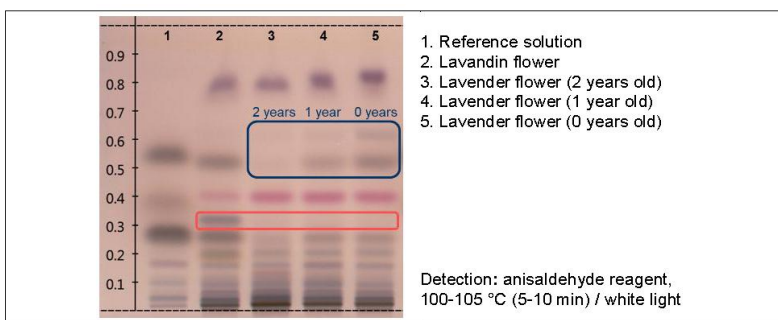


Figure 3. HPTLC chromatograms for identification of lavender flower (*Lavandula angustifolia* Mill.) and discrimination of lavandin flower (*Lavandula × intermedia* Emeric ex Loisel.) (see red rectangle). In addition, old samples (one and two years old) can also be distinguished from the sample of the current year (see blue rectangle). Developing solvent: ethyl acetate, toluene (5:95 V/V). Plate: HPTLC silicagel 60 F₂₅₄.

Gas chromatography (GC) is the technique of choice for essential oils, due to the volatility of their constituents, mainly mono- and sesquiterpenes. However, sometimes, essential oils are adulterated with fatty oils. Triglycerides, the major constituents of fatty oils are not volatile and, consequently, are not detected in the GC analysis of the essential oil: the GC profiles of the pure and adulterated essential oils are similar and the adulteration is not detected. HPTLC is able to distinguish between the pure and the adulterated oil and, in a second analysis, can give information on the fatty oil used as adulterant. As example, Figure 4 shows the case of the detection of this type of adulteration in the essential oil of sage (*Salvia officinalis* L.).

According to the EU regulations [10], stability studies are necessary for the market authorization of an herbal medicinal product. This is another part of the quality requirements where HPTLC has a place. Unless justified, the accepted variation in content of constituents with known therapeutic activity during the proposed shelf-life is $\pm 5\%$ of the declared assay value. Whereas when constituents with known therapeutic activity are unknown (markers are used in this case) the accepted variation is $\pm 10\%$ of the initial assay value.

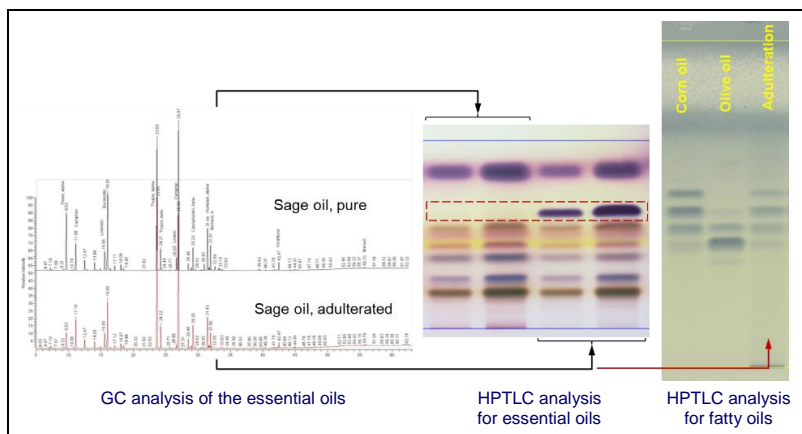


Figure 4. Detection of adulteration of sage essential oil with a fatty oil by HPTLC. The adulteration is not detected by the analysis of the essential oil by gas chromatography (GC), but by HPTLC, where the triglycerides of the fatty oil produce a distinctive zone in the chromatogram of the adulterated oil (see red rectangle). The HPTLC analysis of the essential oil using a method for fatty oils shows that the fatty oil used for the adulteration produces a profile similar to that of corn oil.

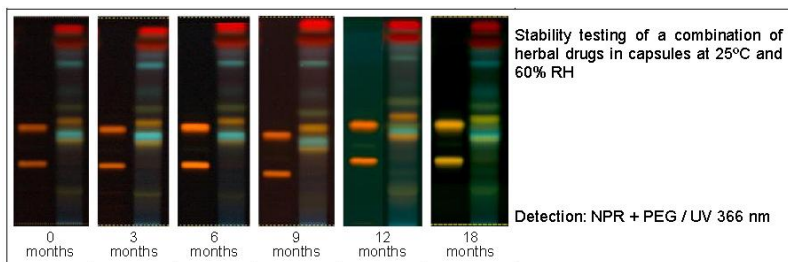


Figure 5. HPTLC chromatograms used for a stability study of a combination of herbal drugs in capsules. For each time point, left track corresponds to reference solution and right track to test solution.

Nevertheless, since the herbal drug or herbal preparation in its entirety is regarded as the active substance, the determination of the stability of the constituents with known therapeutic activity or the markers is not considered sufficient. The stability of other constituents of the herbal drug or the herbal preparation should, as far as possible, also be demonstrated. The HPTLC fingerprint chromatograms are appropriate in this case, as it is shown in Fig. 5.

3. Recent improvements in the Pharmacopoeias

TLC has been included since decades in most of the Pharmacopoeias as identification tool for herbal drugs and herbal preparations. However, a number of issues have been observed over the years with this traditional use, in part due to the technique and in part due to the nature of the herbal materials. First, the variability of the chromatograms obtained, partially due to the inherent variability of the herbal drugs (differences between batches), but also to the lack of intra- and inter-laboratory reproducibility of the analysis. Second, the difficulties on the description and interpretation of the chromatograms. Over the years, the evolution of the description systems in the Ph. Eur. has improved its accuracy by changing from plain text to the use of tables. However, it remains a challenge to describe the natural variability of an herbal drug in a single description of the TLC/HPTLC fingerprint, including the selection of zones to be considered/described and the definition of their position, color and intensity in a way that avoids, as far as possible, ambiguity in the interpretation. At the end, the qualified person in a laboratory has to decide whether the fingerprint of a sample is compliant with that described in the pharmacopoeia. Moreover, in most of the cases,

the pharmacopoeias do not include any system suitability test for qualifying the plate before any interpretation of the chromatograms [11,12].

In order to solve these issues, improvements have been implemented in several pharmacopoeias, that published new general chapters on the analysis of herbal drugs and preparations by HPTLC: the general chapter 2.8.25 (*High-performance thin-layer chromatography of herbal drugs and herbal drug preparations*) in the 9th edition of the European Pharmacopoeia [1] and the general chapters <203> (*High-Performance Thin-Layer Chromatography Procedure for Identification of Articles of Botanical Origin*) and <1064> (*Identification of Articles of botanical origin by High-Performance Thin-layer Chromatography procedure*) in the USP 38 – NF 33 [13].

The first step for **improving reproducibility** is the use of HPTLC instead TLC, because inter-laboratory trials performed in the framework of the Ph. Eur. have demonstrated the higher reproducibility of this technique [11,12].

The second step is the standardisation of the methodology. This is the use of standard operating procedures (SOP) that include detailed descriptions of all relevant parameters, such as preparation of the sample, plate setup and handling, sample application (as band), chamber geometry and saturation, humidity control, developing distance, derivatisation procedure and observation, documentation (as electronic images), and evaluation of the chromatograms. The standards used nowadays in the Ph. Eur. and the USP are following the recommendations of the HPTLC Association (www.hptlc-association.org). The new general chapters of the Ph. Eur. and the USP include detailed description of the common part of the HPLC methodology, while the specific information regarding each method is included in the corresponding individual monograph.

The qualification of the plate is a key factor for improving reproducibility of the HPTLC analysis. It answers the question: Was the HPTLC analysis properly done? Only qualified plates should be used for evaluation of results and for comparison of results of different analyses of the same herbal drug or preparation, performed in the same or in different laboratories.

There are different approaches to the qualification of the plate. In the USP, it is based on two or more reference substances that have just separable R_F or (in most cases) a reference extract, for which results should match description of colors and position, within a specified range. In the HPTLC Association, it is mainly based on reproducible and standardized

HPTLC results, with the definition of exact R_F values. Finally, in the Ph. Eur. a system suitability test (SST) is described in each method and it is based on the separation of 2 substances that have similar retardation factors (R_F values) but that are barely separable under the specified chromatographic conditions. An example of selection of a pair of substances for SST is shown in Fig. 6 for an analysis of flavonoids and phenolic acids [11]. The SST is normally applied on the first track and, in addition to the qualification of the plate, it is also used for normalization of the electronic image of the plate.

As mentioned earlier, one of the main issues with the traditional use of TLC was the **description and interpretation of the chromatograms**. The description has to take into account the sequence and characteristics of the zones (number, position, colour and intensity). The interpretation of the intensity was highly subjective, because there was not a reference to compare with. In order to improve this situation, the new chapter 2.8.25 of the Ph. Eur. has introduced the use of **intensity marker**. The intensity marker is selected from the reference substances used. The reference solution (containing the intensity marker) is applied on adjacent tracks at the normal concentration and diluted one to four. The intensity marker will give different intensities in the two tracks. The intensities of the zones of the chromatogram of the test solution are described comparing to these two different intensities. The meaning of the descriptors used in the Ph. Eur. is illustrated in the Fig. 7.

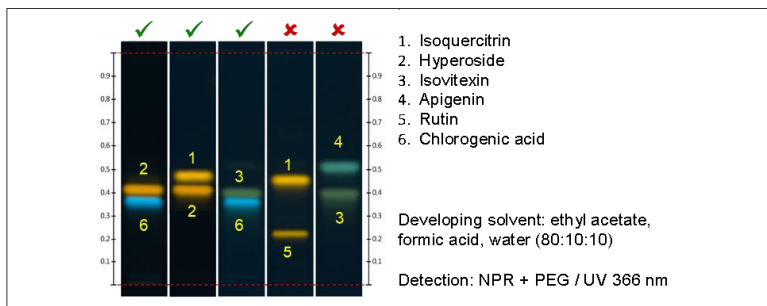


Figure 6. Selection of a pair of substances for the system suitability test (SST) in the analysis of flavonoids with the developing solvent ethyl acetate, formic acid, water (80:10:10 V/V/V/V) on a HPTLC silicagel 60 F₂₅₄ plate. The pairs of the first two tracks are suitable for the SST, and preferable to the pair of compounds of the track three, which are very close together. The pairs of the two last tracks are not suitable because the two compounds tested are too far from each other. NPR: Natural product reagent, PEG: Polyethylenglycol 400.

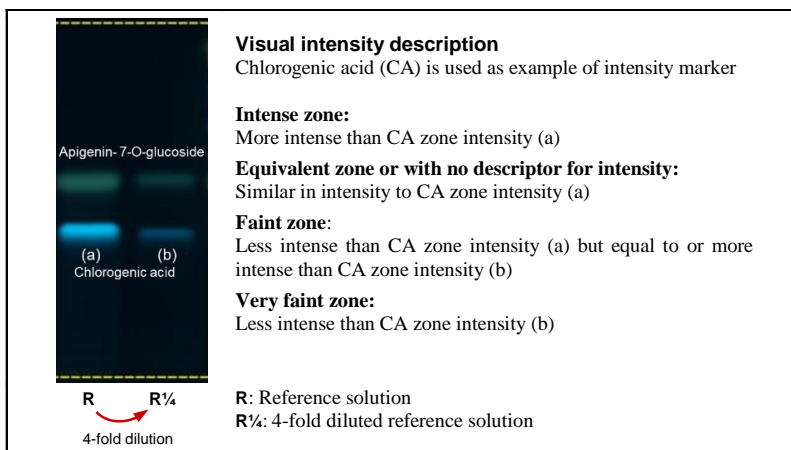


Figure 7. Visual intensity description according to the general chapter 2.8.25 of the Ph. Eur., using chlorogenic acid as example of intensity marker.

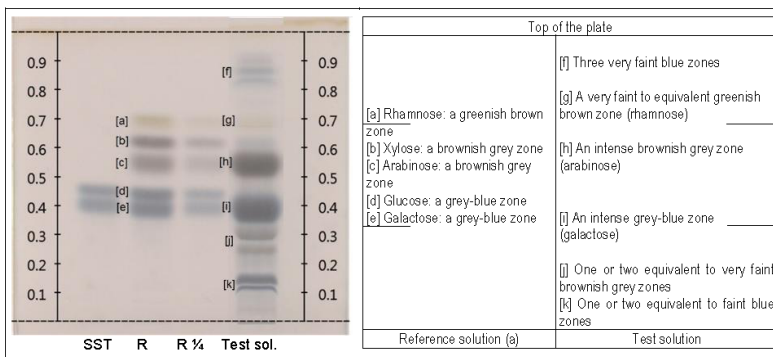


Figure 8. Proposal of description for the identification of acacia and acacia spray/roller dried by HPTLC using the method developed as described in the present chapter (intensity marker: galactose). R: reference solution (a), R¼: 4-fold diluted reference solution (a).

Together with the implementation of the general chapter 2.8.25, the 9th edition of the Ph. Eur. has introduced another significant improvement for the interpretation of the chromatograms, the publication of **colour pictures of the chromatograms**. They are not published in the Pharmacopeia itself but in the Knowledge database. They are not mandatory, but given only as

information. Pictures include type chromatograms, helping with the identification of the zones referred to in the description table of the chromatograms of the individual monographs, as well as pictures of several batches of the herbal drug or preparation to show natural variability. Figure 8 shows an example of a type chromatogram and proposal of description of results according to the new chapter 2.8.25 of the Ph. Eur. for acacia and acacia spray/roller dried. Other Pharmacopoeias and Compendia [13-19] also started to publish pictures of the chromatograms.

4. Development of an HPTLC method

The routine chromatographic identification of polysaccharide rich herbal drugs and preparations thereof, such as gums, mucilages and starches is based on the TLC analysis of the monosaccharides released by hydrolysis. In the 8th edition of the Ph. Eu. [20], TLC identification was described in a limited number of the monographs related to this class of compounds and HPTLC was not described in any of them. In addition, the sample preparation was tedious and applied different conditions of hydrolysis. The TLC methods had also different mobile phases and three different detection reagents. With the aim of setting up an improved and harmonised general method for identification of this type of herbal drugs and preparations, suitable for routine quality control, an HPTLC method was developed and adapted to the requirements of the new Ph. Eur. chapter 2.8.25, published in the 9th edition [1].

In the next paragraphs, the parameters studied and the conclusions obtained will be summarized [21].

For the **preparation of the test solution**, the hydrolysis at 100 °C (1h, oven) and 120 °C (1 h, oven or autoclave), using different concentrations of trifluoroacetic acid (TFA) (100 g/L and 230 g/L) were tested. After the hydrolysis, the need of evaporating the acid (which is time consuming) was tested, as well as the suitability of the use of methanol instead of water as final solvent. TFA at 100 g/L, 120 °C, during 1 h, were the conditions selected for hydrolysis, and the subsequent treatment was considerably shortened by avoiding evaporation of the acid. Methanol as final solvent was considered suitable.

The starting point for the **chromatographic separation** were the TLC methods already described in the Ph. Eur. [20] for ispaghula (seed and husk) guar and guar galactomannan. The separation was performed using one development with acetonitrile, water (85:15 v/v), in a saturated chamber. The main problem of this system was the relatively low R_F s and a limited separation of the monosaccharides. With the aim of improving the separation, other proportions of this binary solvent system were tested, as well as the addition of different proportions of a third solvent, either

acetone or 1-propanol. Saturation with different solvents as well as the use of an unsaturated chamber were also investigated. And, finally, the suitability of multiple developments was verified. An optimised separation was obtained using HPTLC silica gel 60 F₂₅₄ plates conditioned to a relative humidity of 33%, and double development with acetonitrile, water (85:15 v/v) in an unsaturated chamber.

For the **detection**, four derivatisation reagents were tested, and diphenylamine - aniline - phosphoric acid reagent was selected, with observation under white light.

Three pairs of reference substances were tested as candidates for the **system suitability test (SST)**. Galactose and glucose were considered the most suitable pair as SST for the qualification of the plate.

Finally, as **intensity marker**, a monosaccharide was individually chosen for each herbal drug or herbal preparation.

A description to which the chromatogram has to comply was prepared for each herbal drug/preparation, together with the type chromatogram, according to the general chapter 2.8.25 of the Ph. Eur. A proposal for acacia and acacia spray/roller dried is shown in Fig. 8. The application of the method to different herbal drugs and preparations is shown in Fig. 9.

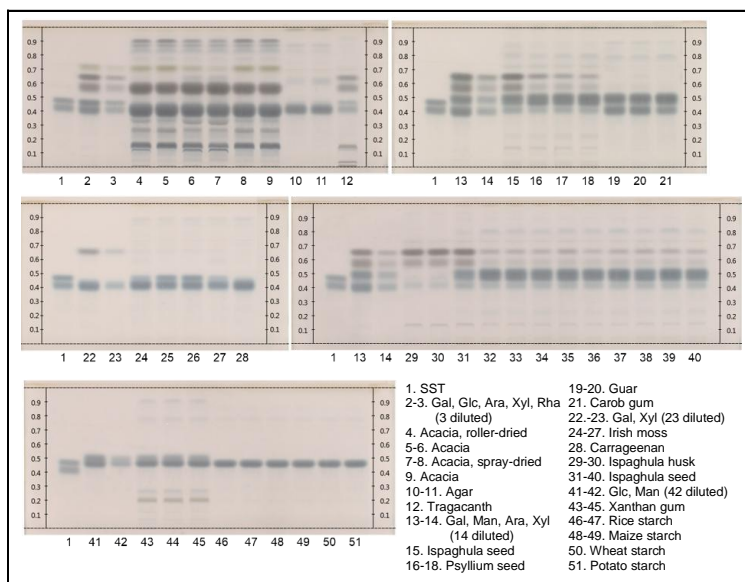


Figure 9. HPTLC chromatograms of several polysaccharide containing herbal drugs and preparations, using the method developed as described in the present chapter.

5. Comprehensive HPTLC fingerprinting

HPTLC is nowadays adopted by the major pharmacopoeias of the world for analysis of herbal drugs and preparations. The current use is generally limited to the visual observation of the fingerprints for identification and detection of adulterations and falsifications. However, standardisation of methodology offers the necessary reproducibility that allows a deeper exploitation of this technique in the field of herbal products. Indeed, the HPTLC fingerprint, as an electronic image of the chromatogram, when generated by a standardized methodology under use of suitable instruments and software, and qualified by a SST, can also provide quantitative information based on the intensity of zones [22]. This information can be used for performing limit tests (e.g. for adulterants), determining content of active constituents or markers, or development of other quality parameters that need quantitative data. This quantitative information can be accessed by converting HPTLC fingerprints (electronic images) into peak profiles from images (PPI) by calculating the luminance from the average of RGB pixels of each line of the track and then plotting it against the RF values. Figure 10 shows this process. The height of the peak in luminance is used as measure of intensity and is compared with the corresponding peak of reference material. This comparison is far more objective than the simple visual comparison of zones intensities.

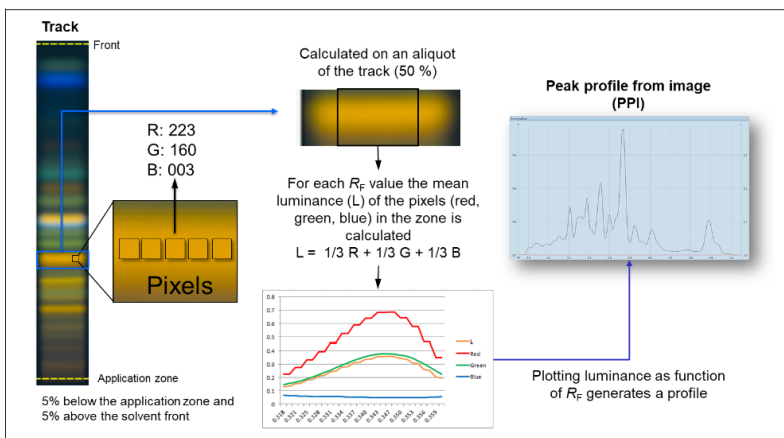


Figure 10. Transformation of the electronic image of the HPTLC chromatogram into the corresponding peak profile from image (PPI).

Based on that, the concept of “comprehensive HPTLC fingerprinting” has been developed [7]: HPTLC fingerprints used for identification, are converted into PPI and used for obtaining information on purity and/or strength/content of the herbal drug or preparation analysed. A single analysis by HPTLC gives comprehensive information on quality and allows the simplification of the quality control process.

The proof of concept has been illustrated in the case of the quality control of the root of Korean angelica (*Angelica gigas* Nakai), known as dang gui and commonly used in the Republic of Korea [7]. It contains decursin and decursinol angelate, which are used as quality markers and a minimum content is required. Two other species of *Angelica*, Japanese angelica (*A. acutiloba* (Siebold & Zucc.) Kitag) and Chinese angelica (*A. sinensis* (Oliv.) Diels), also known as dang gui in their respective countries of origin, can be considered adulterants when mixed with the former. However, the roots of these two species contain Z-ligustilide, which is not present in the root of *A. gigas*. Comprehensive HPTLC fingerprinting of this herbal drug, means that after a single analysis, it is possible to retrieve the following information:

- Identity, based on the visual observation of the fingerprint.
- Distinction from the roots of other 27 *Angelica* taxa and related Apiaceae species, also based on the visual observation of the fingerprint.
- Discrimination of roots of *A. gigas* adulterated with the roots of *A. sinensis* or *A. acutiloba*, based on the PPI analysis of the presence of Z-ligustilide. A 5% of adulterant or even less can be clearly detected.
- Compliance to an established minimum content of the sum of decursin plus decursinol angelate, based on the PPI analysis of the peak that is compared with the corresponding peak of the reference material.

Another example in which the use of comprehensive HPTLC fingerprinting can reduce the number of analyses needed for quality control is the refined dry extract of ginkgo leaf (*Ginkgo biloba* L.) [23]. The USP monograph [13] prescribes an HPTLC identification looking at the fingerprint of flavonoids, and an HPLC assay of flavonoids performed on the aglycons (quercetin, kaempferol and isorhamnetin) released after hydrolysis. The flavonoid content required is 22-27%. The extract can be adulterated with pure flavonoids (e.g. quercetin and rutin) or other herbal extracts rich in flavonoid glycosides releasing quercetin by hydrolysis. The objective of the adulteration is to give the same flavonoid content using less ginkgo leaf extract. For this reason, the USP includes an HPLC limit test for rutin and

quercetin. Comprehensive HPTLC fingerprinting applied to ginkgo products is able to check, after a single analysis:

- Identity of the extract contained in the product, by visual evaluation of the fingerprint.
- Adulterations with quercetin and/or rutin rich materials and the nature of the adulterant, also by visual evaluation. Most common adulterants can be detected: the extracts of sophora fruit or flower bud (*Styphnolobium japonicum* (L.) Schott, syn: *Sophora japonicum* L.), and of buckwheat herb (*Fagopyrum sp* Moench), as well as pure rutin or quercetin.
- Compliance to the USP limit test for quercetin and rutin, using the PPIs obtained from the fingerprints acquired from different detections on the same plate. Results from the HPTLC analysis show a very good correlation with those obtained by HPLC according to the USP. Consequently, the HPLC limit test prescribed by the USP could be avoided by means of a deeper exploitation of the fingerprints obtained in the HPTLC analysis for identification.

6. Conclusions and future prospects

HPTLC is a simple, visual and pragmatic technique, capable of delivering reliable and reproducible results, based on standardized methodology and the use of SST for plate qualification. The improvements introduced in the Pharmacopoeias, especially in the Ph. Eur. and the USP, together with the instrumentation and software allowing to record normalized electronic images of the chromatograms (fingerprints) and their transformation into peak profiles (PPI), open the door to retrieve quantitative information from the analysis performed for identification. Based on that, the concept of comprehensive HPTLC fingerprinting has been introduced. It allows simplification of quality control processes for herbal drug/preparations/products, because from a single HPTLC analysis, information on identity, purity and content can be obtained.

Additionally, HPTLC results generated on different plates can now be compared based on the electronic images of the fingerprint. Images can be stored in an electronic atlas or even in a cloud, which can be accessed by different labs, enabling global exchange and collaboration.

Herbal drugs and herbal preparations have a high chemical complexity and they are considered the active pharmaceutical ingredients in their entirety [10]. The traditional approach of assaying a selected marker, that often represents only 0.02 to 5% of the total composition, has a limited significance for the level of quality and it is under discussion. A more

holistic approach, considering a wider range of constituents would be suitable. In this context, the HPTLC chromatographic profiling of herbal drugs/preparations/products appears as an essential tool to establish its quality [24,25]. Probably, chemometrics will help on that, but how it will develop is still unknown, because it is not only depending on the technical capacities, but on how to establish official criteria of acceptance that can be implemented in a Pharmacopoeia.

Acknowledgements

The authors are grateful to Fundació Maria Francisca de Roviralta and Generalitat de Catalunya (2007PEIR00009-10-A) for the acquisition of laboratory equipment.

References

1. EDQM (European Directorate for the Quality of Medicines and Health Care). 2018. *European Pharmacopoeia*. 9th Ed. Council of Europe, Strasbourg.
2. Cañigüeral, S., Tschopp, R., Ambrosetti, L., Vignutelli, A., Scaglione, F., Petrini, O. 2008, *Pharm. Med.* 22(2), 107.
3. Cañigüeral, S. 2013, *Rev. Fitoter.* 13 (2), 101.
4. Reich, E., Schibli, A. 2006, *High-Performance Thin-Layer Chromatography. For the analysis of medicinal plants*. Thieme, New York.
5. Reich, E., Schibli, A., DeBatt, A. 2008, *J. AOAC Int.* 91, 13.
6. Heck, C.I., Mejia, E.G. 2007, *J. Food Sci.* 72, R138.
7. Frommenwiler, D.A., Kim, J., Yook, C.S., Tran, T.T.T, Cañigüeral, S., Reich, E. 2018, *Planta Med.* 84(6/7), 465.
8. ESCOP (European Scientific Cooperative on Phytotherapy). 2009, *ESCOP Monographs*. 2nd Ed. Supplement 2009. Thieme, Stuttgart.
9. Aprotosoia, A.C., Gille, E., Trifan, A., Luca, V.S., Miron, A. 2017, *Phytochem Rev* 16:761-799.
10. EMA (European Medicines Agency), 2011, *Guideline on quality of herbal medicinal products/traditional herbal medicinal products*. Document EMA/HMPC/201116/2005 Rev. 2. EMA, London.
11. Meier B, Cañigüeral S. 2014, *HPTLC for herbal drugs: A new approach*. In Symposium on herbs. EDQM 50th Anniversary Conference: EDQM, 50 Years of leadership in the quality of medicines. Strasbourg. Available from <https://www.edqm.eu/medias/fichiers/herbals.pdf>. Accessed 27th August 2018.
12. Cañigüeral S. 2016. HPTLC for herbal drugs and herbal drug preparations. In: Symposium on new technologies. European Pharmacopoeia: Tackling future challenges of the quality of medicines together. Tallinn (Estonia). Available from https://www.edqm.eu/sites/default/files/new_technologies_workshop-tallinn-september2016.pdf. Accessed 27th August 2018.

13. United States Pharmacopeial Convention. 2015, *United States Pharmacopeia - National Formulary [USP 38 NF 33]*. United States Pharmacopeial Convention, Inc., Rockville.
14. Chinese Pharmacopoeia Commission. 2008, *TLC Atlas of Chinese crude Drugs in Pharmacopoeia of the People's Republic of China*, People's Medical Publishing House, Beijing.
15. Government of the Hong Kong Special Administrative Region. 2005-2017, *Hong Kong Chinese Materia Medica Standards*, 8 volumes. Available from <http://www.cmd.gov.hk/html/eng/GCMTI/hkcmmms/volumes.html>. Accessed 27th August 2018.
16. Indian Council of Medical Research. 2016, *Quality Standards of Indian medicinal Plants*, 14 volumes. Aravali Printers & Publishers, New Delhi.
17. United States Pharmacopeial Convention. 2015, *United States Pharmacopeia dietary Supplement Compendium*. United States Pharmacopeial Convention, Inc., Rockville.
18. United States Pharmacopeial Convention. 2018 *Herbal medicines compendium*. Available from: <https://hmc.usp.org/>. Accessed 27th August 2018.
19. Upton, R. (Ed.). 1997-2018, *American Herbal Pharmacopoeia and therapeutical Compendium*, 35 volumes. American Herbal Pharmacopoeia, Scotts Valley.
20. EDQM (European Directorate for the Quality of Medicines and Health Care). 2016. *European Pharmacopoeia*. 8th Ed. Council of Europe, Strasbourg.
21. Oudkerk, S., Vila, R., Cañigueral, S. 2017 *Planta Med. Int. Open* , 4, S166.
22. Reich, E., Frommenwiler, D.A., Maire-Widmer, V. 2015, High-performance thin-layer Chromatography for the Identification of botanical Materials and the Detection of Adulteration. In: Reynertson, K.A., Mahmood, K. (Eds.) *Botanicals. Methods and Techniques for Quality & Authenticity*, Chapter 15, Pag. 241-259, CRC Press, Boca Raton.
23. Frommenwiler, D.A., Booker, A., Heinrich, M., Reich, E., Cañigueral, S. 2017, *Planta Med. Int. Open* 4, S190.
24. Cañigueral, S. 2017, HPTLC for herbal drugs and herbal drug preparations in the European Pharmacopoeia. HPTLC 2017 - International Symposium for High-Performance Thin-Layer Chromatography, Berlin. Book of abstracts, O-11. Available from: <https://www.hptlc.com/version-2017/Book-of-abstracts-HPTLC-2017.pdf>. Accessed 10th September 2018.
25. Reich, E. 2017, Can HPTLC help solve the quality problems of botanical dietary supplements?. HPTLC 2017 - International Symposium for High-Performance Thin-Layer Chromatography, Berlin. Book of abstracts, O-9. Available from: <https://www.hptlc.com/version-2017/Book-of-abstracts-HPTLC-2017.pdf>. Accessed 10th September 2018.